



DISSERTATION

Titel der Dissertation:

Sedimentology and modelling of the Mitterndorf Basin

angestrebter akademischer Grad:

Doktor der Naturwissenschaften (Dr. rer. nat.)

Verfasser: Bernhard SALCHER, Mag.
Matrikel-Nummer: 9602551
Dissertationsgebiet: Geologie
Betreuer: Michael WAGREICH, AO. Prof. Mag. Dr.

Wien, am 05.Dezember 2008

Contents

Abstract	2
Kurzfassung	4
Project background and project aim	6
Introduction	6
Study area	7
Methodology and data availability	7
Preliminary Results–Results which were not discussed in the presented articles	9
Preliminary results and implications from the drilling core THER-SCI-1	9
Results regarding the regional geology of the southern Vienna Basin (Rauchenwarth Plateau, Arbesthal Hills, terraces of the Danube	10
References	15
Scientific Articles	23
Article A.....	23
SALCHER, B. and WAGREICH, M. (2008): Climate and tectonic controls on sequence development and river evolution in Austria’s largest Pleistocene basin	
Article B.....	43
SALCHER, B., DECKER, K., MEURERS, B. and WAGREICH, M. (2008): Detection of Pleistocene structures in the southern and central Vienna Basin using first order gravity derivatives, reflection seismic and well data	
Article C.....	65
SALCHER, B., FABER, R. and WAGREICH, M. (2008): Numerical modeling of factors controlling sequence development of Pleistocene alluvial fans, Vienna Basin, eastern Austria	
Appendices	88
Appendix Tab. app. 1, Sample list outcrops.....	88
Appendix Tab. app. 2, Sample list drilling core SCI-THER-1	96
Appendix Tab. app. 3, Heavy mineral assemblages.....	98
 Curriculum Vitae	 104

Abstract

The Mitterndorf Basin is the largest Pleistocene Basin in Austria. The basin is linked to a releasing bend along the major Vienna Basin transfer fault. Basin formation is supposed to start during the Middle Pleistocene. The up to 170 m of accumulated Quaternary sediments show strong variations in their lithofacies reflecting distinct climate oscillations. Massive coarse grained sediments provide huge pore space making the Mitterndorf Basin to one of Europe's largest drinking water reservoirs. Knowledge about the basin's stratigraphy is therefore not only crucial to better understand this important aquifer, basin's subsidence and associated preservation of lithofacies provide also valuable information on Quaternary climate and environment.

Intense field and lab work was supported by computer data processing. All data concerning geology (e.g. drill logs, field and lab data), geophysics (e.g. Bouguer gravity, geoelectric data, seismic data) and geography (e.g. aerial images, topographic information) were integrated in a geographic information system (GIS). This major database builds the platform for all static and forward models.

Within the 3 years of this PhD, 3 scientific papers have been written so far:

Salcher and Wagneich (2008) investigated the impact of climate and tectonic on the lithofacies in the Mitterndorf Basin. The coarse grained, massive facies is associated with high-energetic flood events reflecting a distinct nival regime during glacial times. In contrast, fine grained, well stratified sediments mark periods of rather high discharge to sediment supply ratios during warmer periods. Sequence preservation was provided by subsidence rates of approx. 0.5 - 1 mm/a. High subsidence rates preserve a relatively large record of sequences compared to fluvial terraces which reflect mainly sediments deposited during and shortly after glacials. New ¹⁴C and relative ages demonstrate the strong impact of oscillations in climate on fluvial stratigraphy covering times from the upper period of MIS 3 to the MIS 1.

Salcher, Meurers, Decker, Wagneich (2008) applied a technique in Bouguer gravity filtering to high pass near surface structures. Different first order derivatives of gravity data were used to precisely determine fault locations. Together with drill log information a new and considerably more accurate model of the Mitterndorf Basin's underground was developed. The presented model demonstrated the kinematic (sinistral, pull apart basin) impact on the basin geometry and on fault activity during the Pleistocene. Abundant geophysical and geological data such as 2 D, 3 D seismic, geoelectric, log and outcrop data were used to verify coincidence of structural features with gravity anomalies gained from derivatives. Additionally, numerical models were carried out to better understand effectiveness of derivatives and better interpret gravity anomaly features. Results do not only demonstrate the impact of faults on landscape development. It could be demonstrated that diverse geomorphologic features have a tectonic origin such as scarps, grabens and valleys. Salcher, Meurers, Decker, Wagneich (2008) have been among the first to apply gravity high pass filtering technique in general and the first who demonstrate the suitability in a continental Pleistocene Basin.

Salcher, Faber, Wagneich (2008) used a numerical model approach to investigate climate induced aggradation and degradation cycles, the influence of subsidence and the impact of base-level change (Danube) on this large Pleistocene basin within a time frame of 25 ka. Models were carried out as landscape evolution models describing long term changes in size, shape and relief of landforms. Models were calibrated on real world conditions benefiting from abundant data of the study area. New codes were tested and implemented. Software (SedTec) provided excellent calibration possibilities, helping to make models more realistic. Our models showed that adjustments in sediment supply mainly impact basin's sequence evolution. Strong alterations in sediment supply are related to changing climate, ranging from cool or cold to warm and rather wet conditions. The effect of subsidence is minor compared to climate and only gets relevant over longer time spans. The impact of the axial main river (Danube) is principally strong and fast but

has no relevance for the study area. Both factors are especially relevant during long lasting warm periods.

Kurzfassung

Die Mitterndorfer Senke ist das größte Pleistozän Becken in Österreich. Das Becken hat sich entlang der sinistralen Wiener Becken Transfer Störung ausgebildet. Im Bereich dieser wichtigen Blattverschiebung haben sich durch fortlaufende Bewegung Störungsflächen gekrümmt („befreiende Krümmung“ oder auch releasing bend) und Platz für die Beckenformation geschaffen. Die bis zu 170 m mächtigen quartären Sedimente spiegeln die deutlichen Klimaveränderungen während des Quartärs in ihrer Lithofacies wider. Die massiven, grobkörnigen Sedimente stellen ein sehr großes Porenvolumen und damit auch ein bedeutendes Aquifer dar. Es ist eines der größten Europas. Die Kenntnis der Beckenstratigraphie ist damit nicht nur entscheidend um dieses Aquifer besser zu verstehen, sondern auch um die in der Lithofacies vorhandene Information zur Klimatik und Umwelt besser zu verstehen.

Intensive Feld- und Laborarbeit wurde durch computerisierte Datenprozessierung unterstützt. Die gesamten Daten, betreffend Geologie (z.B. Bohrlogs, Feld- und Labordaten), Geophysik (z.B. Bouguer Schwere, Geoelektrikdaten, Seismikdaten) und Geographie (Luftbilder, Topographische Information) wurden in ein Geographisches Informationssystem integriert. Diese große Datenbank stellt die Plattform für alle statischen und gerichteten Modelle dar.

3 wissenschaftliche Arbeiten wurden bisher geschrieben und eingereicht:

Salcher and Wagreeich (2008) haben den Einfluss von Klima und Tektonik auf die Lithofacies des Mitterndorfer Beckens untersucht. Die grobkörnige, massive Fazies steht im Zusammenhang mit hochenergetischen Flutereignissen die ein ausgeprägtes nivales Regime während der Glaziale anzeigt. Im Gegensatz dazu stehen feinkörnige, gut geschichtete Sedimente die Perioden eines großen Verhältnisses von Niederschlag zu Sedimenttransport zeigen. Günstige Sequenzenpreservationseigenschaften wurden durch Subsidenzraten von etwa 0.5 – 1 mm/a geschaffen. Die Subsidenzraten sind in der Regel auch groß genug um einen großen Teil warmzeitlicher Information vor Erosion zu bewahren. Dieser Teil fehlt in fluviatilen Terrassen häufig. Neue ¹⁴C und relative Alter die aus dem Studiengebiet entstammen beweisen den starken Einfluss klimatischer Oszillationen auf das Klima und auf die fluviale Stratigraphie im Zeitraum von MIS3 bis MIS1.

Salcher, Meurers, Decker, Wagreeich (2008) haben eine Technik verwendet um Bouguer Schweredaten auf ihre hochfrequenten Anteile zu filtern und oberflächennahe Strukturen zu beleuchten. Verschiedene erste Ableitungen wurden verwendet um eine genaue Störungslokation zu erhalten. Zusammen mit Loginformationen aus Bohrungen wurde ein neues und genaues Modell des Mitterndorfer Beckenuntergrundes erstellt. Das Modell zeigt den kinematischen Einfluss auf die Beckengeometrie und auf Störungsaktivität während des Pleistozäns. Reichhaltige Information wie 2D, 3D Seismik, Geoelektrik-, Log- und Erdbebenaktivitätsdaten wurden verwendet um die Übereinstimmung der Strukturen mit den Schwereanomalien zu demonstrieren. Zusätzlich wurden Computermodelle gerechnet um die Effektivität der Ableitungen zu beweisen und auch um Dargestelltes besser zu interpretieren. Resultate zeigen nicht nur den Einfluss von Störungen auf die Landschaftsentwicklung. Es konnte gezeigt werden dass diverse geomorphologische Strukturen tektonisch bedingt sind wie Z.B. Böschungen, Gräben und Täler.

Salcher, Faber, Wagreeich (2008) haben klimatisch bedingte Aggrations- und Degrationszyklen, den Einfluss von Subsidenz und Änderungen des fluviatilen Akkomodationslevels mittels eines numerischen Modells untersucht. Der Modellierungszeitraum betrug 25.000 Jahre. Die Modelle, so genannte „Landschaftsevolutionsmodelle“, beschreiben Langzeitänderungen von Oberflächenformen. Die Modelle haben von den reichlich vorhandenen Daten profitiert und wurden an den naturalistischen Bedingungen des Untersuchungsgebietes kalibriert. Diesbezüglich wurde der Programmcode erweitert und implementiert. Die resultierenden

Modelle zeigten dass Änderungen der Sedimentzufuhr die stärksten Auswirkungen auf das System haben. Starke Änderungen der Sedimentzufuhr hängen direkt mit den klimatischen Bedingungen im Einzugsgebiet zusammen. Der Einfluss von Subsidenz ist geringer und wird erst nach einer längeren Zeit deutlich. Änderungen des Akkomodationslevels wirken sich prinzipiell stärker und schneller aus, haben aber für die Mitterndorfer Senke keine Bedeutung. Beide können sich während längeren, klimatisch wärmeren Perioden besonders deutlich auswirken.

Project background and project aim

This work forms part of the Austrian Science Fund FWF project P18203-N10. The Mitterndorf basin ("Mitterndorfer Senke"; Tollmann, 1985; Fink, 1973; Küpper 1954; Küpper, 1952) comprises one of Europe's largest shallow groundwater reservoirs (Tollmann, 1985; Reitinger et al. 1973) and provides a significant source for raw materials. Economically important groundwater plants are situated in the basin, including the 3rd Vienna waterline Moosbrunn, and other drinking water supplies of this most densely populated area of Austria. The vulnerability of this shallow groundwater reservoir is extremely high. Several severe pollution cases including chlorinated hydrocarbons from waste sites and industrial plants are currently under restoration (Forschungszentrum Seibersdorf, 1992). Considering the economic importance of the MB, detailed knowledge on the basin fill is surprisingly poor. Especially the sedimentology of the up to 170 m thick massive gravels and intervening fine-grained layers is poorly known. Previous studies did almost exclusively deal with hydrogeological aspects (WASY, 1992; Berger, 1989; Prohaska 1983; Küpper 1954; Küpper 1950).

The principal aim of the project was the analysis of the Pleistocene sediments and tectonics. Therefore, research was mainly focusing on the basin's stratigraphic and kinematic evolution. Numerical landscape evolution models helped to understand the interaction of factors which control the basin's sequence development.

Introduction

External factors like climate, tectonic and base-level change are considered to act as main factors controlling the sequence development of fluvial (e.g. Leeder et al., 1998; Bull, 1991; Langbein et al., 1958) or alluvial fan systems (e.g. Harvey, 1992; Bull 1977). These factors control transport conditions and whether a system undergoes aggradation or degradation. The climatic factors influence the sediment supply and runoff power from the catchment (e.g. Wells and Harvey, 1987). Alterations in discharge and sediment supply affect the river planform and consequently the lithofacies development (e.g. Vandenberghe, 2008; Vandenberghe, 2008). Especially during the Pleistocene, where climatic oscillations are very distinct, climate change has a fast and strong impact on the energy level of a system (e.g. Mol et al., 2000).

Tectonic and base level change, as long term effects, control the available sequence accumulation space (Holbrook et al., 2006; Blum and Törnqvist, 2000). Tectonic subsidence generally provides accumulation space and subsequently leads to a sequence lowering below a possible depth of removal and incision. Uplift triggers incision and terrace formation (e.g. Bridgland, 2008; Starkel, 2003). Local shifts in base level elevation may often be associated by downstream changes relating to sea level drop. However, influence on sea level change on streams decreases with distance to the sea strand and has no influence on continental settings which are far of sea (Blum and Törnqvist, 2000). Alterations in base level are then a local effect (e.g. incision of an axial main river, lake level fall). Climate and tectonics gain the principal influence on fluvial systems which are purely continental (Shanley and Mc Cabe, 1994; Blum, 1993).

To understand the sedimentological and tectonic built up of Austria's largest and most important Pleistocene basin, research focused on the lithofacies and associated sequence development. The article: "Climate and tectonic controls on sequence development and river evolution in Austria's largest Pleistocene basin" (Salcher B. and Wagreich M., 2008) deals with basin's sequence and lithofacies evolution.

Since the introduction by Vail et al. (1977) the application of sequence stratigraphy on sedimentary basins is commonly associated with hydrocarbon exploration surveys in marine and nearshore depositional systems. The knowledge on basin stratigraphy and kinematics premise a comprehensive geophysical and geological record (e.g. 3D and 2D seismic, drill log information, e.g. Strauss et al., 2006).

Application of sequence stratigraphic concepts in purely fluvial settings is limited even though sequences have been recognized in continental rocks (Weissmann et al., 2005; Blum and Price, 1998; Shanley and Mc Cabe, 1998; Aitken and Flint, 1995; Shanley and

Mc Cabe 1994). Near surface features, such as Pleistocene fluvial basin fills and faults, are normally not in the focus of hydrocarbon exploration. Consequently, the structural knowledge of very young infillings is often comparable poor if information is not provided by separate surveys. However, common near-surface exploration surveys provide only punctual (drillings) or sectional (GPR, geoelectric and 2D seismic surveys) data. The knowledge on uppermost basin parts concerning its structural and sedimentological build-up remains then often fragmentary. The article "Gravity derived fault maps as constraints on the evolution and geomorphology of Austria's largest Pleistocene basin" (Salcher B., Decker, K., Meurers B., Hoelzel M., Wagreich M., 2008) introduces in new geophysical methods to detect shallow fault systems. Precise fault constraint together with numerous, deep groundwater drillings allowed building a high resolution model of basin's geometry. Derived faults maps explain not only Pleistocene tectonics but could e.g. address drainage development to regional tectonics at the transition to the Pannonian Basin (Eisenstadt Basin) or show the relevance of extensional Plio-Pleistocene kinematics on the geomorphology of Vienna Basin Miocene hills (Rauchenwarth Plateau and Arbesthal Hills). However, with this detailed structural data, knowledge on the distinct sequence extension and the influence of subsidence on the Mitterndorf basin's development was significantly improved.

The interaction of climatic, tectonic and baselevel relevant factors (influence of the axial main river, Danube) on the sequence development were investigated by a numerical modelling approach in the article: "Numerical modelling of factors controlling development of two Pleistocene alluvial fans, Vienna Basin, eastern Austria" (Salcher B., Faber F., Wagreich M., 2008). The numerical models were carried out as landscape evolution models and calibrated on real world conditions using a new adapted code (SedTec by R. Faber). Results show the impact and the time relevance of factors on the basin's fluvial system in a simulated time frame of 25 ka.

Study area

The Pleistocene Mitterndorf Basin forms as pull apart in a releasing bend along the major, active, sinistral strike-slip Vienna Basin Transfer fault (e.g. Hinsch et al., 2005) sizing about 50 km in length and about 10 km in width. Active faulting is indicated by earthquake data (Reinecker and Lenhardt, 1999), geodetic data (Grenerczy et al., 2006, Grenerczy et al., 2002; Höggerl, 1980) and growth faults. In the north where subsidence rates are the highest, Pleistocene sequences reach thicknesses of more than 170 m. In the southern basin part, two mountain front alluvial fans toe out into the basin. Both fans cover approximately two third of the basin.

Lithofacies of basin's sequences reflect a distinct development of massive, crudely bedded, coarse grained sediments during glacial periods and finer grained, stratified sediments during interstadials or interglacials. Sequences which are associated with glacial periods become thick. In contrast, sediments which were formed during warmer periods have only minor thicknesses in the range of only some meters.

Basin subsidence in the range of 1 mm/a (Högerl, 1980) acted sequence preserving lowering sediments below a possible depth of incision and removal (cf. Blum and Törnqvist, 2000). New OSL ages and biostratigraphic data from boreholes point to middle to late Middle Pleistocene ages (Fig. 2) supporting relatively high subsidence rates and confirming suggested ages from Küpper (1950) and Decker et al. (2005). Results show an estimated maximum time span for sedimentation of not much more than approx. 250.000 – 300.000 years.

Methodology and data availability

Information on basin stratigraphy was gained out of more than 2000 drillings, more than 20 gravel pits and several drilling cores. Wells were commonly drilled for groundwater prospection or hydrocarbon exploration. Log data is available in a large database (HADES well database) which was allocated by the courtesy of the Government of Lower Austria. This dataset was completed by digitising further analogue paper logs of the drilling

archive at the Austrian Geological Survey. Special software (well master by Heinz Reitner, Geological Survey of Austria) was used to visualize data in a GIS (Arc View 3.2). Sediments in outcrops respectively gravel pits, were generally analysed regarding their lithofacies, their sedimentary, frost and tectonic induced structures. However, faults were only evident in strata older than Pleistocene (thus not in the Mitterndorf Basin). Occurring paleosols and overbank fines were analyzed regarding their freshwater mollusc assemblages and pollen content (almost all samples lack pollen). Furthermore, charcoals were picked, and if mass was sufficient (minimum of ~ 15 mg), sent for ^{14}C dating (CEDAD radiocarbon centre, Lecce). Sand fractions were analysed regarding their heavy mineral assemblages (commonly taken at the top and the bottom of an outcrop, see appendix Tab. app. 3). Approximately 1700 digital photos have been made for documentation purposes.

The scientific drilling THER-SCI-1 (coordinates Austrian grid, east zone: $x = 743200$, $y = 303568$, geographic net: latitude = $47^{\circ}52'22.6038''$, longitude = $16^{\circ}14'37.00824''$) delivered valuable drilling cores (appendix Tab. app. 2). The drilling site was chosen after the first year of the thesis under consideration of all available drillings and outcrops to offer the best relation in stratigraphic information to drilling costs. The drilling site was situated at almost the same position like the drilling BR-FELIX-2-8 (well database of the Government of Lower Austria; Fig. app. 1). The driller's lithologic log was found to encounter most dateable material in relation to the (relative shallow) depth. Dateable material comprises commonly thin layers of fine grained deposits of inferred rather warm periods (see article A, p. 23) which are appropriate for correlation. Total depth of the drilling was 40.5 m. The drilling was fully cored. The difficulty was to get the sediment largely undisturbed and under the absence of light to the surface (for subsequent OSL dating). Four drilling companies have been evaluated under these considerations. Unfortunately, experiences were generally low, but the company "Insond" (Vienna) was found to bring most drilling experience. Best core results were achieved by rotary technique without flush. Flushed sections, cored with liners (8 to 14 m below surface) were unusable for our purpose. Through the impossibility to use liners, encountered sample material was hammered out into (almost) light impermeable plastic core tubes in 0.5 m steps (Fig. app. 2). Through the compaction of the sediment, hammering into the tubes did disturb sediments only marginally. Cores have been analyzed regarding their age, fossil content (freshwater molluscs), soil composition, palaeo-magnetism, heavy mineral spectra and grain size. Soil, palaeo-magnetism and freshwater mollusc analysis is still in progress. OSL ages, heavy mineral and preliminary palaeo-magnetism data are presented below, in the appendices Tab. app. 3 and Fig. app. 2, respectively.

New modelling techniques in geophysics were applied to provide a precise picture of the basin tectonics using Bouguer anomaly derivatives, 3D seismic, 2D seismic, well and geoelectric data. Seismic, Bouguer anomaly and some of the well data were allocated by the courtesy of OMV E & P.

The digital elevation model (10 m in ground resolution, by the courtesy of the Government of Lower Austria) built the main basis for all geomorphic analyses. High resolution laserscan images (some cm in ground resolution) were not available or too expensive for basin wide application, respectively.

The analysis of high resolution aerial images was necessary to make statements on southern Vienna Basin's stream evolution during the late- to postglacial history. Data from special flight missions which focused the detection of prehistoric settlement was found to be very useful. Special aerial data was provided by Dr. M. Doneus (Dept. for Prehistory and Medieval Archaeology, University of Vienna). Furthermore the location of prehistoric sites in the southern Vienna Basin helped to make statements on the impact of prehistoric flood limits and river change (time range approx. < 5000 a B.P.).

Historical maps (first and second military survey of the Austrian-Hungarian Empire, 1763-1785 and 1806-1869, respectively) were used to get information on the original stream course (without or only minor anthropogenic alterations) and to differentiate between natural (e.g. fault scarps) and artificial topographies (e.g. military trenches). To process data, streams and topographic information was digitized (by the courtesy of the Institute and Museum of War History of Hungary, ARCANUM, Budapest).

Earthquake data was used to know seismic activity and energy in different tectonic segments of the Vienna Basin Transfer fault. Data was allocated by the ZAMG (Central Institute for Meteorology and Geodynamics, Vienna).

All data and derivatives were integrated into a GIS (Arc View and Arc GIS) building the main database for all further computer-aided operations.

Appendix Tab. app. 1 shows all samples taken in the field. Appendix Tab. app. 2 lists samples from the drilling core THER-SCI-1. The spreadsheets contain additional information like e.g. exact position, local description, ages, picture references, etc.

The complete digital dataset will be stored on a file named "Mitterndorf_FWF_AP18203" at the server Geo183 at the University of Vienna, Department of Geodynamic and Sedimentology and at an author's hard disc. Of course, no statements on the duration and maintenance of the stored data at the university can be made. Sample material of outcrops and drilling cores are stored at the Department's magazine. Freshwater mollusc assemblages stay with Prof. C. Frank (Dep. of Anthropology, University of Vienna).

Preliminary Results – Results which were not discussed in the presented articles

As shown in the articles much research has been done during the 3 years of this PhD. Not all of the derived data could be integrated into the scientific articles presented above. Some work is still in progress or has just recently finished. Several new results or results which have not been published so far are presented in this chapter. The very laborious determination of freshwater molluscs is still in progress and will be finished in January to February 2009. Several ten thousand (!!) freshwater molluscs shells have been already sieved, picked and determined (determination by Prof. Frank, Dep. of Anthropology, Vienna). Results are very promising, giving relative ages and detailed knowledge on the palaeo-environment. Palaeo-magnetic work (Dr. Robert Scholger, Montanuniversität, Leoben) and soil analysis of the scientific drilling "THER-SCI-1" (Prof. Fran Ottner, Univ. of Natural Resources and Applied Life Sciences, Vienna) is still under progress. However, preliminary data on the palaeo-magnetic work is presented in Fig. app. 1. New data which have not been published so far comprises e.g. results from OSL dating (Prof. Markus Fiebig, Univ. of Natural Resources and Applied Life Sciences, Vienna; Prof. Frank Preusser, Dep. of Geological Sciences, Bern) heavy mineral and grain size analysis. OSL dating results of the scientific drilling "THER-SCI-1" are presented below. Heavy mineral assemblages of almost all outcrops of the Mitterndorf Basin as well as assemblages from adjacent areas can be found in appendix Tab. app. 3.

Preliminary results concerning the drilling core of THER-SCI-1 and unpublished results concerning the southern Vienna Basin outside the study area (Danube Terraces, Rauchenwarth Plateau and Arbesthal Hills) are presented below. Implications from aerial images and historical maps were integrated in the articles. However, several hundred digitized features (e.g. palaeo-meanders or scarps) are too numerous to be presented in a print form.

Preliminary results and implications from the drilling core THER-SCI-1

Küpper (1950) was probably the first which recognize the importance of climate on the sequence development in the Mitterndorf Basin. The application of sequence stratigraphy at the Mitterndorf Basin has been presented in the article "Climate and tectonic controls on sequence development and river evolution in Austria's largest Pleistocene basin" (Article A, p. 23). The article focuses on the youngest basin development mainly relying on ^{14}C ages. Ages of drillings cores were not available. Three OSL ages of the scientific core THER-SCI-1 are now available. Ages confirm the assumed early to middle Middle Pleistocene age of the Mitterndorf Basin. Samples of the upper sections (KTH3 and KTH4), were taken from fine clastic channel sediments which clearly differ in lithofacies from the thick sequences of underlying and overlying massive gravels. Samples give (feldspar) ages of 134 ± 10 ka (~ 16.7 m below surface) and 135 ± 9 ka (~ 16.1 m below surface) before past, respectively. These ages are therefore in good accordance with

preliminary interpretations concepts of sequence stratigraphy (appendix Fig. app. 1). Channel and paleosol deposits mark formations during rather warm periods (see article A). Ages reflect the transition time from MIS 6 to MIS 5 which corresponds well to the Riß/Würm interglacial. The age of the sample KTH1 (at ~ 37.2 m) seem to relatively young (feldspar age of 246 ± 24 ka). A several dm thick dark, red brown paleosol at $\sim 33 - 33.8$ m below surface indicates very long formation times, at least of several ten thousand years (F. Ottner pers. com.). This paleosol must therefore represent a long interstadial of even interglacial. However, results have to be compared with freshwater mollusc fauna assemblages (in progress) and final results from palaeo-magnetism to verify age information.

The transitions from thick, massive gravel units with rather thin units of interbedded channel and overbank deposits to deposits which are dominated by soils and overbanks reflect also the transition in the subsidence speed (see appendix Tab. app. 2). Higher subsidence creates more accumulation space (sensu Blum and Törnqvist, 2000) and thicker units of massive gravels. The alluvial fan formation and the distinct sequence development (see article C, p. 65) of the Piesting and Schwarza River fan is associated with basin subsidence. Low or no subsidence does not provide or only provides minor accumulation space. The basin subsidence which is assumed to start around the formation of the dark paleosol at $\sim 33-33.8$ m did preserve these sequences from erosion.

Results regarding the regional geology of the southern Vienna Basin (Rauchenwarth Plateau, Arbesthal Hills, terraces of Danube)

An analysis of the Rauchenwarth Plateau (RWP) and Arbesthal Hills (ATH) adjacent to the Mitterndorf Basin was undertaken to find out more on the role of active tectonics (e.g. fault scarps, fluvial activity is very minor) and to find exposed material which comprises the base of the Mitterndorf basin. Indications for active tectonics were found (e.g. "Kuku Berg" at $\sim x: 762000, y: 324550$, Austrian grid east zone). The analysis of several new outcrops, give new implications on the regional geology of the Pleistocene. The tectonic geomorphology of the Rauchenwarth Plateau and the Arbesthal Hills is described in detail in the article B, p. 43.

The Neogene Hills of the Rauchenwarth Plateau and Arbesthal Hills and the Wiener Berg east of the RWP (see Fig. 2 and 10 of the Article B, p. 43), mark a some kilometres wide ridge along the Danube River. It crosses the Vienna Basin extending from the Alps to the Little Carpathians. Seismic, drilling and outcrop data show that the Rauchenwarth Plateau and the Arbesthal Hills consist of mostly marine-lacustrine, fine clastic sediments of the Pannonian. Seismic data constrain those to at least Middle to Upper Pannonian sediments (Harzhauser and Tempfer, 2004; Harzhauser et al. 2004; Strauss et al., 2006; Bernhard et al. 1992). A strong lithologic difference is comprised by some thick layers of sandy gravels which are patchy covering the RWP and ATH. To the north, these Neogene hills are delimited by the Danube for which these hills are cut bank. Due to the uplift of the Alpine-Carpathian orogen (Decker and Peresson, 1996) the Danube River was forced to incise into the bedrock (see article A). Terrace remnants cover the northern part of the Neogene Hills at different elevations corresponding to different ages (Fink, 1954). Terraces have a rather flat topography and occur on an about 2 km wide, continuous zone along the river. Drillings (Hades drilling database, by the courtesy of the Government of Lower Austria) show that these terraces have a common thickness of up to c. 10 m and comprise commonly sandy gravels to cobbles with intervening, up to some dm thick layers of sands. Geological maps of Vienna (Austrian Geological Survey, 1985) and adjacent areas to the east (Bruck an der Leitha, Austrian Geological Survey, 1985) mark patchy occurrences of Pleistocene (Danube) terraces and equivalents on the almost entirely Neogene hill chain. New results derived from new outcrops at the Rauchenwarth plateau, drillings and heavy mineral assemblages indicate that these southern, patchy occurrences of gravels must be older than Pleistocene.

Gravels pits of the Arbesthal Hills are almost all inactive and strongly overgrown. Here observations do rather rely on drillings and older outcrop descriptions. Gravel pits at the

Rauchenwarth Plateau (see sample list appendix Tab. app. 1) show commonly crudely bedded, well imbricated, sandy gravels. Gravels may show cross stratification. Cobbles or boulders do not occur. Matrix content of silts and clays can become high in some places – grain supporting is then not fulfilled. Sediments show a slight overall tilt towards west, reflecting the general inclination of the Rauchenwarth Plateau towards west (Hinsch et al. 2005). The fluvial gravels are interbedded by fine laminated silts and clays which sometimes contain thin layers of sand. Ripples, light clayey concretions and water escape structures are recognizable in places. Clays, silts and sands are coloured. Colours range from yellow to red brown. Clays may become very dark reflecting a very high organic content (possible lignites).

The interbedded fine grained sediments attain thicknesses of up to few meters and are interpreted as overbank deposits. Soils are generally missing. Samples show that they do not contain pollen or freshwater molluscs. One sample contained pieces of thin, some millimetres long, columnar charcoals.

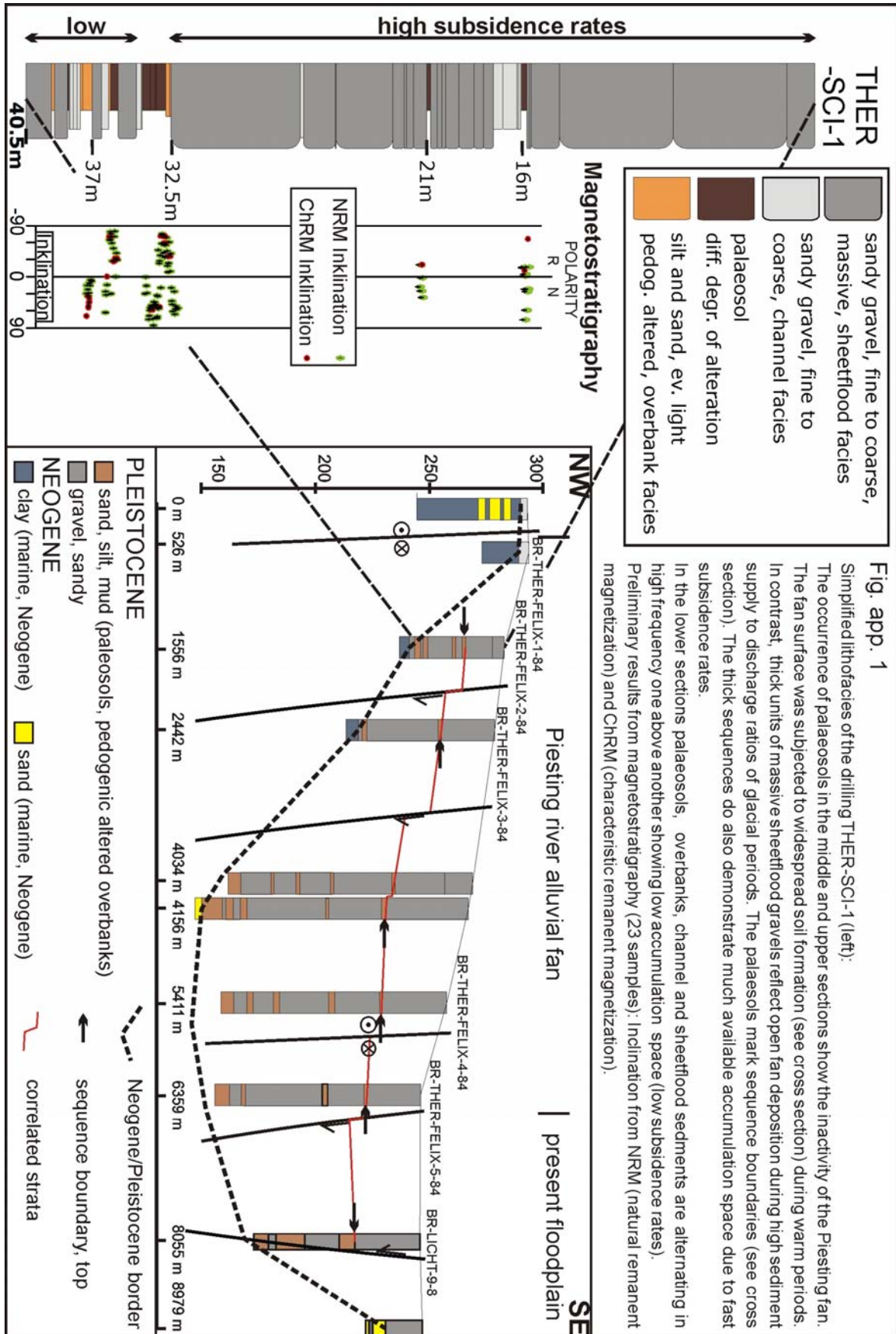
The gravel pits are not very deep, compared to the deep pits in the Mitterndorf Basin. Only one outcrop (Rauchenwarth, see sample list) had a depth of more than 10 m meters, showing that the crudely bedded to stratified gravels of the upper sections merge into well cross stratified sands without any clear discordance. The gravels decrease clearly in grain size and were almost completely displaced by sands towards the base of the outcrop. Fine gravels do then cover the sands only with a thin some cm thick lag at the base of erosive scours or cover individual bedding planes with an mm thin veneer. The occurrence of fine gravels is often associated with a change in colour from yellow to rust brown (Fig. app. 3a). Heavy mineral assemblages of the sandy section are clearly marked by a higher garnet content and some lower content of staurolite (appendix Tab. app. 3). Assemblages are comparable to samples of (Upper) Pannonian sands taken from the eastern limits of the Mitterndorf Basin along the Leitha Mountains (outcrop HS2, see appendix Tab. app. 1). A nearby sand pit with Upper Pannonian sands (inactive Götzendorf sand pit; Brix, 1989) shows similar heavy mineral assemblages. As most of the Rauchenwarth Plateau and Arbesthal Hills are mapped to be of late Pannonian age (Austrian Geological Survey, 1985) such an age would not surprise.

In contrast to sandy sections, the upper gravel sections do clearly differ in heavy mineral content demonstrating different provenance areas and different palaeo-transport directions.

A driller's lithologic log of a nearby drilling (62-B/3-D, well database of the Government of Lower Austria) in the village of Rauchenwarth recognized a very distinct sequence development of four, 6 m thick units of sandy gravels which are interbedded by three 8-9 m thick units of clays and sands (lithofacies is not described in detail in the log) to a depth of more than 50 m below surface.

The difference in provenance, the fact that gravels show no recognizable unconformity to the cross stratified Upper Pannonian sands, very dark clays (lignites?) and the observations from nearby drillings lead to the conclusion that sediments are deltaic deposits older than Pleistocene or Pliocene. Source areas reflect a marine/lacustrine influenced (stratified sands) and an alpine fluvial influenced provenance (gravels). Heavy mineral assemblages from Danube sands at high elevated terraces (e.g. Husz, 1964; Szabo, 1959; see appendix Tab. App. 3) show similar assemblages to these fluvial, sandy gravels (high garnet, low green hornblende, rather high epidot content). The stratified sands have equal assemblages like Upper Pannonian marine/lacustrine strata. These sands could be interpreted as deltaic sands reworked at a sea/lake shore. A sediment bypass of the palaeo-Danube through the Vienna into the Pannonian Basin can be assumed since the Late Miocene (M. Harzhauser pers com.; cf. Gabris and Nádor, 2007). An Upper Pannonian deltaic complex of a palaeo-Danube at this position seems therefore plausible. However, it can be suggested that the patchy coverage of fluvial sediments on top of the Rauchenwarth Plateau and the Arbesthal Hills does not reflect classical Pleistocene terraces (sensu Fink, 1954) but rather reflects remnants of a local lake delta or floodplain of the palaeo-Danube.

Figures





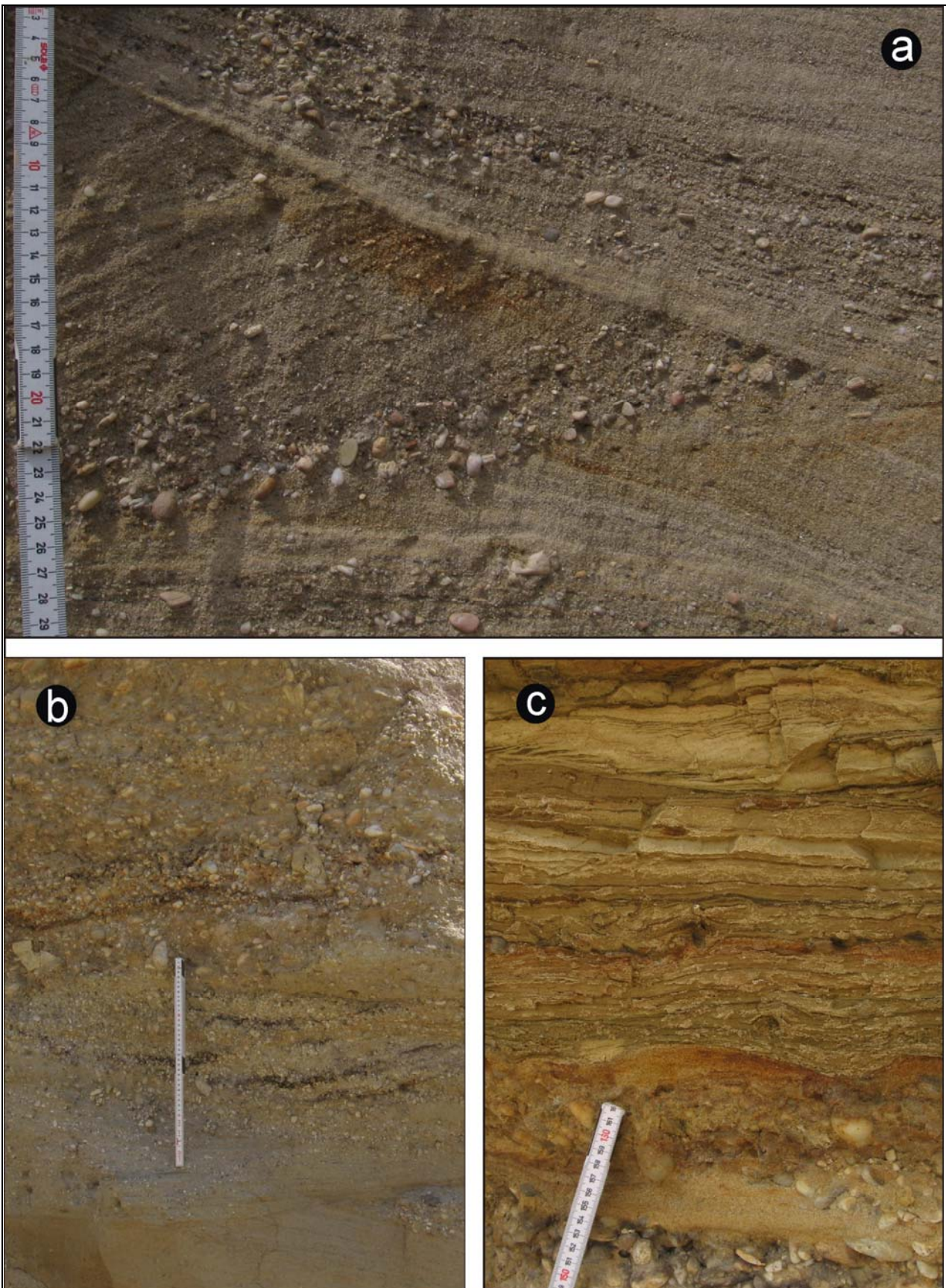


Fig. app. 3 **Upper Pannonian deltaic sediments of the Rauchenwarth Plateau**

(a) well stratified sands and gravels of the upper

(b) transition area: fluvial gravels to well stratified sands, no discordance

(c) upper fluvial gravel section: laminated, sandy to muddy infillings of a channel, the sandier sections may show ripples

References

- Aitken, J.F., Flint, S.S., 1995. The application of high-resolution sequence stratigraphy to fluvial systems: a case study from the Upper Carboniferous Breathitt Group, eastern Kentucky, U.S.A. *Sedimentology*, 42: 3-30.
- Allen, P.A., Densmore, A.L., 2000. Sediment flux from an uplifted fault block. *Basin Research*, 12: 367-380.
- Allen, P.A., Allen, J.R., 2005. *Basin Analysis*. Blackwell, Oxford.
- Amorosi, A., Farina, M., Severi, P., Preti, D., Caporale, L., Di Dio, G., 1996. Genetically related alluvial deposits across active fault zones: an example of alluvial fan-terrace correlation from the upper Quaternary of the southern Po Basin, Italy. *Sedimentary Geology*, 102: 275-295.
- Amy, L.A., Peakall, J., Talling, P.J., 2005. Density and viscosity stratified gravity currents: Insights from laboratory experiments and implications for submarine flow deposits. *Sedimentary Geology*, 179: 5-29.
- Anderson, R.S., Humphrey, N.F., 1990. Interaction of weathering and transport processes in the evolution of arid landscapes. In: T.A. Cross (Editor), *Quantitative Dynamic Stratigraphy*. Prentice-Hall, Englewood Cliffs, NJ, pp. 349-361.
- Andres, W., Bos, J.A.A., Houben P., Kalis, A.J., Nolte, S., Rittweger, H., Wunderlich, J., 2001. Environmental change and fluvial activity during the Younger Dryas in central Germany. *Quaternary International*, 79: 89-100.
- Beidinger, A., Decker, K., 2008. Geophysical, Geomorphological and Geological Studies at the active Lasseer Segment of the Vienna Basin Fault System, *Trabajos de Geologia, YORSGET - International Meeting of Young Researchers in Structural Geology and Tectonics*, Oviedo, Spain.
- Berger, E., 1989. *Analyse der Funktionsfaktoren des Grundwasserspeichers Mitterndorfer Senke*, Amt der NÖ Landesregierung, Wien.
- Bernhard, M., Niesner, E., Holub, B., 1992. *Geophysikalisch-hydrologische Untersuchungen jungtertiärer Tiefensüßwasser im Raum Wien: Teil A*, Montanuniversität Leoben, Wien, 112 pp.
- Blair, T.C., McPherson, J.G., 1994. Alluvial fans and their natural distinction from rivers based on morphology, hydraulic processes, sedimentary processes, and facies assemblages. *Journal of Sedimentary Research*, A64(3): 450-489.
- Blakely, R., 1995. *Potential theory in gravity and magnetic applications*. Cambridge University Press, 441 pp.
- Blum, M.D., Price, D.M., 1998. Quaternary alluvial plain constriction in response to glacio-eustatic and climatic controls, Texas Gulf Coastal Plain. In: K.W. Shanley, McCabe, P.J. (Editor), *The Relative Role of Eustasy, Climate, and Tectonism in Continental Rocks*. SEPM, Special Publication, pp. 31-48.
- Blum, M.D., Törnqvist, T.E., 2000. Fluvial responses to climate and sea level change: a review and look forward. *Sedimentology*, 47: 2-48.
- Bogaart, P.W., Van Balen, R.T., Kasse, C., Vandenberghe, J., 2003. Process-based modelling of fluvial system response to rapid climate change-I: model formulation and generic applications. *Quaternary Science Reviews*, 22: 2077-2095.
- Boogart, P.W., van Balen, T., 2000. Numerical modeling of the response of alluvial rivers to Quaternary climate change. *Global and Planetary Change*, 27: 147-163.
- Bridge, J.S., Leeder, M.R., 1979. A simulation model for alluvial stratigraphy. *Sedimentology*, 26: 617-644.
- Bridgland, D., Westaway, R., 2008. Climatically controlled river terrace staircases: A worldwide Quaternary phenomenon. *Geomorphology*, 98: 285-315.
- Brix, F., 1989. *Zur Geologie und Lithostratigraphie der Sandgrube Götzendorf an der Leitha*, Niederösterreich. *Anzeiger der Österreichischen Akademie der Wissenschaften*, 126: 33-42.
- Brix, F., Schulz, O., 1993. *Erdöl and Erdgas in Österreich*. Museum of Natural History, Vienna, Wien, 688 pp.

- Bull, W.B., 1962. Relations of alluvial fan size and slope to drainage basin size and lithology, in Western Fresno County, California. US Geological Survey, Professional Paper, 430b: 51-53.
- Bull, W.B., 1977. The alluvial fan environment. *Progress in Physical Geography*, 1: 222-270.
- Bull, W.B., 1991. *Geomorphic response to climate change*, New York.
- Bull, W.B., 1991. *Geomorphic Responses to Climate Change*. Oxford University Press, New York, 326 pp.
- Bull, W.B., 1996. Global climate change and active tectonics: effective tools for teaching and research. *Geomorphology*, 16: 217-232.
- Chwatal, W., Decker, K., Roch, K.H., 2005. Mapping of active capable faults by high-resolution geophysical methods: examples from the central Vienna Basin. *Austrian Journal of Earth Sciences*, 97: 52-59.
- Clevis, Q., de Boer, P., Wachter M., 2003. Numerical modelling of drainage basin evolution and three-dimensional alluvial fan stratigraphy. *Sedimentary Geology*, 163: 85-110.
- Collins, P.E.F., Worsley, P., Keith-Lucas, D.M., Fenwick, I.M., 2006. Floodplain environmental change during the Younger Dryas and Holocene in Northwest Europe: Insights from the lower Kennet Valley, south central England. *Palaeogeography, Paleoclimatology, Palaeoecology*, 233: 113-133.
- Cowie, P.A., Attal, M., Tucker, G. E., Whittaker, A.C., Naylor, M., Gansas, A., Roberts, G. P., 2006. Investigating the surface process response to fault interaction and linkage using a numerical modelling approach. *Basin Research*, 18: 231-266.
- Culling, W., E., H., 1960. Analytical theory of erosion. *Journal of Geology*, 68: 336-344.
- De Chant, L.J., Pease, P.P., Tchakerian, V.P., 1999. Modelling alluvial fan morphology. *Earth Surface Processes and Landforms*, 24: 641-652.
- Decker, K., Peresson, H., 1996. Tertiary kinematics in the Alpine Carpathian-Pannonian system. links between thrusting, transform faulting and crustal extension, *Oil and Gas in Alpidic Thrustbelts and Basins of Central and Eastern Europe*. EAGE Special Publication, London, pp. 69-77.
- Decker, K., Peresson H., Hinsch R., 2005. Active tectonics and Quaternary basin formation along the Vienna Basin Transform fault. *Quaternary Science Reviews*, 24: 305-320.
- Demoulin, A., Campbell, J., De Wulf, A., Muls, A., Arnould, R., Görres, B., Fischer, D., Kötter, T., Brondeel, M., Van Damme, D., Jacqmotte, J., M., 2005. GPS monitoring of vertical ground motion in northern Ardenne-Eifel: five campaigns (1999-2003) of the HARD project. *International Journal of Earth Sciences (Geologische Rundschau)*, 94: 515-524.
- Döppes, D., Rabeder, G., 1997. *Pliozäne und pleistozäne Faunen Österreichs*. Austrian Academy of Sciences, Vienna.
- Edel, J.-B., Fluck, P., 1989. The upper Rhenish Shield basement (Vosges, Upper Rhinegraben and Schwarzwald): main structural features deduced from magnetic, gravimetric and geologic data. *Tectonophysics*, 169(303-316).
- Fink, J., Majdan, H., 1954. Zur Gliederung der pleistozänen Terrassen des Wiener Raumes. *Jb.Geol.B.A.*, 97(2): 211-249.
- Fink, J., 1955. Das Marchfeld. *Verh. Geol. B.-A., Spec. Vol. D*: 88-116.
- Fink, J., 1958. *Die Bodentypen Niederösterreichs*, Wien.
- Fink, J., 1966. *Die Paläogeographie der Donau*. Schweizerbart'sche Verlagsbuchhandlung, Stuttgart.
- Fink, J., 1973. Zur Morphogenese des Wiener Raumes. *Z. Geomorph. N.F., Suppl.*, 17: 91-117.
- Fink, J., 1977. Jüngste Schotterakkumulationen im österreichischen Donauabschnitt. *Erdwissenschaftliche Forschung*, 13: 190-211.
- Fink, J., Kukla, G., 1977. Pleistocene climates in central Europe. *Quaternary Research*, 7: 363-371.

- Fodor, L., 1995. From transpression to transtension. Oligocene-Miocene structural evolution in the Vienna Basin and the East Alpine-Western Carpathian junction. *Tectonophysics*, 242: 151-182.
- Frank, C., 1997. Stillfried - Typusprofile. In: D. Döppes, Rabeder G. (Editor), *Pliozäne und pleistozäne Faunen Österreichs*. Österreichische Akademie der Wissenschaften, Wien.
- Frank, C., Rabeder, G., 1997. Willendorf in der Wachau. In: D. Döppes, Rabeder G. (Editor), *Pliozäne und pleistozäne Faunen Österreichs*. Österreichische Akademie der Wissenschaften, Wien.
- Frank, C., 1997. Wienerberg. In: D. Döppes, Rabeder, G. (Editor), *Pliozäne und pleistozäne Faunen Österreichs*. Austrian Academy of Sciences, Vienna, pp. 148-150.
- Frank, C., Rabeder, G., 1997a. Laaerberg. In: D. Döppes, Rabeder, G. (Editor), *Pliozäne und pleistozäne Faunen Österreichs*. Austrian Academy of Sciences, Vienna, pp. 88-92.
- Frank, C., Rabeder, G., 1997b. Mannswörth. In: D. Döppes, Rabeder, G. (Editor), *Pliozäne und pleistozäne Faunen Österreichs*. Austrian Academy of Sciences, Vienna, pp. 102-105.
- Frank, C., Rabeder, G., 1997c. Fischamend an der Donau. In: D. Döppes, Rabeder, G. (Editor), *Pliozäne und pleistozäne Faunen Österreichs*. Austrian Academy of Sciences, Vienna, pp. 79-80.
- French, H.M., 2007. *The periglacial environment*. Wiley.
- Frostik, L.E., Reid, I., 1989. Climatic versus tectonic controls of fan sequences: lessons from the Dead Sea, Israel. *Journal of the Geological Society, London*, 146: 527-538.
- Fuchs, W., 1981. Geological mapping reports 1978, map Bruck an der Leitha. *Verh. Geol. B.-A., Spec. Vol. D*, 1979(1): A91-A95.
- Fuchs, W., Grill, R., 1984. Geological map of Vienna and its surroundings. In: J. Fuchs, Grill, R. (Editor). *Austrian Geological Survey, Vienna*.
- Fuchs, W., Herrmann, P., 1985. Geological map of Vienna. In: W. Fuchs (Editor). *Austrian Geological Survey, Vienna*.
- Gabris, G., Nagy, B., 2005. Climate and tectonically controlled river style changes on the Sajó-Hernád alluvial fan (Hungary). *Geological Society of London, Special Publication*, 251: 1-7.
- Gabris, G., Nador, A., 2007. Long-term fluvial archives in Hungary: response of the Danube and Tisza rivers to tectonic movements and climate changes during the Quaternary: a review and new synthesis. *Quaternary Science Reviews*, 26: 2758-2782.
- Gangl, G., 1993. Die geologischen Vorerkundungen und die Grundwasserverhältnisse beim Donaukraftwerk Freudenau: Teil I: Geologische Vorarbeiten für das Donaukraftwerk Freudenau am Stadtrand von Wien. *Mitteilungen des Institutes für Bodenforschung und Baugeologie, Abteilung Baugeologie: reihe Angewandte Geowissenschaften, Universität für Bodenkultur*, 3: 55-68.
- Granser, H., 1987. Three-dimensional interpretation of gravity data from sedimentary basins using an exponential density-depth function. *Geophysical Prospecting*, 35: 1030-1041.
- Granser, H., Meurers, B., Steinhauser, P., 2006. Apparent density mapping and 3D gravity inversion in the eastern Alps. *Geophysical Prospecting*, 37(3): 279-292.
- Grenerczy, G., Kenyeres, A., Fejes, I., 2000. Present crustal movement and strain distribution in Central Europe inferred from GPS measurements. *Journal of Geophysical Research*, 105: 333-358.
- Grenerczy, G., Kenyeres, A., Fejes, I., 2006. Crustal deformation between Adria and the European platform from space geodesy. In: N. Pinter, Grenerczy, G., Weber, J., Stein, S., Medak, D. (Editor), *The Adria Microplate: GPS Geodesy, Tectonics and Hazards*. Earth and Environmental Sciences, NATO Science Series IV, pp. 321-334.
- Grill, R., 1971. *Berichte über Begehungen auf den Blättern Wien und Preßburg der Österreichischen Karte 1:200.000; Mapping Reports regarding the geological maps of Vienna and Bratislava 1:200.000*, Vienna.
- Grill, R., 1973. *Berichte über Begehungen auf den Blättern Wien und Preßburg der Österreichischen Karte 1:200.000; Mapping Reports regarding the geological maps of Vienna and Bratislava 1:200.000*, Vienna.

- Harvey, A.M., 1987. Alluvial fan dissection: relationships between morphology and sedimentation. In: L. Frostick, Reid, I. (Editor), *Desert Sediments: Ancient and Modern*. Geological Society of London, Special Publication, pp. 87-103.
- Harvey, A.M., 1992. Control on sedimentary style on alluvial fans. In: P. Billi, Hey, R. D., Thorne, C.R., Tacconi, P. (Editor), *Dynamics of gravel bed rivers*, pp. 519-535.
- Harvey, A.M., 1996. The role of alluvial fans in the mountain fluvial systems of Southeast Spain: Implications of climatic change. *Earth Surface Processes and Landforms*, 21: 543-553.
- Harvey, A.M., Silva, P.G., Mather, A.E., Goy, J.L., Stokes, M., Zazo, C., 1999a. The impact of Quaternary sea-level and climatic change on coastal alluvial fans in the Cabo de Gata ranges, southeast Spain. *Geomorphology*, 28: 1-22.
- Harvey, A.M., 2002a. Effective timescales of coupling within fluvial systems. *Geomorphology*, 44: 175-201.
- Harvey, A.M., 2002b. The role of base-level change in the dissection of alluvial fans: case studies from southeast Spain and Nevada. *Geomorphology*, 45: 67-87.
- Harzhauser, M., Tempfer, P., M., 2004. Late Pannonian Wetland Ecology of the Vienna Basin based on the Molluscs and Lower Vertebrate Assemblages (Late Miocene, MN 9, Austria). *Cour. Forsch.-Inst. Senckenberg*, 246: 55-68.
- Harzhauser, M., Daxner-Höck, G., Piller, W.E., 2004. An integrated stratigraphy of the Pannonian (Late Miocene) in the Vienna Basin. *Austrian Journal of Earth Sciences*, 95/96: 6-19.
- Harzhauser, M., Daxner-Höck, G., Piller, W.E., 2004a. An integrated stratigraphy of the Pannonian (Late Miocene) in the Vienna Basin. *Austrian Journal of Earth Sciences*, 95/96: 6-19.
- Harzhauser, M., Tempfer, P., M., 2004b. Late Pannonian Wetland Ecology of the Vienna Basin based on the Molluscs and Lower Vertebrate Assemblages (Late Miocene, MN 9, Austria). *Cour. Forsch.-Inst. Senckenberg*, 246: 55-68.
- Havinga, A.J., 1972. A palynological investigation in the Pannonian climate region of Lower Austria. *Review of Palaeobotany and Palynology*, 14: 319-352.
- Havlicek, P., Holásek, O., Smoliková, L., Roetzel, R., 1998. Zur Entwicklung der Quartärsedimente am Südostrand der Böhmisches Masse in Niederösterreich. *Jb. Geol. B.-A.*, 41: 51-71.
- Hinsch, R., Decker, K., Wagreich, M., 2005. 3-D mapping of segmented active faults in the southern Vienna Basin. *Quaternary Science Reviews*, 24: 321-336.
- Högerl, N., 1980. Repeated Levelling and Vertical Crustal Movements. *Problems and Results. Rock Mechanics, Suppl.* 9: 201-212.
- Holbrook, J., Scott, R.W., Oboh-Ikuenobe, 2006. Base-level buffers and buttresses: A model for upstream versus downstream control on fluvial geometry and architecture within sequences. *Journal of Sedimentary Research*, 76: 162-174.
- Hrubes, M., 1994. New knowledge of the Pliocene and Quaternary sediments in the northern part of the upper Moravian Basin. *Zpravy o Geologických Vyzkumech v Roce*, 1993: 41-43.
- Hrubes, M., Ctyroka, J., 1999. Preliminary results of mapping on Olomouc map sheet. *Zpravy o Geologických Vyzkumech v Roce*, 1998: 20-22.
- Husz, G., 1965. Zur Kenntnis der quartären Sedimente des Seewinkelgebietes. *Wissenschaftliche Arbeiten aus dem Burgenland*, 32: 147-205.
- Joó, I., 1992. Recent vertical surface movements in the Carpathian Basin. *Tectonophysics*, 202: 129-134.
- Jung, K., 1961. *Schwerkraftverfahren in der angewandten Geophysik*. Akademische Verlagsgesellschaft, GeestandPortig, 348 pp.
- Klaus, W., 1962. Zur Pollenanalytischen Datierung von Quartärsedimenten im Stadtgebiet von Wien, südlichen Wr. Becken und Burgenland. *Verhandlungen Geologische Bundesanstalt*: 20-38.
- Knobloch, E., 1963. Pliocene plant assemblages of the Moravian part of the Vienna Basin. *Zpravy geol. vysk UUG, Praha, Prague*, pp. 271-772.
- Koukal, V., Wagreich, M., 2008. Das Rohrbacher Konglomerat (Rohrbach-Formation, Pliozän?) im südlichen Wiener Becken. *Journal of Alpine Geology*, 49: 56-57.

- Krieger, I.M., Dougherty, T., J., 1959. A mechanism of non-Newtonian flow in suspension of rigid spheres. *Transactions of the Society of Rheology*, 3: 137-152.
- Krzyszowski, D., 1990. Middle and Late Weichselian stratigraphy and palaeoenvironments in central Poland. *Boreas*, 19: 333-350.
- Krzyszowski, D., Stachura, R., 1998. Neotectonically controlled fluvial features, Walbrzych Upland, Middle Sudeten Mts, southwestern Poland. *Geomorphology*, 22: 73-91.
- Küpper, H., 1950. Zur Kenntnis des Alpenabbruchs am Westrand des Wiener Beckens. *Jb.Geol.B.A.*, 94.
- Küpper, H., Papp, A., Thenius, E., 1952. Über die stratigraphische Stellung des Rohrbacher Konglomerates. *Akademie der Wissenschaften, mathematisch naturwissenschaftliche Klasse*, 161: 441-453.
- Langbein, W.B., Schumm, S., A., 1958. Yield of sediment in relation to mean annual precipitation. *Am. Geophys. Union*: 1076-1084.
- Leeder, M.R., Harris, T., Kirkby, M.J., 1998. Sediment supply and climate change: implications for basin stratigraphy. *Basin Research*, 10(1): 7-18.
- Lefort, J.P., Agarwal, B.N.P., 1999. Gravity evidence for an alpine buckling of the crust beneath the Paris Basin. *Tectonophysics*, 258: 1-14.
- Lopes Cardozo, G.G.O., Edel, J.B., Granet, M., 2005. Detection of active crustal structures in the Upper Rhine Graben using local earthquake tomography, gravimetry and reflection seismics. *Quaternary Science Reviews*, 24: 339-346.
- Mahel, M., 1972. Geological map of the Little Carpathians. *Geologický Ústav Dionýza Štúra*, Bratislava.
- Miall, A.D., 1977. A review of the braided river depositional environment. *Earth Science Review*, 13: 1-62.
- Militzer, H., Weber, F., 1984. *Angewandte Geophysik*, Bd. 1: Gravimetrie und Magnetik. Springer, 353 pp.
- Mol, J., 1997b. Fluvial response to Weichselian climate changes in the Niederlausitz (Germany). *Journal of Quaternary Science*, 12: 43-60.
- Mol, J., Vandenbergh, J., Kasse, C., 2000. River response to variations of periglacial climate in mid-latitude Europe. *Geomorphology*, 33: 131-148.
- Nemec, W., Postma, G., 1993. Quaternary alluvial fans in southwestern Crete; sedimentation processes and geomorphic evolution. In: M. Marzo, Puigdefabregas C. (Editor), *Alluvial Sedimentation. Spec. Publ., Int. Ass. Sedimentol.*, pp. 235-276.
- Neugebauer-Maresch, C., Peticzka, R., Frank, C., Urban, B., 2008. *Krems-Hundssteig - Mammutjäger der Eiszeit. Mitteilungen der Prähistorischen Kommission 67.* Österreichische Akademie der Wissenschaften, Wien.
- Niedermayr, G., Seemann, R., 1974. Vorläufiger Bericht über sedimentpetrographische und mineralogische Untersuchungen an Höhlensedimenten des Pfaffenberges bei Deutsch-Altenburg (NÖ.). *Die Höhle*, 25(1): 3-11.
- Oldfield, F., 2005. *Environmental change*.
- Penck, A., Brückner, E., 1909. *Die Alpen im Eiszeitalter*, 1-3, Leipzig, 1199 pp.
- Peresson, H., Decker, K., 1997. Far-field effects of Late Miocene subduction in the Eastern Carpathians: E-W compression and inversion of structures in the Alpine-Carpathian-Pannonian region. *Tectonics*, 16(1): 38-56.
- Piffil, L., 1971. Zur Gliederung des Tullner Feldes. *Annals Museum of Natural History*, 75: 292-310.
- Plan, L., Pavuza, R., Seemann, R., 2006. Der Nasse Schacht bei Mannersdorf am Leithagebirge, NÖ (2911/21) - eine thermal beeinflusste Höhle am Ostrand des Wiener Beckens. *Die Höhle*, 57(1-4).
- Prohaska, W., 1983. Die geologischen und hydrogeologischen Verhältnisse am Westrand des südlichen Wiener Beckens, University of Vienna, Wien, 161 pp.
- Rabeder, G., 1997. Deutsch-Altenburg 1. In: D. Döppes, Rabeder, G. (Editor), *Pliozäne und pleistozäne Faunen Österreichs. Austrian Academy of Sciences, Vienna*, pp. 241-274.

- Ratschbacher, L., Merle, O., Davy, P., Cobbold, P., 1991a. Lateral extrusion in the eastern Alps, part I: boundary conditions and experiments scaled for gravity. *Tectonics*, 10(2): 245-256.
- Ratschbacher, L., Frisch, W., Linzer, H.-G., 1991b. Lateral extrusion in the eastern Alps, part II: structural analysis. *Tectonics*, 10(2): 257-271.
- Raymo, M.E., 1997. The Timing of Major Climatic Terminations. *Paleocenography*, 12(4): 577-585.
- Reinecker, J., Lenhardt, W., 1999. Present-day stress field and deformation in eastern Austria. *International Journal of Earth Sciences*, 88: 532-550.
- Reitinger, J., et al., 1973. Mensch und Wasserwirtschaft im südlichen Wiener Becken. *Österr. Wasserwirtschaft*, 25 (1/2): 15-22.
- Reynisson, R.F., Ebbing, J., Skilbrei, J.R., 2007. Magnetic and gravity field in an intergrated approach to the sub-basalt imaging problem.
- Ritter, J.B., Miller J.R., Enzel, Y., Wells, S.G., 1995. Reconciling the roles of tectonism and climate in Quaternary alluvial fan evolution. *Geology*, 23: 245-248.
- Roberts, N., 1995. Climatic forcing of alluvial fan regimes during the Late Quaternary in Konja basin, south central Turkey. In: J. Lewin, Macklin, M.G., Woodward, J. (Editor), *Mediterranean Quaternary River Environments*. Balkema, Rotterdam, pp. 205-217.
- Rotstein, Y., Edel, J.-B., Gabriel, G., Boulanger, D., Schaming, M., Munsch, M., 2006. Insight into the structure of the Upper Rhine Graben and its basement from a new compilation of Bouguer Gravity. *Tectonophysics*, 425: 55-70.
- Rousset, D., Bayer, R., Guillon, D., Edel, J.-B., 1993. Structure of the southern Rhine Graben from gravity and reflection seismic data. *Tectonophysics*, 221: 135-153.
- Royden, L.H., 1985. The Vienna Basin: A thin -skinned pull-apart basin. In: K.T. Biddle, Christie-Blick, N., (Editor), *Strike slip deformation, basin formation and sedimentation*.
- Ruszkiczay-Rüdiger, Z., Fodor L., Bada, G., Leél-Össy, Sz., Horváth, E., Dunai, T.J., 2005. Quantification of Quaternary vertical movements in the central Pannonian Basin: A review of chronologic data along the Danube River, Hungary. *Tectonophysics*, 410: 157-172.
- Salcher, B., Faber, R., Wagneich, M, 2008. Numerical modeling of factors controlling sequence development of Pleistocene alluvial fans, Vienna Basin, eastern Austria. *Geomorphology* (in review).
- Salcher, B., 2008. Sedimentology and modelling of the Mitterndorf Basin, PhD thesis. University of Vienna, Vienna, 178 pp.
- Salcher, B.a.W., M., 2008. Climate and tectonic controls on sequence development and river evolution in Austria's largest Pleistocene basin. *Quaternary International* (in review).
- Salcher, B.C., Meurers, B., Decker, K., Wagneich., M, 2008. Detection of Pleistocene structures in the southern and central Vienna Basin using first order gravity derivatives, reflection seismic and well data. submitted for publication.
- Sauer, R., Seifert, P., Wessely, G., 1992. Guidebook to excursion in the Vienna Basin and the adjacent Alpine-Carpathian thrustbelt in Austria. *Mitteilungen der Österreichischen Geologischen Gesellschaft*, 85: 1-264.
- Schaller, M., von Blanckenburg, F., Hovius, N., Kubik, P.W., 2001. Large scale erosion rates from in situ produced cosmogenic nuclides in European river sediments. *Earth and Planetary Science Letters*, 188(3-4): 441-458.
- Schenkóvá, Z., Schenk, V., Pospisil, L., Kottbauer, P., 1995. Seismogeological pattern of a transition area between the Eastern Alps and Western Carpathians. *Tectonophysics*, 248: 235-245.
- Schumm, S.A., 1977. *The fluvial system*. Wiley, New York, 338 pp.
- Schumm, S.S., Holbrook, J., 1999. Geomorphic and sedimentary response of tectonic deformation: a brief review and critique of a tool for recognizing subtle epeirogenic deformation in modern and ancient settings. *Tectonophysics*, 305: 287-306.
- Shanley, K.W., Mc Cabe, P.J., 1994. Perspectives on the sequence stratigraphy of continental strata. *American Association of Petroleum Geologists, Bulletin*, 78: 544-568.
- Shanley, K.W., Mc Cabe, P.J., 1998. Relative Role of Eustasy, Climate, and Tectonism in Continental Rocks. *SEPM, Special Publication*, 59, 234 pp.

- Shepard, D., 1968. A two-dimensional interpolation function for irregularly-spaced data. *Proceedings of the 1968 ACM National Conference*: 517-524.
- Siegenthaler C., H., P., 1993. Pleistocene Rhine gravel: deposits of a braided river system with dominant pool preservation. In: J.L. Best, Bristow., C.S. (Editor), *Braided Rivers*. Geological Society Special Publication, London.
- Silva, P.G., Harvey, A.M., Zazo, C., Goy, J.L., 1992. Geomorphology, depositional style and morphometric relationship of Quaternary alluvial fans in the Guadalentin depression (Murcia, southeast Spain). *Zeitschrift fuer Geomorphologie*, 36: 325-341.
- Slingerland, R.S., Harbaugh, J.W., Furlong, K.P., 1994. *Simulating clastic sedimentary basin*. Prentice-Hall, Englewood Cliffs, NJ, 220 pp.
- Starkel, L., 1995a. Evolution of the Carpathian valleys and the Forecarpathian Basins in the Vistulian and Holocene. *Studia Geomorphologica Carpatho-Balcania*, 29: 5-40.
- Starkel, L., 2003. Climatically controlled terraces in uplifting mountain areas. *Quaternary Science Reviews*, 22: 2189-2198.
- Stock, J.D., Montgomery, D.R., 1999. Geologic constraints on bedrock river incision using the streampower law. *Journal of Geophysical Research*, 104: 4983-4993.
- Strauss, P., Harzhauser, M., Hinsch, R., Wagreich, M., 2006. Sequence Stratigraphy in a classic pull apart basin (Neogene, Vienna Basin). A 3D seismic based integrated approach. *Geologica Carpathica*, 57(3): 185-197.
- Survey, A.G., 1984. *Geologische Karte von Wien und Umgebung*, Geological map of Vienna and surroundings, Wien.
- Survey, A.G., 1985. 59 Wien. In: W. Fuchs (Editor), Wien.
- Survey, A.G., 1985. 60 Bruck an der Leitha. In: W. Fuchs (Editor), Wien.
- Szabo, P., 1959. Angaben zur Entwicklung des Flussnetzes im Wiener Becken und auf ungarischem Gebiet während des Quartäres, aufgrund von Schwermineralien, University of Vienna, Wien.
- Szádeczky-Kardoss, E., 1937. Über die Entwicklungsgeschichte des Leithaflusses. *International Review of the Hungarian Geographical Society*, 65: 50-54.
- Szafián, P., Horváth, F., 2006. Crustal structure in the Carpatho-Pannonian region: insights from three-dimensional gravity modelling and their geodynamic significance. *International Journal of Earth Sciences*, 95: 50-67.
- Timár G., S., P., Horváth F., 2005. Late Quaternary dynamics of the Tisza River: Evidence of climatic and tectonic controls. *Tectonophysics*, 410: 97-110.
- Tollmann, A., 1985. *Geologie von Österreich*, 2. Deuticke, Vienna, 710 pp.
- Tucker, G., Slingerland, R., L., 1994. Erosional dynamics, flexural isostasy, and long-lived escarpments: A numerical modeling study. *Journal of Geophysical Research*, 99(B6): 12229-12243.
- Van Husen, D., 1987. *Die Ostalpen in den Eiszeiten*. Geologische Bundesanstalt, Geological Survey of Austria, Vienna.
- Van Husen, D., 2000. Geological Processes during the Quaternary. *Mitt. Österr. Geol. Ges*, 92: 135-156.
- Vandenbergh, J., 2001. A typology of cold-based rivers. *Quaternary International*, 79: 111-121.
- Vandenbergh, J., 2002. The relation between climate and river processes, landforms and deposits during the Quaternary. *Quaternary International*, 91: 17-23.
- Vandenbergh, J., 2003. Climate forcing of fluvial system development: an evolution of ideas. *Quaternary Science Reviews*, 22: 2053-2060.
- Vandenbergh, J., 2008. The fluvial cycle at cold-warm-cold transitions in lowland regions: A refinement of theory. *Geomorphology*, 98(3-4): 275-284.
- Viall, P.R., Mitchum, R.M., Todd, R.G., Widmier, J.M., Thompson, S., Sangree, J.B., Bubb, J.N., Hatlelid, W.G., 1977. *Seismic Stratigraphy-Applications to Hydrocarbon Exploration*. American Association of Petroleum Geologists, Memoir, 26(47-212).
- Viseras, C., Calvache, M.L., Soria, J.M., Fernández, J., 2003. Differential features of alluvial fans controlled by tectonic or eustatic accommodation space. Examples from the Betic Cordillera, Spain. *Geomorphology*, 50: 181-202.
- Walker, M., 2006. *Quaternary dating methods*. Wiley, 286 pp.
- WASY, 1997. *Grundwassermodellierung Mitterndorfer Senke*, Gov. Lower Austria.

- Weissmann, G.S., Mount, J.F., Fogg G.E, 2002. Glacially driven cycles in accumulation space and sequence stratigraphy of a stream-dominated alluvial fan, San Joaquin Valley, California, U.S.A. *Journal of Sedimentary Research*, 72(2): 240-251.
- Weissmann, G.S., Bennett, Lansdale, A.L., 2005. Factors controlling sequence development on Quaternary fluvial fans, San Joaquin Basin, California, USA. *London Spec. Pub.*, 251: 169-186.
- Wells, S.G., Harvey, A.M., 1987. Sedimentologic and geomorphic variations in stream generated alluvial fans, Howgill Fells, northwest England. *Geological Society of America, Bulletin*, 98: 182-198.
- Wessely, G., 1988. Structure and development of the Vienna Basin in Austria. In: L.H. Royden, Horváth, F. (Editor), *Memoir 45. American Association of Petroleum Geologists*, pp. 333-346.
- Willgoose, G., Bras, R.L., Rodriguez-Irtube, I., 1991. Results from a model river basin evolution. *Earth Surface Processes and Landforms*, 16: 237-254.
- Willis, K., J., Rudner, E., Sümegi, P., 2000. The full-glacial forests of central and southeastern Europe. *Quaternary Research*, 53: 203-213.
- Zámolyi, A., Székely, B., Draganits, E., Timár, G., 2008. Neotectonic control on river sinuosity at the western margin of the Little Hungarian Plain. *Geomorphology*, in press.
- Zeng, H., 1988. Estimation of the degree of polynomial fitted to gravity anomalies and its application. *Geophysical Prospecting*, 37(8): 959-973.
- Zentralanstalt für Meteorologie und Geodynamik, Z., 2008. *Catalogue of earthquakes in Austria 1201-2008*, Vienna (ZAMG).
- Zych, D., Meurers, B., Steinhauser, P., 1993. Gravity map of the Vienna Basin and adjacent areas. *Austrian Geological Survey, Vienna (Geologische Bundesanstalt)*.

Climate and tectonic controls on sequence development and river evolution in Austria's largest Pleistocene basin

Abstract

Controls of climatic and tectonic relevant factors on the deposition of lithofacies is demonstrated from Austria's largest Pleistocene sedimentary basin. The coarse grained, massive facies is associated with high-energetic flood events reflecting a distinct nival regime during glacial times. In contrast, fine grained, well stratified sediments mark periods of rather high discharge to sediment supply ratios during warmer periods. Sequence preservation was provided by subsidence rates of approx. 0.5 - 1 mm/a. High subsidence rates preserve a relatively large record of sequences compared to fluvial terraces which reflect mainly sediments deposited during and shortly after glacials. ¹⁴C and relative ages demonstrate the strong impact of oscillations in climate on fluvial stratigraphy covering times from the upper period of MIS 3 to the MIS 1.

Abundant sediment supply and the associated increase in accumulation space (Blum and Törnqvist, 2000) as well as tectonic factors affect not only the sequence development but also the geomorphology of two mountain front alluvial fans which toe out into the Mitterndorf Basin. High discharge to sediment supply ratios lead to fan incision and to abandonment of fan surfaces. During phases of reduced sediment supply the effect of subsidence results in headcut erosion, and, if sufficient time is available, may lead to total through trenching. Abandoned fan surfaces are exposed to widespread soil formation which mark sequence boundaries to the following coarse grained, massive facies reflecting high sediment supply to discharge ratios.

1. Introduction

The main controlling factors on erosion and deposition of alluvial-fluvial sediments are supposed to be changes in precipitation behaviour, the vertical shift of vegetation zones and related influence on weathering (e.g. Leeder et al., 1998; Bull, 1996; Bull, 1991;). Long term preservation of alluvial sequences is generally associated with tectonic forcing (Starkel, 2003; Blum and Törnqvist, 2000) preventing possible incision and removal either through uplift or subsidence. Relation between climate and terrace formation has been recognized since a long time (e.g. Penck and Brückner, 1909). Climatically controlled terrace sediments are well developed in uplifted mountainous areas of central Europe (e.g. Starkel, 2003; Krzyszkowski and Stachura, 1998; Mol et al., 2000; Amorosi et al., 1996; Fink, 1966; Penck and Brückner, 1909). Terraces have a typically rather coarse grained nature representing high energy (braided) conditions related to glacials (e.g. Van Husen, 2000; Vandenberghe, 2002). Lithofacies of Interglacial or Interstadial periods are generally known to be finer-grained and less massive, representing higher discharge to sediment supply ratios, i.e. dominantly overbank fines. River patterns rather tend to be meandering. Deposits of warm periods are generally lower in thicknesses and are more prone to erosion. A switch to braided conditions and associated lateral stream erosion may cause removal of most traces of previous (meandering) systems (Vandenberghe, 2008) if uplift rates are not sufficient to prevent erosion. As a consequence most terraces lack significant fluvial deposits associated with warm periods. Quaternary uplift rates in the range of 50 - 100 m for central Europe (Starkel, 2003) are relatively low compared to subsidence rates often exceeding 1 mm/a, determined for some central European Quaternary Basins (e.g. Rheingraben, Pannonian Basin, Mitterndorf Basin, Lasse Basin) by precise levelling (Decker et al., 2005; Demoulin et al., 2005; Ruszkiczay-Rüdiger et al., 2005; Joó, 1992;). As subsidence rates directly control the chance of sequence preservation (Blum and Törnqvist, 2000), relatively high rates are supposed to preserve a more complete record of sequences within such basins as compared to fluvial terraces.

Application of sequence stratigraphic concepts in purely fluvial settings are limited (e.g. Weissmann et al., 2002; Blum and Price, 1998; Amorosi et al., 1996; Aitken and Flint, 1995). The significant impact of Quaternary glacial-interglacial cycles on alluvial

sequence development in a basin-scale has been described by Shanley and McCabe (1994) and Weissmann et al. (2005).

In this study we present a climate and subsidence controlled depositional model for fluvial lithofacies in a Quaternary pull-apart basin of Eastern Austria. In our model, sediment supply and stream discharge control the characteristics of lithofacies and sedimentary structures in short term way. Subsidence is supposed to act as a long term effect. Base level factors are found to play no relevant role. The presented model is mainly based on ^{14}C ages and biotic climate signals (pollen and terrestrial snails) covering oxygen isotope stage 3 to 1 (Middle Pleniglacial to Holocene). Fluvial facies are shown to be deposited in stratigraphic cycles controlled by the impacts of Glacials and Interglacials.

2. Regional setting and study area

Several Quaternary basins formed during the youngest kinematic history of the Miocene Vienna Basin. These basins are linked to releasing bends along the active sinistral strike-slip Vienna Basin Transfer fault (Mitterndorf Basin, Lasse Basin, e.g. Hinsch et al., 2005) and to normal faults, which splay off from this fault system which extend to the West Carpathians. Active faulting is indicated by earthquake data (Reinecker and Lenhardt, 1999), geodetic data (Grenerczy et al, 2006; Grenerczy et al 2002; Höggerl, 1980) and growth faults. The largest of these Quaternary sub-basins is the Mitterndorf Basin (Fig. 2) with an area of approximately 270 km². The Mitterndorf Basin is a tight, elongated strike slip pull-apart basin with a width of not more than 9 km and a length of approximately 50 km. Pleistocene sequences of the Mitterndorf Basin reach thicknesses of more than 170 m in the areas of highest subsidence rates in the north. In the southern part, two mountain front alluvial fans toe out into the basin. The northern, smaller Piesting River alluvial fan (Piesting fan) and the southern distally confined Schwarza River alluvial fan (Schwarza fan) cover approximately two third of the basin. Both fans are inactive. Adjacent to the fans, in the western and northern basin parts, alluvial rivers provide sediments to the basin's floodplain covering approximately one third of the basin. The underlying strata of the Mitterndorf Basin mostly consist of lower to upper Pannonian (Middle Miocene) strata which generally comprise fine-grained lacustrine (fine sands, clays and marls) and deltaic sediments (alternating sands, gravels or thin layers of lignite). Pliocene fluvial conglomerates (Rohrbacher Konglomerat; Koukal and Wagreich, 2008; Küpper, 1952) are present below the southernmost Mitterndorf basin.

2.1. Drainage areas and present climate

The Piesting River alluvial fan, at the western margin of the basin sizes about 75 km², the adjacent Schwarza River alluvial fan sizes about 120 km². The Schwarza fan is confined filling the southern part of Mitterndorf Basin. Drainage basin of Piesting fan covers approx. 280 km², with highest elevation of 1723 m above sea level and an elevation of the fan apex of 310 m above sea level. Mean fan gradient is $\sim 0.45^\circ$. Average drainage height is (~ 688 m). The drainage basin of the Schwarza fan covers about 660 km², with highest elevation of 2076 m above sea level and a fan apex of about 370 m above sea level. Mean gradient is $\sim 0.35^\circ$. Average drainage height is (~ 905 m). Weak glaciation and permanent snow cover (~ 80 km²) of highest elevations during the Pleniglacial is evident in the Schwarza drainage basin (Van Husen, 1987; Fig. 9). Modern climate in the basin is affected by continental, Pannonian climate with warm and rather dry summers and cold winters. Mean annual temperature range around 9° C, mean annual precipitation totals less than 700 mm. Rainfall occurs mainly during spring and autumn. Precipitation of the Alpine hinterland clearly differs with values of more than 1800 mm at highest elevations (hydrologic survey of lower Austria, 2007).

3. Methodology and data availability

Information on basin stratigraphy was gained out of more than 2000 drillings, more than 20 outcrops, mainly gravel pits, and several drilling cores. Additional work was done for field mapping. Wells were mostly drilled for groundwater prospection and hydrocarbon exploration (digital well data base HADES, by courtesy of the Government of Lower Austria). This dataset was completed by digitising further analogue paper logs of the drilling archive at the Austrian Geological Survey. The sediment in the cores was assessed for grain size and clay mineralogy. ^{14}C ages derive from charcoals (6 samples), or, if carbonaceous plant material was not sufficient, from terrestrial mollusc shells (4 samples, Tab. 1). Organic material was almost exclusively found in fine grained overbank deposits which may appear slightly pedogenic altered.

Topographic information on drainage area was derived from digital elevation models in 10 m resolution. Information on river plan forms and palaeo-meanders derive from coloured orthofotos, infrared orthofotos and non orthogonal aerial images. Topographic and aerial data was provided by courtesy of the Government of Lower Austria and the Department for Prehistory and Medieval Archaeology of the University of Vienna.

4. Facies assemblages (Fig. 3)

4.1. Debris flow facies assemblages

The debris flow assemblage is limited to some sequences at a several hundred meter broad zone along the western Alpine front. This facies consists of massive, matrix supported gravels and cobbles with no or very few internal structures (Fig. 3a). The matrix consists of sand with a low, varying amount of silt and clay. Matrix content is generally high. Gravels display different degrees of carbonatic cementation. In drillers lithologic logs this facies is described as sandy gravels to cobbles which may be interrupted by conglomeratic layers of gravels to cobbles. High content of matrix, large clasts and the complete absence of sedimentary structures demonstrate deposition under high energy mass flow conditions. Gravitationally driven debris flows are the consequence of slope failures along the Alpine front, triggered by heavy rainfalls and/or snowmelt. Slope failure is supposed to be facilitated by low vegetation coverage during cold periods

4.2. Sheetflood facies assemblages

The sheetflood facies assemblages consist of (loamy) clayey to sandy, medium gravels to cobbles which are massive or crudely bedded (Blair and Pherson, 1994; Miall, 1977). Units may sporadically contain dm thick clusters of open framework gravels or thin lenses of stratified sands. Sediment is often slightly cemented but does also rarely appear as several meters thick conglomerate. The tops of individual beds may be covered with thin (some cm), lateral extensive silts and sands (up to several tens of meters). Depositional process is interpreted mainly as suspended grain fall at the end of high-magnitude flood events. The southern Schwarza fan contains generally some coarser grained clasts due to higher energy conditions (larger drainage area, glaciated hinterland). The gravel and cobble components are dominated by carbonates (dolomites and lime stones) which are typical of the Northern Calcareous Alps hinterland. In contrast to the Piesting fan, the Schwarza fan contains a significant amount of metamorphic clasts (quartzites, granitic gneisses, marbles) which derive from metamorphic and basement units to the south (Austrian Geological Survey, 1984). Due to this difference in source rocks, both fans can be clearly differentiated by their clast lithologies and heavy mineral assemblages. In driller's lithologic logs the sheetflood facies assemblage is recognized as fine- to coarse-grained gravels or cobbles with different degrees of sand and loam. Logs show occasional conglomeration of gravel and cobble units, especially at basal layers of the Mitterndorf Basin. Sheetflood deposits are laterally extensive and most common in the Piesting and Schwarza River alluvial fan strata. In the mid to the upper drill-sections sheetflood facies

is recognized to become very thick. Growth strata due to (asymmetric) subsidence cause increasing thicknesses towards the basin centre to more than 30 m. Sequences are interrupted by dm to m thick soils or often pedogenic altered overbank deposits. Thicknesses of soils and overbanks increase at deeper basin sections. Thickness of the sheetflood facies assemblage decreases (Fig. 4). Frost induced deformations like cryoturbations may be well developed (Fig. 7b; cryoturbations correspond to periglacial involutions; cf. French, 2007). Today, both alluvial fans of the Mitterndorf basin are inactive and dissected by their feeder streams (Piesting respectively Schwarza River).

4.3. Channel facies assemblages

The channel facies assemblage consists of generally stratified sandy, fine gravels to cobbles. Boulders may occur occasionally. Cobble and gravel units are clast supported. Alternating cross strata with open frame work gravel, sandy gravel and sand is common, where sediment often show an upward fining tendency. Open-framework gravels may also occur as several dm long and several cm thick bedload sheets or as a basal lag overlying an erosional contact. The largest clasts such as cobbles and boulders are concentrated in planar strata and are commonly imbricated. The channel facies assemblage is distributed on the present floodplain of the Mitterndorf Basin (Fig. 2). Alluvial rivers (Leitha and Piesting River, Fischa Creek) are meandering mixed load dominated. Well developed sedimentary structures are typical. Some dm thick fine grained successions may also be distributed on the fan surface, demonstrating brief episodes of flooding at the onset of stream incision. Several m thick sequences relating to incised-valley fills do rarely occur within the sheetflood facies of the alluvial fans. Channel fillings are commonly lateral not extensive deposits of stratified fluvial sediments within the sheetflood assemblage.

Distinct, frost induced deformations like cryoturbations are not developed within the youngest channel facies assemblage, indicating warmer conditions during and after deposition. The often coarse-grained nature, upward fining tendencies, presence of a basal lag and erosive contacts support deposition under a relatively high energetic level. Overbank deposits are common within this facies assemblage. In the subsurface individual units of this facies cannot be correlated between wells because lithologic well log reports are not always detailed enough to differentiate this facies assemblage from the sheetflood facies assemblage.

4.4. Overbank facies assemblage

The overbank facies assemblage consists of tabular, commonly laterally extensive sheets of sand and silt. They show little variation in mean grain size or internal structure. Overbank fines appear massive or, rarely, laminated. Sheets are often interrupted by some dm thick layers of fluvial gravels or cobbles. Fluvial gravels and cobbles are sometimes conglomerated. Individual strata packages of overbank fines can reach thicknesses of almost 2 m but are commonly few dm thick. Top banks often show light pedogenic alteration. The top strata of the overbank facies assemblage may sometimes show evidences of frost influence such as ice wedge casts or cryoturbations.

Overbank deposits are rich in terrestrial molluscs and dispersed, columnar, few mm long pieces of carbonificated plant remnants. Terrestrial mollusc fauna assemblages commonly indicate rather warm and humid climate (C. Frank pers. com.). In driller's lithologic logs, the overbank facies assemblage is recognized as yellow-brown to brown mostly sandy and/ or gravely loam. Thicknesses of the overbank facies assemblage have a general tendency to increase with decreasing distance to the basin's centre. Similar, the colour of overbanks has a tendency to get more yellowish-brown towards the basin centre and gets more reddish towards the Basin margins (Küpper, 1950).

In the stratigraphically older part, closer to the basement of the Mitterndorf Basin fill, the number and thicknesses of individual overbank facies packages increase in the profiles. The frequency and degree in conglomeration of gravels and cobble layers generally

increases clearly within the deepest sections of the Mitterndorf Basin. Pedogenic alteration is more intense close to the basement.

In the northern part of the floodplain overbank facies assemblage is generally recognized to become sandier, less loamy and lighter in colour indicating less pedogenic alteration. Furthermore, the overbank deposits are less extensive but are more frequent and have a tendency to become lower in thicknesses ranging from only some cm to few dm. Nevertheless, thicknesses of up to several meters are rare but may be recognized in some drilling sections. A general tendency of an increase in number and thickness of overbank facies assemblages at the deepest parts of the basin is equally to the southern part with the difference that the pedogenic alteration is much lower.

In the uppermost (Holocene) floodplain successions, overbank deposits are generally very frequent. Peat bog formation (Havinga, 1972; Klaus, 1962) is enforced through the relative impermeability of the overbank fines. Distribution of peat bogs and wetlands do coincide over large parts with the main depocenter of the Mitterndorf Basin which is interpreted as sag pond (Hinsch et al. 2005; Decker et. al 2005).

4.5. Paleosol Facies assemblage

Moderately to strong pedogenic altered sediments contrast through their darker colours and their higher clay content from other sediments. This alteration is recognizable in the increase of reddish to brownish colours, depending on the alteration degree, accompanied by the concentration of the iron-ion content. Alteration may also be accompanied by biogenic activity and the presence of root traces.

Paleosols are evident and frequently recognized in drillers log in the alluvial fan and southern floodplain strata as commonly up to some dm, brown to grey-brown sandy loams. Drilling cores show that these brown to red brown loams lie on coarse grained, sheetflood sediments of the fans. Strong pedogenic altered sediments are concentrated in the lowermost sections of the Mitterndorf Basin (up to ~ 15 m above the basin floor) which formed on overbanks or channel sediments. However, distinct soil sequences were not identifiable, possibly because of erosion of upper horizons. They are laterally very extensive in the Piesting River alluvial fan and southern floodplain strata and are more common than in the Schwarza River fan succession. This might reflect a generally stronger erosion potential of higher energetic conditions at the Schwarza fan. Some lower subsidence in the southernmost parts of the basin and associated lower preservation space might also cause stronger erosion. If preserved, thicknesses are generally increasing towards the central parts the Mitterndorf Basin from few dm to up to 1.5 m.

The increase in pedogenic alteration in the lowermost sections of the Mitterndorf Basin is primarily accompanied by a stronger coloration (dark brown to dark red brown, Hue 5YR 4/4 – 5YR 3/2, USGS rock colour chart) which is associated with a higher content of clay minerals. These relatively mature paleosols, close to the basement must have had at least several 10.000 years to develop (F. Ottner pers. com.). Such formation times do exceed the duration of interstadials considerably. Consequently, we these paleosols must have been formed during an interglacial.

5. Absolute ages:

Age assignments for the fill of the Mitterndorf Basin vary considerably and, so far, were only based on biostratigraphy and/or lithofacies correlations. During our study, absolute ages were for the first time derived for some outcrops, mainly from samples of the overbank facies assemblage in the upper part of the basin fill (Tab. 1).

5.1. Outcrop 1 (Fig. 5)

3 ages derive from the uppermost overbank facies assemblage of the distal Schwarza River alluvial fan in a distal fan area. The top of the highest overbank set (~ 1.5 - 2 m) is pedogenic altered, indicating the presence of backwater (hydromorphic soil) and biogenic activity (worm traces). On its top, frost influences (cryoturbations and frost influenced

soil morphology patterns, Fig. 5b) are well recognizable. Deeper sets may also be affected by (weak) pedogenic alteration but do not show frost influence. The topmost overbank set is situated under a thick sequence of massive gravels (sheetflood facies) approx. 11-12 m below the surface (Fig. 5a). Two ages from 30 – 50 cm below give ages of 40460 ± 650 and 47766 ± 1400 a BP, respectively (dispersed charcoal, samples S1 and S2). Approx. 5 m below, a further age was gained from charcoal of a ~ 1.5 m thick overbank set (45672 ± 1000 a BP, sample S3, Fig. 5c). A further age of a carbonificated root from the same overbank set gave an age of > 46000 a BP (S4). The root was in situ, emanating from coniferous wood (no resin channels; O. Cichocki pers. com.) The overbank sequence is laterally extensive and exposed in large parts of the outcrop which sizes ~ 0.5 km². A continuation of this overbank sequence below the city of Wr Neustadt is indicated by drillings and by outcrop data (Klaus, 1962; Grill, 1971; Grill 1973).

5.2. Outcrop 2 (Fig. 6)

In outcrop 2, 2 ages were derived from silty to sandy laminated overbank fines which underlie an approximately 2-3 m thick sequence of massive gravels with a weak unconformity. The ~ 2 m thick overbank fines are in turn underlain by a several meters thick sequence of stratified gravels. A fine, weak horizontal layering within the overbanks is recognizable. Some weak influence of a former active layer may affect the uppermost sediments. Overbanks are rarely interrupted by thin layers of sandy fine gravels. The grain size distribution is very homogenous with the sequence. Remnants of coalified (carbonaceous) plant material in overbank deposits were insufficient for ¹⁴C dating. Ages derive from terrestrial snail shell fragments, even though incorporation of older carbonates may lead to anomalously old ages or in case of pedogenic alteration to anomalously young ages (Walker, 2006). Contemporary snails of the same species to correct ages were not available. Results give therefore only imprecise age information. Overbanks are grey to yellowish and are not or only very light pedogenic altered. Ages from this sequence derive from ~ 20 cm (43326 ± 1000 ; S5) and ~ 100 cm (35884 ± 600 , S6) below the top of the overbank deposits. Those ages are similar to the ages reported before suggesting deposition during MIS3. However, data from snail carbonate has to be treated with caution and point to a certain kind of failure as ¹⁴C ages from outcrop 2 appear younger in stratigraphically lower parts.

5.3. Outcrop 3 (Fig. 7)

Outcrop 3 is dominated by the channel facies assemblage. Aggradation was provided by the Piesting River. At least 4 aggradational events are marked by clear unconformities. One charcoal sample (sample S7) has been taken from a ~ 30 cm thick layer of dark brown, clayey, pedogenic altered sediment, ~ 1.7 m below the surface and ca. 70 cm below an 1 m thick silty to sandy overbank deposit. The few cm thick layer is laterally not extensive and embedded in stratified fluvial gravels. The up to 1 m thick overbank cover is laterally extensive and can be found in several nearby outcrops. Overbanks are sometimes eroded, topped by up to 1 m of well stratified fluvial gravels, or cut by small, several meters wide channels. Channel fillings are also well stratified and may show resedimented remnants of overbank fines (Fig. 7a).

The whole succession of stratified fluvial gravels and overbank fines is interpreted as crevasse splay of the nearby Piesting River. The extension of the splay deposits is visible in aerial images as fine network of small tributary channels.

A second sample (S8, dispersed snail shells) has been taken from a sand lens in yellow coloured gravels (sample S8) near the base of the outcrop, 4.5 m below the surface. This sediment is strongly affected by cryoturbation processes as the overlying light brown and the underlying red to dark brown gravel. This brown gravel has high matrix content with inclusions of dark brown paleosols and light overbank fines. Sample S7 has an age of 8999 ± 65 a BP (calibrated), sample S8 40785 ± 1000 a BP. An Early Holocene age of sample S7 is also clearly indicated by terrestrial snail assemblages (C. Frank pers. com.).

5.4. Outcrops 4 and 5

Samples from outcrops 4 and 5 were too old for ^{14}C dating. Both outcrops are situated at the basin margins (Fig. 2). In outcrop 4 (sample S9), a sample from a spherical charcoal piece (approximately 1.5 cm in diameter) has been taken from fluvial gravels (~ 1 m below the surface). A statement about the age of gravel deposition is therefore problematic. Sample material S10 (outcrop 5) consists of terrestrial mollusc shells sieved from a cemented, few dm long, coarse sandy lense within fluvial gravels of the palaeo-Schwarza River. Both samples have ages older than 45000 BP.

6. Stratigraphic packing

Overbank deposition seems to have been widespread in the Mitterndorf Basin during periods of MIS 3 as suggest by a cluster of ^{14}C age and by terrestrial snail assemblages. Thick sheetflood dominated facies of the alluvial fans overly rather thin soils respectively pedogenic altered overbank fines with an unconformity. Increasing tectonic subsidence towards the central parts of the Mitterndorf Basin is evident from growth strata of sheetflood sediments between these unconformities (Fig. 4). Overbanks are much more frequent and have a tendency to be less altered in the central parts, below the floodplain of the Mitterndorf Basin than in the western parts within the strata of the alluvial fans (Küpper, 1950). This tendency refers to a lower exposure time on the floodplain and a longer exposure time on the alluvial fans. However, close to the basement pedogenic alteration may become very high.

Preliminary data on terrestrial mollusc assemblages (C. Frank pers. com.) confirm the suggested early to middle, Middle Pleistocene age of the lowest sequences of the Mitterndorf Basin (Decker et al. 2005, Küpper, 1950). Fluvial sediments, overbank fines and paleosols have erosive contacts and are alternating in high frequency one above the other. Long exposure times and low accumulation space, indicated by erosive contacts and alternating sequences, thus represent low subsidence rates (Blum and Törnqvist 2000) at the beginning of the Mitterndorf basin formation.

To the north, the Mitterndorf basin decreases in width to approximately 3 km. Here, higher subsidence rates lead to thickening of Pleistocene channel sediments of up to 170 m (Berger, 1989; Salcher et al. 2008; Fig. 8). The overbank facies assemblage lacks evidence of significant pedogenic alteration and had a higher chance of preservation which is also evident by the presence of more and also thinner sheets of overbank deposits. The present development of the Mitterndorf Basin's floodplain is dominated by meandering river patterns.

Subsidence triggers weak valley incision (headcut development) at the alluvial fans and valley fill deposits during times of high sediment supply. Evidences for valley fills are given by outcrop and core data from the Piesting River and the Schwarza River alluvial fan. The upper Piesting fan incised-valley fill (Fig. 3d, outcrop 6) consists of coarse clastic, stratified channel deposits with few fine clastic infillings of some meters wide channels (overbanks). The base of this incised valley is ~ 10 m below the recent surface. Channel facies assemblage can be well distinguished by its lithofacies from the underlying respectively adjacent sheetflood facies assemblage. The width of this valley is not exceeding some hundred meters. Fining upward sequences on basal lags demonstrate processes of valley filling. Schwarza River alluvial fan valley fill are represented in outcrop 1.

7. Depositional Model

The stratigraphy of the Pleistocene Mitterndorf Basin reflects the response of alluvial/fluvial systems to climate change and varied subsidence.

^{14}C ages demonstrate widespread depositions of overbank fines in the Mitterndorf basin during at least the upper stage of MIS 3 (which is in the range of radiocarbon measurements). In the stratigraphical context of the Mitterndorf Basin, deposition of overbank fines indicates rather high discharge to sediment supply ratios. Rather warm

climatic conditions during periods of MIS3 in eastern Austria are demonstrated by fossil records (Neugebauer-Maresch, 2008; Frank, 1997; Frank and Rabeder 1997;). Typical terrestrial snails assemblages of MIS3 found in the overbanks confirm ^{14}C ages and suggest a generally moderate climate with the presence of trees. Presence of trees during periods of overbank formation is also documented by a fossil record of an insitu root. The occurrence of trees in the Pannonian area during MIS 3 and, in refuges, even during MIS 2 could be demonstrated by Willis (2000).

Frozen ground on the top of some overbank successions point to a strong climatic decline. As vegetation cover determines the amount of sediment available (Schumm, 1977) a strong climatic decline and associated periglacial conditions lead to an increase of debris supply (Vandenberghe, 2002; Van Husen, 2000). The consequence of high sediment supply was a switch to bed load dominated runoff behaviour. Alluvial channels which were cut in the fan's surface during warm periods were filled, the intersection points of the streams move to upper fan positions. Aggradation on the entire surface of the fans took now place. A generally low vegetation cover is also supposed to trigger the number of slope failure and debris flow deposits along the Alpine front. Datable material dispersed in overbanks (outcrop 1, 2, 3) below the sheetflood facies demonstrate that the last strong aggradational phase must have been taking place younger than approximately 40.000 a. Many studies from north, east European and Alpine areas prove aggradation during or shortly after the maximum of the last glaciation (e.g. Vandenberghe, 2003; Mol, 1997; Krzyszkowski, 1990; Penck and Brückner 1909;). In accordance with these studies and dated material of the Mitterndorf Basin sequences, the last strong aggradation phase affecting the Mitterndorf Basin is supposed to happen during MIS 2.

During glacial conditions most of the annual precipitation of the Alpine drainage areas was in the form of snow which resulted in an extended glacial network in the central Alps (Van Husen, 1987; Penck and Brückner 1909). The limit of permanent snow cover was in the range of ~ 1500 m. The drainage area of the Schwarza River alluvial fan was affected by smaller valley glaciers. The generally lower lying drainage area of the Piesting River alluvial fan lacks glaciation (Van Husen, 1987). The run off behaviour under such conditions is characterized by very low or no discharge during the winter and peak discharge during the summer (Vandenberghe, 2001). Similar to the Pleistocene "brown gravels" of the Rhine (Siegenthaler and Huggenberger, 1993) the sheetflood facies assemblage of the Mitterndorf fans is supposed to be rapidly accumulated under high magnitude floods during peak discharge conditions. High energy conditions are indicated by the massive lithofacies, large clasts and the horizontal bedding of gravel sheets. Frozen subsoil may also play a certain role, preventing water from draining in the underground and increasing the amount of discharge (Bogaart et al., 2000). High energetic bed load dominated streams were eroding the uppermost fine sediments (Vandenberghe, 2001). This process may reflect the absence of upper soil horizons which were formed on the surface of the alluvial fans during warmer periods. Thicknesses of the sheetflood facies assemblage demonstrate that aggradation on the Piesting fan was much lower than on the Schwarza fan during MIS 2. Sheetflood deposits approximately 11.5 km from the Schwarza fan apex reach a thickness of 11 - 12 m, sheetflood deposits approximately 6.4 km from the Piesting River apex reach a thickness of only 3 m. Height, size and glaciation of the Schwarza River drainage area caused more sediment supply and a larger peak runoff which resulted in an increased transport capacity. The consequence was a stronger aggradation on the Schwarza fan in contrast to the Piesting fan. Even though the drainage area of the Schwarza fan is almost 3 times larger than the drainage area of Piesting fan, the fan area is only double size. Lateral confining of the Schwarza fan on both sides (Alps) may have caused a smaller fan area and an additional impact on the growth of the sequences. Higher subsidence in the area of the Piesting fan may not be the reason for a larger fan size as the gradient to fan size relationship is inverse (Bull, 1977): Lower subsidence results rather in larger fans, higher subsidence rather in smaller fans (e.g. Viseras, 2003).

At the beginning of the Late Glacial many European Rivers in mid latitude experienced incision (e.g. Timár et al., 2005; Vandenberghe, 2002; Starkel 1995). The Danube which

is the receiving stream for all tributaries of the Austrian Northern Alps is supposed to incise much later. Large quantities of debris which were transported from intensive glaciated northern Alps are supposed to prolongate the incision phase up to the beginning of the Holocene (Van Husen, 2000). In the Mitterndorf Basin, the switch from a braided pattern to a meandering river with well developed sedimentary structures can be assumed to happen before 9000 a BP along the Piesting River (Fig. 7a, sample S7, outcrop 3). Cut and fill structures and overbank deposition at the top section of outcrop 3 (Fig. 7) show a transition to erosive conditions. Overbank deposition and well stratified fluvial gravels point to a general shift to a higher discharge/sediment supply ratio, in contrast to the massive bedded, coarser grained sediments below. Age results from pedogenic altered sediment in 2 m depth, (E. Draganits pers. com.), close to contemporary Schwarza River and about ~ 14 km from the Schwarza fan apex, point to a switch from an aggradational braided pattern to a cut and fill, meandering river pattern at < 13.700 B.P.. The youngest channel sediments are not affected by cryoturbations indicating a rather warm climate during and after deposition.

As age data is limited, more detailed information on the influence on the sedimentary pattern during the Late Glacial (e.g. Younger Dryas; c.f. Collings et al., 2006; Andres et al., 2001) can not be made. After the switch to a meandering pattern, at the onset of incision, flood events could have led to overtopping of the incised valley and brief episodes of deposition on the fan (cf. Weismann et al., 2002). However, alluvial fans are supposed to be inactive at the latest at the beginning of the Holocene. Presently, the Piesting River is held within a 5 m deep (far apex, some 11 km) incised valley, with an intersection point located at a rather distal fan location. With incision and associated inactivity of the alluvial fans, fan surfaces were exposed to widespread soil formation (Fig. 9). The thin sequences of soil which formed on the fan surfaces constitute sequence boundaries to the sheetflood sediments of following glacials.

During the Holocene, vegetation around the Mitterndorf Basin demonstrates a generally warmer climate with even warmer periods than present (*Quercus* dominance at the second stage of the Atlantic Period; Havinga, 1972; Klaus, 1962). While black earth formation is widespread in the southern Vienna Basin lowlands, the formation of peat bogs is strictly limited to the northern part of the Mitterndorf Basin (Havinga, 1972; Soil map of lower Austria). Peaty and marshy soils point to an extension during Boreal, Atlantic and Subboreal periods (Havinga, 1972). The climatic transition to warmer and wetter conditions is associated with a clear increase in overbank deposition in the upper few m of the floodplain. Overbanks are recognized as grey sand, silt or loam in driller's lithologic logs. The Holocene peat bogs are often underlain by some cm to dm thick overbanks. Fine grained overbanks act as aquicludes and are supposed to promote peat bog formation. The fact that peat bogs only occur within the limits of the Mitterndorf Basin (Havinga, 1972) refer to an influence of subsidence on its formation.

8. The role of the base level – tectonic subsidence

Tectonic, climate and base-level related factors are generally assumed to act as main influencing factors on alluvial fan development (Bull, 1977). So far the discussion was mainly focused on the role of climate, causing the fastest and strongest response of streams upon these three controlling factors.

8.1. Influence of base level

The Danube, which is the base level and receiving river for all tributaries in the southern Vienna Basin, is not supposed to have a large impact on incisional or aggradational behaviour of streams. Fluctuations in elevations of Danube River within the Vienna Basin are very minor. Elevation of terraces of the late Middle Pleistocene (MIS 6, Riß) above the contemporary floodplain of the Danube is not exceeding ~ 15 m, demonstrating generally low incision. The terrace deposited during and after MIS 2 (Van Husen, 2000) is situated just few meters above the contemporary Danube. The uplift of the Alpine-Carpathian block (Decker and Peresson, 1996) cause preservation of the Danube terraces

(cf. Bridgland and Westaway, 2008; Starkel, 2003). Uplift and continuous slow incision is also supported by the fact that the Danube is separated from underlying Neogene sediments just by few meters of fluvial sediments (Gangl, 1993). As incision rates were low during the Pleistocene, the adjustment of tributaries on the Danube level is supposed to be minor. The complete absence of fluvial terraces in the northern parts of the Mitterndorf basin point to an higher influence of Mitterndorf basin subsidence than base level fall through climatically induced incision of the Danube during the Holocene.

8.2. The role of subsidence

Subsidence accumulation space & Provides preservation of the stratigraphic record through lowering of deposits below a possible depth of incision and removal (Blum and Törnqvist, 2000). The chance of preservation is highest in the basin centre where subsidence rates are the highest (Fig. 9) and is decreasing towards the basin edges and towards south where subsidence rates get lower. Differences in subsidence rates are demonstrated by growth strata (growth) of alluvial fan sequences (Fig. 4). Interestingly, the sheetflood facies assemblage according to MIS2 is higher at the Schwarza River alluvial fan even though subsidence rates are similar or even something lower compared to the Piesting River alluvial fan (compare outcrops 1 and 2). As subsidence rates control the accumulation space (Blum and Törnqvist, 2000; Weissmann et al., 2002), the deposition of thicker MIS2 sequences on the Schwarza fan imply not only a larger drainage area (Fig. 9), but also higher erosion potential of subsequent aggradation events. Higher erosion potential is reflected by less preserved paleosols in the stratigraphic record of the Schwarza fan compared to the Piesting fan where paleosols or pedogenic altered overbanks are more frequent in driller's lithologic logs.

Precise levelling measurements show an actual subsidence of $\sim 1\text{mm/yr}$ (Höggerl, 1980) of the Mitterndorf Basin. Preliminary results of terrestrial mollusc assemblages confirm the suggested early to middle, Middle Pleistocene age of the basin (Decker et al. 2005). Only $\sim 170\text{ m}$ of Pleistocene sediments (Berger, 1989) refer to some lower Pleistocene subsidence values for the Mitterndorf Basin as calculated from present precise levelling measurements. Levelling data may reflect effects of compaction or strong water withdrawal in the basin. Withdrawal of hydrocarbons in the central Vienna Basin is known to bias levelling data (Brix and Schulz, 1993).

As peat bog extension is limited to tectonic sag ponds in the northern part of the basin (Hinsch et al. 2005) subsidence is supposed to have an additional influence on its formation - beside the climatic effect. Rapid subsidence is known to trigger deposition of overbank fines (Bridge and Leeder, 1979; Schumm, 1977). The increasing number of overbank deposits in the upper few m of the northern floodplain parts may reflect an influence on flooding frequency through an increase of accumulations space (sensu Blum and Törnqvist, 2000).

A further effect of subsidence might be the formation of some meters deep incised-valleys at the fans. Incipient distal headcut development at the Piesting fan is evident at the present fan surface. Subsidence may trigger or enforce distal fan incision and lead to total trough trenching (Harvey, 1987, 1996, 2002; Fig. 9) if subsidence remains higher than aggradation rates. Filling of the incised-valley is supposed to happen during periods of high sediment supply to discharge ratios during or shortly after glacials.

9. Conclusions

Significant different sedimentary lithofacies assemblages were recognized in Austria's largest Pleistocene basin. Facies distribution and packing is supposed to be subjected to a cyclic development depending mainly on glacial cycles and subsidence as a long term effect (Fig. 9). In this context, lithofacies is related to times of glacials, interstadials or interglacial periods.

Glacial Periods

Aggradation during glacial periods is mainly the consequence of a decrease in vegetation cover and an increase in periglacial conditions. Congelifraction produced large quantities leading to high debris input (Van Husen, 2000). Nival regime caused discharge peaks in runoff and provided high energetic transport of sediments into the basin which is represented by the sheetflood facies assemblage. Transport of large sediment quantities lead to a consequent filling of incised valleys and to a subsequent aggradation of streams onto the alluvial fans. A larger drainage area of the Schwarza River alluvial fan system and more transport capacity through glaciation led to a generally thicker sequence of the sheetflood facies assemblage compared to the Piesting River alluvial fan. The typical coarse grained nature of valley fillings and alluvial fan sediments represent the high energy conditions.

End of glacial periods

Aggradation of sediments was prolonged into periods after the Pleniglacial. The Danube, which is the receiving streams for all southern Vienna Basin streams, was not able to incise before the early Holocene (Fink, 1977; Piffel, 1971, Van Husen, 2000). A weak base level influence on its tributaries might therefore affect the streams as early at that time. Sparse age data constrain the switch to a meandering pattern and incision of the Piesting and Schwarza River somewhere around between ~ 14.000 and 9.000 years. Incision of streams leave the fan surface abandoned. Fan surfaces got subsequently exposed to soil formation.

Interglacial – Interstadial Periods

During times of interglacial periods ratios of discharge to sediment load ratios are high. River planforms are shifted to meandering pattern. Discharge conditions are moderate and not dominated by a distinct (glacio-) nival regime. The consequence is a decrease in discharge energy and an associated reduction in mean grain size. Decrease of sediment load lead to a general increased deposition of overbank fines in case of flood events. Lithofacies shifts from massive, matrix supported gravels represented by sheetflood flood facies assemblage to well stratified, sandy gravels represented by the channel facies assemblage. High discharge to sediment load ratios cause incision of Piesting and Schwarza River into fan surfaces and intersection point movement to distal positions. The abandoned fan surfaces are affected by widespread soil formation. Soils mark the sequence boundary to next depositional event around glacial periods (Fig. 4).

Subsidence

Subsidence has a long term effect on fan deposition in contrast to the short term effects of climatic oscillations. It provides accumulation space and increases the change of sequence preservation (Blum and Törnqvist, 2000). Rather low accumulation during warm periods is enforcing the effect of tectonic subsidence. Sequences of the northern Mitterndorf Basin may not only reflect a climatic effect but also the effect of tectonic sag ponding recognizable in a surpassing number of overbank fines and peat bog formation. Both are supposed to represent the lowering below a possible depth of incision and removal which is associated with and increase in flood activity (Blum and Törnqvist, 2000). Subsidence (or base level fall on which the fans toe out) may also trigger headcut development on the Mitterndorf Basin fans which may subsequently lead to total trough trenching and to incised valleys if sufficient time is available.

Acknowledgements

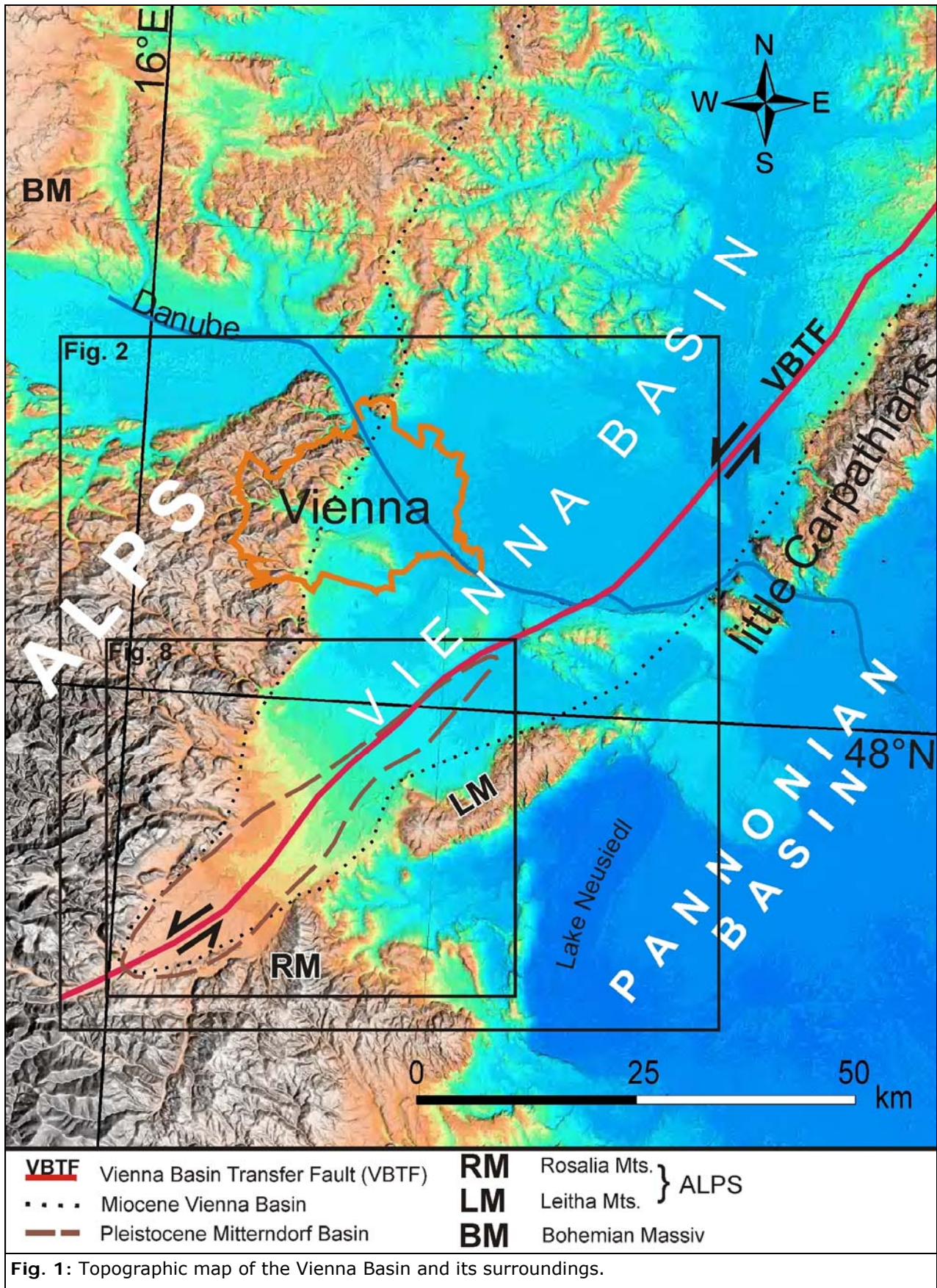
This project was funded by the Austrian Science Fund FWF, Project 18203. We thank the Government of Lower Austria and OMV E & P AG and for providing data).

Table

Sample number	time B.P:	sample material	geographic pos. long	geographic pos. lat	Depth below surface approx. (m)
S1	40460 ± 650	charcoal fragments	16.202151	47.791492	12
S2	47766 ± 1400	charcoal fragments	16.202151	47.791492	12
S3	45672 ± 1000	charcoal fragments	16.243413	47.872900	16-17
S4	> 46000	charcoal fragments	16.201264	47.790889	16-17
S5	43326 ± 1000	shell fragments of freshwater snails	16.284142	47.877247	2.7
S6	35884 ± 600	shell fragments of freshwater snails	16.284142	47.877247	3.5
S7	8999 ± 65	charcoal fragments	16.323420	47.933846	1.7
S8	40785 ± 1000	shell fragments of freshwater snails	16.321948	47.934982	4.5
S9	> 45000	charcoal fragments	16.169111	47.818465	1
S10	> 45000	shell fragments of freshwater snails	16.104743	47.740081	7.5

Tab. 1: Sample ages

Figures



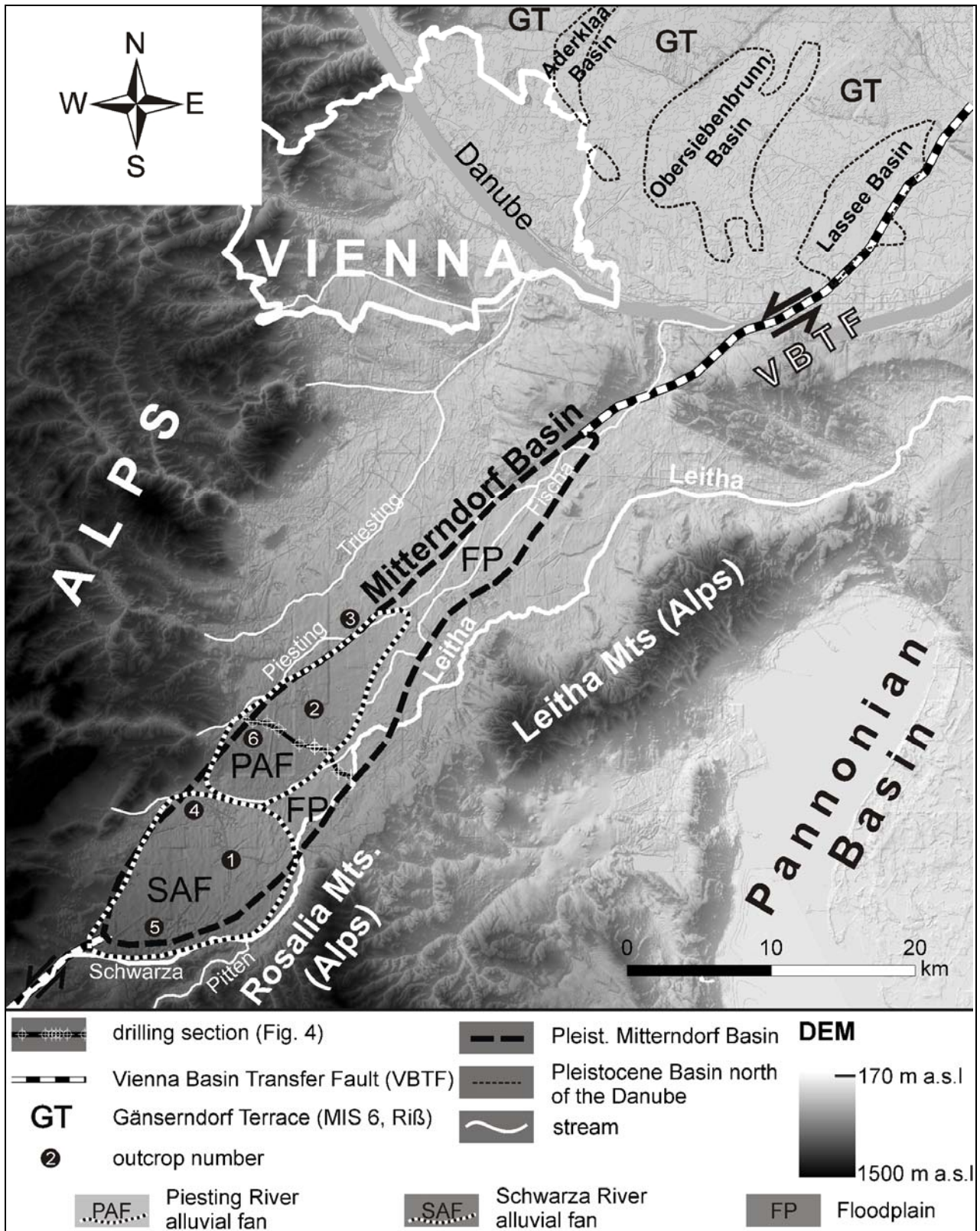


Fig. 2: Overview of the study area showing southern and central Vienna Basin's Pleistocene basins and streams. These basins are linked to releasing bends along the Vienna Basin Transfer Fault (VBTF, Mitterndorf Basin, Lassesee Basin) and to normal faults, which splay off from this sinistral strike-slip fault system (Obersiebenbrunn and Aderklaa Basin). Both alluvial fans of the Mitterndorf Basin (Piesting and Schwarza River alluvial fan) are distally trenched and inactive. Fast subsidence rates suppress the formation of terraces in the Mitterndorf Basin. Distinct terrace levels are evident north of the Danube (MIS 6 Danube terraces). Terrace levels point to some uplift of the Alpine Carpathian system.

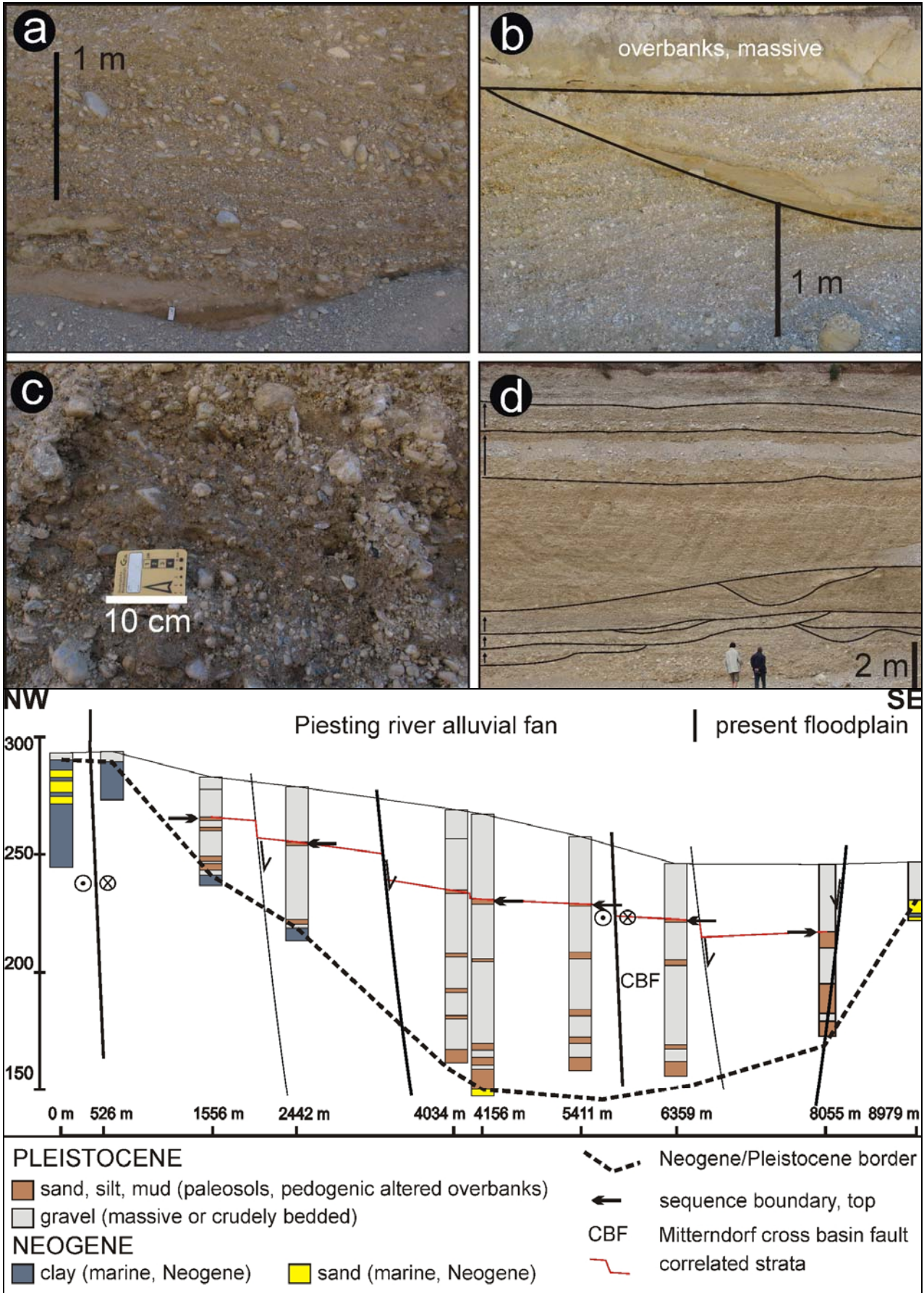


Fig. 4: Cross section through the Piesting River Alluvial fan and the Floodplain of the Mitterndorf Basin. Lateral extensive paleosols or pedogenic altered sediments are interbedded into thick units of massive or crudely bedded gravels. Paleosols reflect long exposure times marking sequence boundaries. The massive gravels reflect short and intense aggradation events during and shortly after glacials.

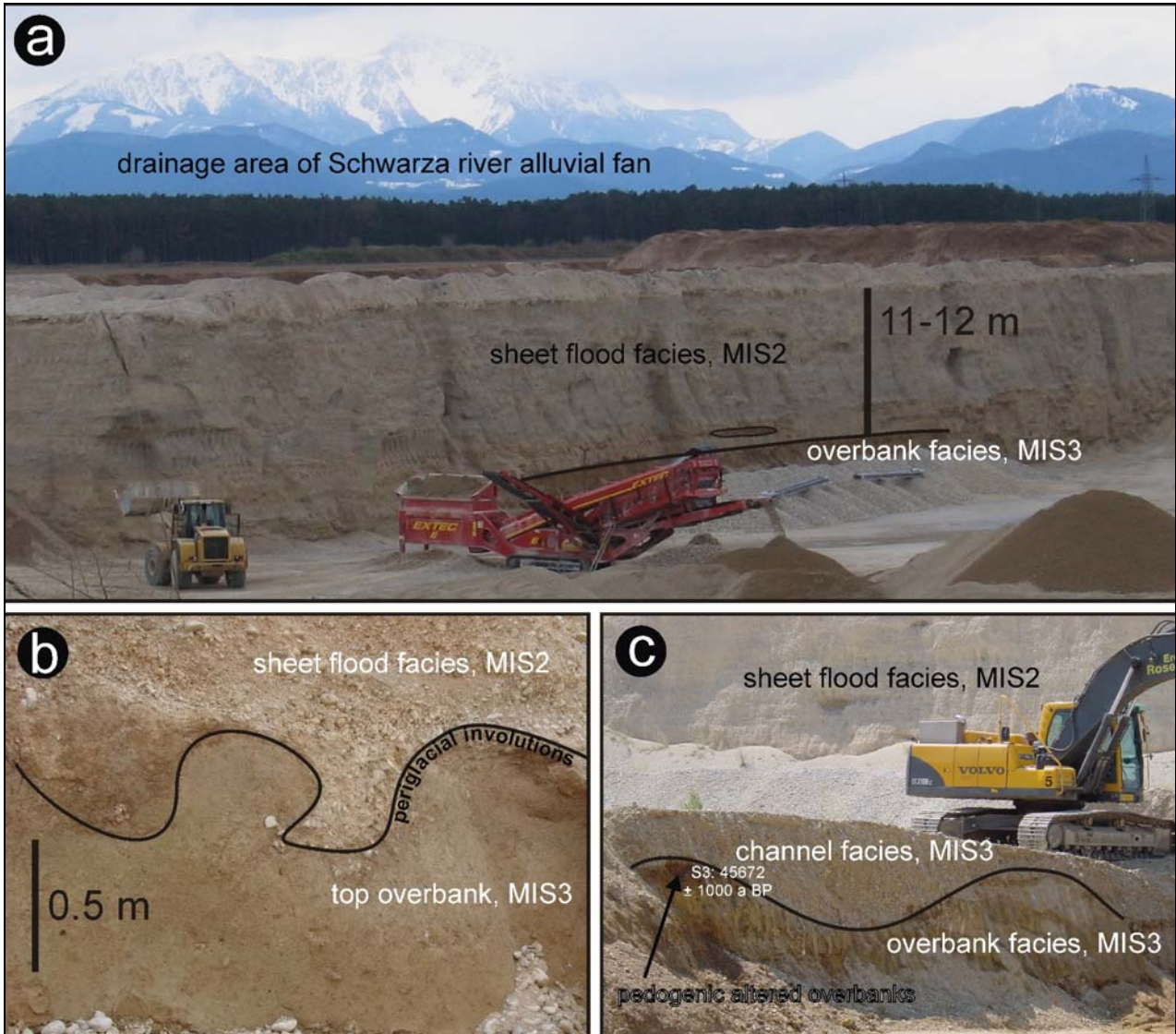


Fig. 5: Outcrop 1, Schwarza River alluvial fan:



Fig. 6: Outcrop 2, Piesting River alluvial fan: The outcrop is situated at a rather distal location of the fan. Distal position is obvious as massive gravels deposits are relatively thin. They top laminated overbank fines which are related to rather warm-periods.

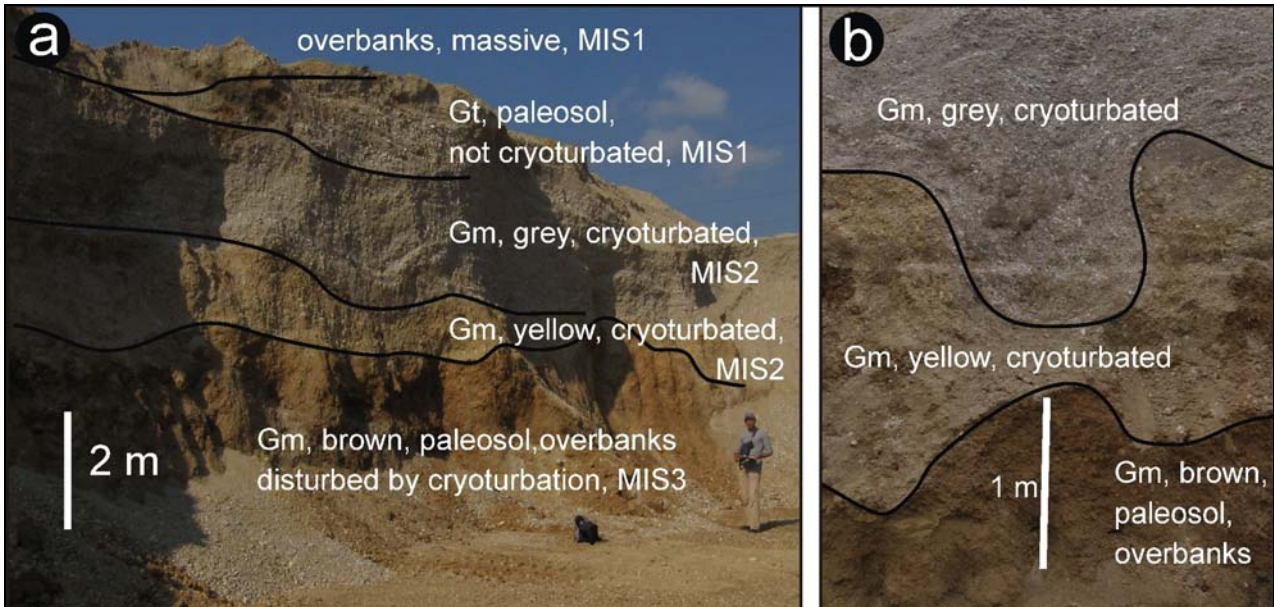


Fig. 7: Outcrop 3, Piesting River

Sediments show at least 4 erosive contacts, reflecting rather minor accumulation space (7a). Except of the upper, well stratified channel facies, sediments are affected by distinct periglacial involutions (cryoturbations, b).

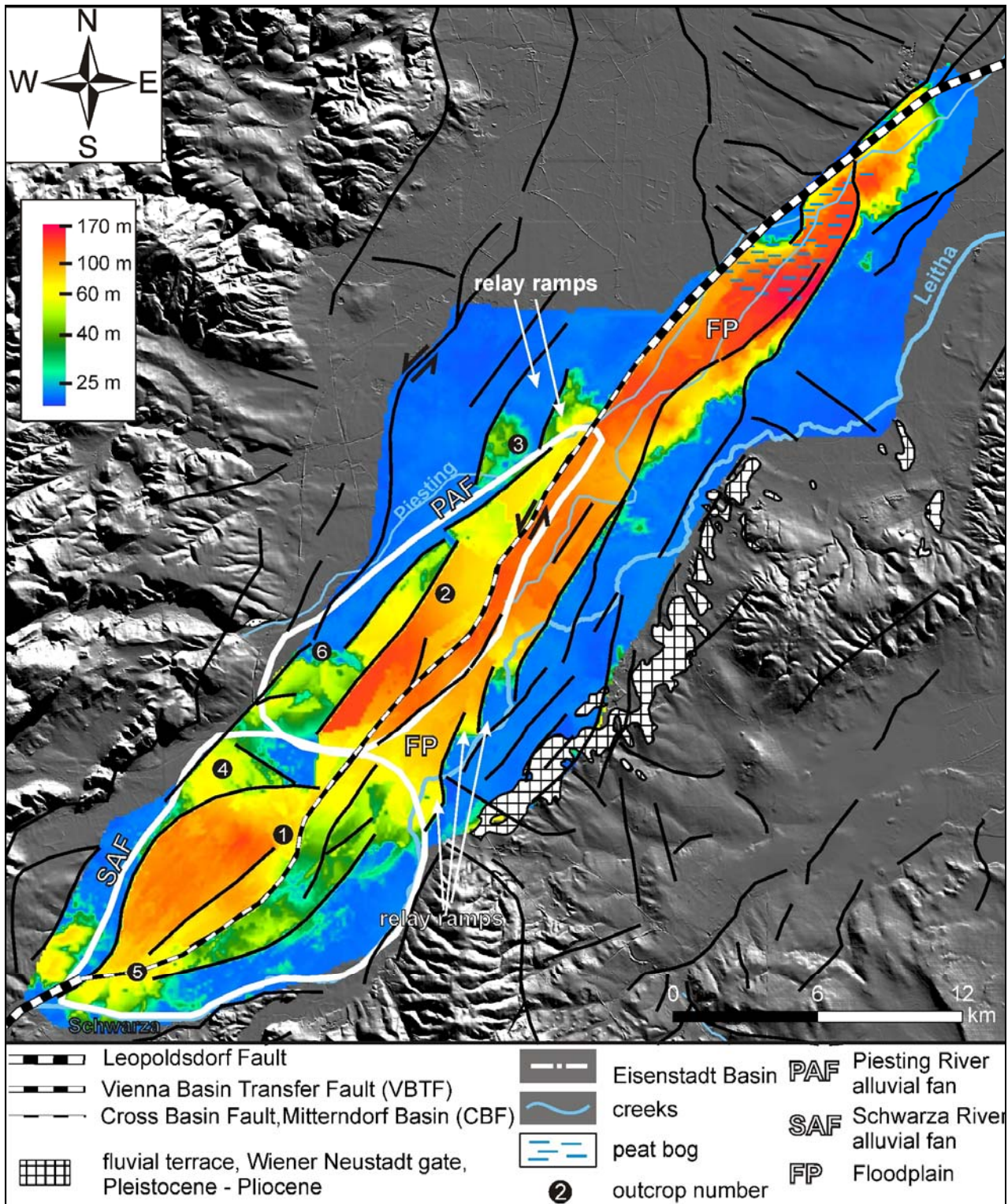


Fig8: Thickness map of the Mitterndorf Basin Pleistocene Sediments calculated from c. 2000 drillings. Subsidence rates which can be inferred by sediment thicknesses control the creation of accumulation space and the sequence preservation potential (Blum and Törnqvist, 2000). Strong differences in thickness of the sheetflood facies of the Piesting and Schwarza River alluvial fan indicate that the sequence development is primary an effect of drainage area size (modified after Salcher et al., 2008).

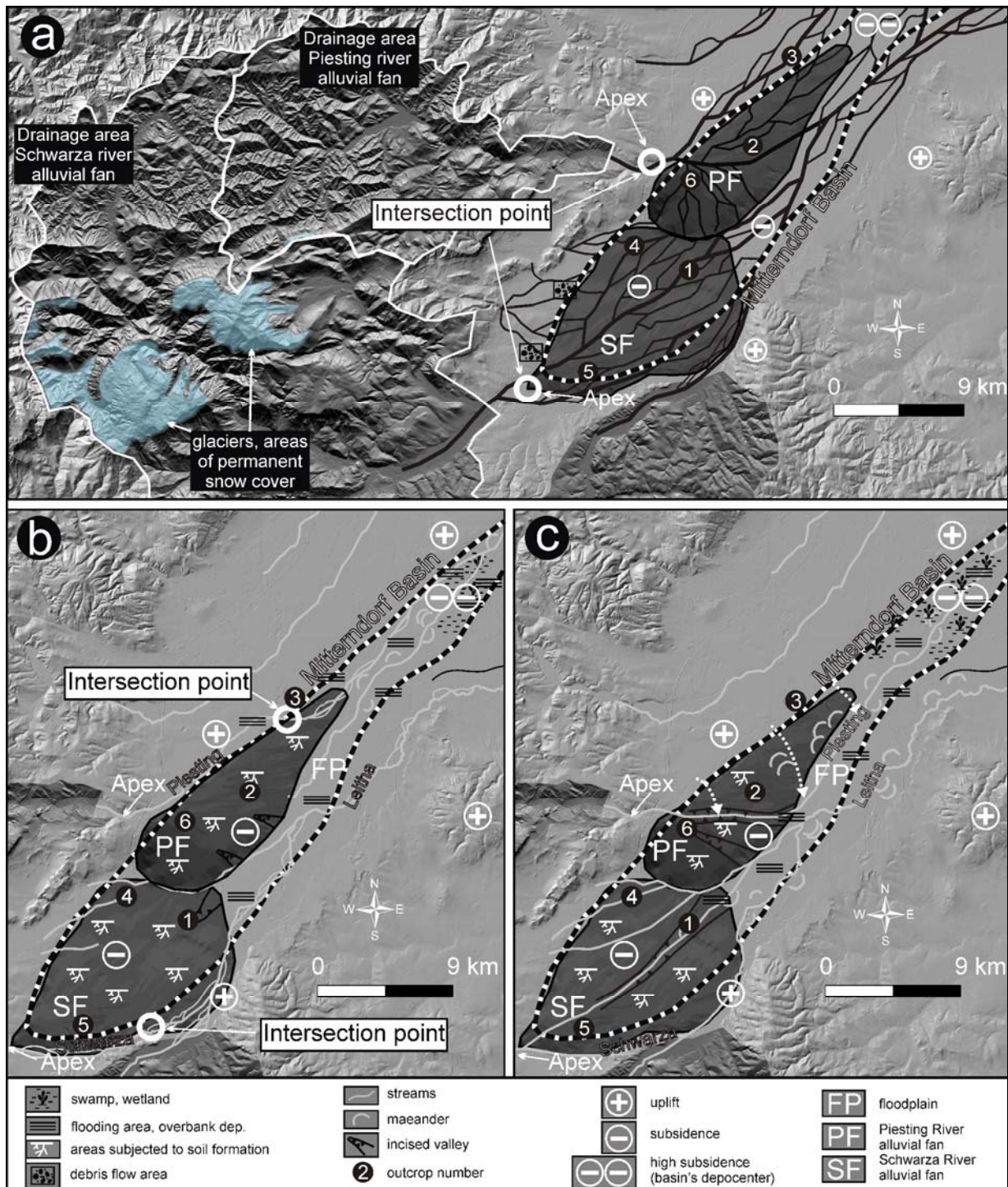


Fig. 9: (a) Situation of the Mitterndorf Basin during the last glacial maximum. High ratios in sediment supply to discharge are associated with high accumulation space and intersection points close to the apex.

(b) With the beginning of a warmer period, sediment supply decreases, discharge is increasing causing change in river planform and increasing deposition of overbank fines. Streams tend to incise leading to an intersection point movement to downfan position. Ongoing subsidence leads to headcut development along the now inactive alluvial fans. Fan surfaces are subjected to widespread soil formation

(c) During longer lasting warm periods tectonic influence becomes more prevalent. Rivers have meandering planforms, flooding and associated deposition of overbank fines is frequent. Alluvial fans are now inactive. The relatively stable position of the Danube and high subsidence rates suppress the preservation of terraces. However, subsidence may lead to ongoing headcut development and complete through trenching at both alluvial fans.

Detection of Pleistocene structures in the southern and central Vienna Basin using first order gravity derivatives, reflection seismic and well data

Abstract

The active Vienna Basin Transfer Fault system is related to the formation of several Pleistocene basins with depths of up to 170 m (e.g. Mitterndorf and Lassees Basin) and areas covering up to 270 km². In this study we present the suitability of conventional Bouguer gravity data to highlight near surface basin and tectonic structures by a relatively simple high pass filtering process. Different first order derivatives of gravity data are used to precisely determine shallow fault locations. The obtained fault locations are validated against geophysical and geological data such as 2 D, 3 D seismic, geoelectric, drill log information and outcrop data. Additionally, numerical models were carried out to better understand effectiveness of derivatives and better interpret shallow gravity anomaly features.

Using this technique a new and considerably more accurate model of Austria's largest Pleistocene Basin, the Mitterndorf Basin, was developed, demonstrating the kinematic (sinistral, pull apart basin) impact on the basin geometry and on fault activity during the Pleistocene. We also show the impact of Plio- to Pleistocene tectonics in a more regional framework, along the Danube in the southern and central Vienna Basin and the evolution of the Eisenstadt Basin at the transition to the Pannonian Basin. Results demonstrate the major impact of faults on landscape development. The precise constrain of near surface faults allowed to link diverse geomorphologic features to a tectonic origin such as scarps, grabens, valleys and erosional gullies.

1. Introduction

The Vienna Basin area is characterized by a complex tectonic evolution during the Quaternary, which has significant impact on erosion, sedimentation, and the regional landscape evolution. Available studies highlight a number of Quaternary strike-slip and normal faults, which evolved from Miocene structures (Hinsch et al., 2005; Peresson and Decker, 1996; Chwatal et al., 2005; Beidinger et al., 2008). These faults lead to differential vertical movements forming a mostly tectonically controlled relief within a basin with generally very low relief energy. There, even small vertical offsets may have an impact on the course and deposition of rivers and alluvial fans (Salcher and Wagreich, 2008; Salcher et al., 2008). In addition, faults delimit several Quaternary basins, which are characterized by subsidence during the Quaternary acting as sediment traps in a fluvial environment (Fink 1955; Fink, 1965; Decker et al., 2005).

Attempts to identify and sort the contribution of tectonic forcing on sedimentation and landscape evolution from Pleistocene climatic controls so far were severely limited by the fact that Quaternary faults were only inaccurately mapped and that Quaternary fault maps only covered small parts of the basin (Decker et al., 2005; Hinsch et al., 2005). This is particularly true for the active Vienna Basin strike-slip fault system, which hosts two up to 170 m thick Quaternary fluvial basins (Mitterndorf-, Lassees Basin). Tectonic analyses and seismic data indicated that these basins are delimited by a geometrically complex array of surface breaking faults controlling the local relief. Quantitative data on fault location and fault dip, however, were not available so far. The central objectives of the current paper therefore are (1) to develop a methodology to map Quaternary faults throughout the basin, and (2) to evaluate the impact of these faults on sedimentation and geomorphology.

The precise determination of near-surface fault locations and their exact course over larger areas is a difficult task for basinal settings. Commonly applied high-resolution geophysical methods for near-surface fault mapping like resistivity, ground penetrating radar or reflection seismic only provide fault data for 2D vertical sections. Such information is difficult to link into a consistent fault map. We therefore use gravity data, which are available for the entire Vienna Basin, to obtain regional fault maps. Bouguer anomaly data have previously been used for getting insights into the general structural

build up of the basin (Zych et al., 1993). This data, however, requires advanced processing in order to image faults at high resolution. Studies from other basins show that derivatives of the Bouguer anomaly such as the high-pass filtered vertical gradient and the horizontal gradient are suitable for enhancing structural information (e.g. Zeng, 1988; Edel and Fluck, 1989; Lopez Cardozo et al., 2005; Rotstein et al., 2006; Reynisson et al., 2007). In the first part of the paper we therefore combine these two Bouguer gravity derivatives in order to produce a regional map with precise near-surface fault locations. The derived fault maps are validated using locally available independent geophysical data (2D reflection seismic) and well data. Validation shows that gravity data reliably map Quaternary faults and that the combined use of the horizontal and vertical gradient even allows assessing the dip direction of faults. The latter feature appears particularly important as it discriminates hanging wall and footwall of faults with vertical slip components, which exert control on sedimentation and erosion. The resulting high-resolution fault map is further used for a detailed discussion of the impact of individual faults on Quaternary sedimentation and landscape evolution.

2. Regional setting and tectonic evolution of the Vienna Basin

The Vienna Basin is a Miocene thin-skinned pull-apart basin (Royden, 1985; Wessely, 1988; Fig. 1), which formed at a major releasing bend of the Vienna Basin Transfer Fault between the Eastern Alps and the Western Carpathians (Austria, Slovakia and Czech Republic; Ratschbacher et al., 1991; Fodor, 1995; Decker et al., 2005). The tectonic history of the basin is characterized by major kinematic changes during the Miocene, Pliocene and Quaternary.

Middle to Upper Miocene pull-apart formation (Badenian to Pannonian; c. 16 – 7 Ma) includes the formation of NE-striking divergent strike-slip faults with negative flower structures and extensional strike-slip duplexes. Major strike-slip faults enter the basin at its SW and NE corner, respectively. These faults are linked by en-echelon N- to NNE-striking listric normal faults (Fodor, 1995; Decker, 1996; Decker et al., 2005), which are associated with substantial horizontal extension and up to 5.6 km normal faulting (Steinberg-, Leopoldsdorf Fault System). Middle to Upper Miocene growth faulting led to rapid basement subsidence and to the deposition of up to 4.3 km marine, brackish, lacustrine and fluvial sediments (Wessely, 1988; Sauer et al., 1992).

Pull-apart subsidence ended during the Upper Miocene as shown by fault inversion and the termination of pull-apart sedimentation during the Upper Pannonian (between 9 and 5.3 Ma; Peresson and Decker, 1997). This kinematic change may be correlated to the onset of major regional surface uplift. The latter is evident from the complete regression of the Parathethys lake system, the absence of Pliocene sediments, and the occurrence of marine or brackish sediments of Middle to Late Miocene age at elevations of up to 440 m at the present basin margins (Decker, 1996). The formation of staircase terraces along the Danube (Fink, 1955) proves that surface uplift continued into the Pleistocene (Starkel, 2003; Bridgland et al., 2008). Incision of the river into bedrock at the eastern margin of the Vienna Basin is further constrained by cave sediments from the outliers of the Little Carpathians (Hainburg Mountains). Caves located between 100 and 170 m above the Danube are filled with fluvial sediments, which are dated to the Villafrancian (Lowermost Pleistocene; Niedermayr and Seemann, 1974; Rabeder, 1997).

Pliocene to Early Pleistocene tectonics includes NE-SW-directed extension and the formation of NW-striking normal faults and grabens, which cut older faults of Miocene the pull-apart basin. The event is dated by sediment ages from the Upper Moravian Graben (Pleistocene to Early Pleistocene; Knobloch, 1963; Hrubes, 1994; Hrubes and Ctyroka, 1998) and the age of deformed sediments in the Vienna Basin proper (Decker et al., 2005).

Late Pleistocene to present deformation is characterized by sinistral slip along the Vienna Basin transfer faults system and by the reactivation of part of the Middle to Late Miocene faults in the Vienna Basin. The transition from NE-directed extension to renewed strike-slip faulting is not well dated but apparently occurred during the Middle Pleistocene. Active sinistral faulting along a strike-slip system extending from the southern Vienna

Basin to the E margin of the basin and the West Carpathians is indicated by earthquake data (Reinecker and Lenhardt, 1999), geodetic data (Höggerl, 1980; Grenerczy, 2002; Grenerczy, 2006) and growth faults, which delimit several Quaternary basins within the Miocene pull-apart structure (Fig. 2, Fig. 10). These basins are linked to releasing bends along the VBTF (Mitterndorf Basin, Lasse Basin) and to normal faults, which splay off from the sinistral strike-slip fault system (Aderklaa, Obersiebenbrunn Basin; Decker et al., 2005). Seismic data covering the Mitterndorf and Lasse Basin show that both Quaternary basins overly negative flower structures (Fig. 4), which include numerous faults arranged in strike-slip duplexes or overstepping en-echelon patterns (Hinsch et al., 2005; Beidinger and Decker, in press). Faults converge into a single masterfault at depth.

3. Morphology and sedimentology of the southern Vienna and Eisenstadt Basin

3.1 Pleistocene Mitterndorf Basin (southern Vienna Basin)

The Mitterndorf Basin (MB) is Vienna Basin's largest and deepest Pleistocene sub-basin with Pleistocene sediment thicknesses of more than 170 m (Fig. 7; Berger, 1989). The basin is characterized by a NE-trending floodplain, which is encroached by the alluvial fans of the Piesting and Schwarza at the W and SW basin margin, respectively (Fig. 2). Steep and straight scarps delimit the northern part of the floodplain from plateaus hill countries with surface exposures of Upper Miocene (Pannonian) strata. The scarp delimiting the Rauchenwarth Plateau W of the Mitterndorf Basin is traced over a length of about 15 km. Scarp heights reach up to ~ 60 m. To the NE, a smaller Neogene ridge delimits the basin with an up to 30 m high morphological scarp on a length of about 3 km. The Pleistocene basin fill overlies Pannonian sediments with a non-conformity or a slight angular unconformity. The fluvial sediments reach a thickness of more than 170 m in the deepest parts of the basin (Fig. 7). Recent and historical wetlands along this depocenter are a consequence of tectonic subsidence and sag pond formation (Decker and Peresson, 1996). Precise levelling data from this part of the basin indicate active subsidence at rates between 0.6 and 1 mm/a (Höggerl, 1980). Active subsidence of the basin is also corroborated by the absence of Pleistocene fluvial terraces, which, however, are prominent along the Danube river N of the Mitterndorf floodplain (Fink, 1955; Fuchs and Grill, 1984). The recent drainage pattern of the southern Vienna Basin is strongly influenced by continuous subsidence in the NE-trending MB pull apart basin, the general tilt of the southern Vienna Basin and the fluvial history of the Danube forming the fore-flood of its southern tributaries (Triesting, Piesting and Fischa, Fig. 2).

The stream dominated alluvial fans of the Piesting and Schwarza Rivers form the most obvious morphological structures of the basin. Both fans are inactive. The last period of activity is associated with the deposition of coarse, massive sheetflood gravels during MIS 2 Pleniglacial (Küpper, 1950; Salcher and Wagreeich, 2008). The alluvial fan facies represents an alternating sequence of up to c. 2 m thick paleosols or pedogenic altered overbank fines, and coarse up to c. 35 m thick massive gravels. Paleosol sequences formed on inactive alluvial fans during warm periods (cf. Weissmann et al., 2002; Salcher and Wagreeich, 2008). These extensive sequences can be correlated between wells across an area larger than 100 km². The distinct sequence development allows a good correlation between wells and offer markers to constrain fault locations between wells (Fig. 5 and 6). Results from mollusc assemblages of cored overbank fines close to the bottom of the basin indicate a Middle Pleistocene age for the basal strata of the Mitterndorf Basin (cf. Küpper, 1952; Decker et al., 2005; Salcher and Wagreeich, 2008).

3.2. Neogene hills along the Danube in the Vienna Basin

The elevations of the Rauchenwarth Plateau and the Arbesthal Hills (Neogene Hills) extend from the outskirts of Vienna across the southern Vienna Basin to the Little Carpathians (Fig. 2). The elevations size about 140 km² and are separated by the Vienna Basin Transfer Fault, marking distinct morphological ridges in the Vienna Basin of up to

90 m above the present Danube level. Both consist of mostly marine to lacustrine fine-grained sediments and fine to coarse grained deltaic sands and sandy gravels. Lithofacies, heavy mineral data and correlations of the sediments to dated successions in the central Vienna Basin indicate Late Pannonian ages (Salcher, 2008; cf. Harzhauser et al., 2004a).

The northern parts of the Neogene Hills are covered by Pleistocene fluvial terraces of the Danube forming at least four different levels of different ages (Fink, 1966; Fink, 1977). Drill data show that gravels reach a thickness of commonly not more than 10 m. Terrace ages were supposed to correlate to all major glacial events during the Pleistocene (Fink, 1966; MIS 16 to 2). This interpretation, however, appears uncertain as it is mostly based on morphological terrace correlations (e.g. Fuchs, 1981, Fuchs and Herrmann 1985) disregarding the tectonic impact of Pleistocene and active faulting within the Vienna Basin. Biostratigraphic data from mammals and molluscs suggest Early Pleistocene and upper Middle - Late Pleistocene ages for the uppermost and lowest terrace levels, respectively (Frank, 1997; Frank and Rabeder, 1997, a,b,c). As expected, faunas suggest that terraces formed during rather cool periods (Döppes and Rabeder, 1997).

The whole Rauchenwarth Plateau and its Pleistocene terraces are tilted towards northwest by faulting at the major Leopoldsdorf fault (offsets of up to 4000 m, Hinsch et al., 2005). Two NW striking, up to 5 km long and 2 km wide grabens divide the plateau into three parts (Fig. 9). Minor and larger NW striking gullies incise into the plateau following the overall slope of the plateau. Gullies have asymmetric cross profiles (Fig. 9). NW trending morphological features are also evident from Arbesthal Hills east of the Rauchenwarth Plateau. Parallel ridges are separated by discontinuous valleys and straight, steep scarps (Fig. 9, Fig. 11). The spacing between the steeply flanked ridges is only some hundred meters. The elevated block of the Arbesthal Hills is tilted towards southeast by faulting at the Engelhartstetten fault. Pannonian strata disappear below alluvium of the Leitha River. The small valleys separating the ridges have undulating profiles and are discontinuous.

3.3. Eisenstadt Basin – transition southern Vienna to Pannonian Basin

The Eisenstadt Basin (EB, c. 570 km²) is located between the southern Vienna Basin in the West and the Pannonian Basin (little Hungarian Plain) in the East. It has a depth of up to 2000 m, comprising mainly marine/lacustrine Pannonian and Sarmatian sands and clays (Brix and Schulz, 1993).

Two low mountain ranges (Leitha and Rosalia Mts.) and a low saddle between these ranges delimit the EB from the southern Vienna Basin. This only 15 to 20 m high and ~ 1.5 to 2.5 km wide saddle forms a first-order drainage divide between the Vienna Basin and the Pannonian Basin system. A strong morphological difference is obvious between the almost plane southern Vienna Basin with highly active fluvial systems of large Alpine drainage areas and the EB, which is deeply incised by small creeks with low discharges (Fig. 2).

NW directed fluvial headward erosion of minor creeks of the western EB lead to a continuous incision into the low saddle separating the southern Vienna Basin and the EB. Similarly, subsidence and associated NE directed normal faulting of the MB lowers this saddle from the western side. These processes may lead to future drainage shortcut from the Alps to the Pannonian Basin.

Tectonic geomorphologic features are well preserved within the EB due to low fluvial activity. Features are aligned in NW direction in the western EB paralleling the main drainage of the Leitha Mts. (Fig. 2, Fig. 11). The drainage pattern switches abruptly to the northeast in the centre of the basin.

4. Methodology

In the current study we assess possibilities to apply derivatives of Bouguer gravity data for mapping near-surface faults. Detailed fault information is used to constrain the tectonic, syntectonic depositional and geomorphologic history of large Pleistocene (sub-) basins

within the Miocene Vienna pull-apart basin. Analyses focus on the southern and central Vienna Basin. Bouguer anomaly data are used to assess strong density differences in near-surface strata to locate faults, which control the accumulation of Pleistocene sediments and the local geomorphology, respectively.

Bouguer anomaly data are well-known to highlight major faults in sedimentary basins (e.g. Granser, 1987; Rousset et al., 1993; Lefort and Agarwal, 1999; Lopes Cardozo et al., 2005; Granser et al., 2006; Szafián and Horváth, 2006). These data, however, are improper for mapping faults at the high local resolution needed for detailed structural assessments of near-surface fault patterns as addressed in the current study (Fig. 4). First order derivatives (vertical and horizontal gradient) have been calculated to enhance gravity signals (Blakely, 1995; see appendix for details). The high-pass filter properties of these derivatives are particularly appropriate to depict near-surface with high lateral density contrast such as the faults in the MB Mitterndorf Basin. These datasets (Fig. 4) are used for interpreting and locating faults. The resulting fault map is validated using integrated seismic, well geomorphologic and outcrop data.

2D and 3D reflection seismic acquired for hydrocarbon exploration cover large parts of the southern and central Vienna Basin. Data was used by courtesy of OMV Austria (Fig. 4). About 2000 drillings were evaluated to map stratigraphic marker horizons such as the base of Pleistocene sediments or laterally extensive paleosols within the Pleistocene succession, and to obtain information on the stratigraphy of Pleistocene sediments (Fig. 6; Salcher and Wagreich, 2008). Similar to the seismic datasets drilling logs were used to verify gravity derived fault locations (Fig. 5) and to constrain the relative ages of faults with respect to mapped Pleistocene strata. Data from about 1000 of these drillings were further used to calculate a thickness map of the Mitterndorf basin's Pleistocene sediments using an inverse distance algorithm for gridding point data (Shepard, 1968), which was modified to account for faults. In the modified algorithm mapped faults act as interpolation break lines (Fig. 7). Wells were mostly drilled for groundwater prospection and hydrocarbon exploration (digital well data base HADES, by courtesy of the Government of Lower Austria). This dataset was completed by digitising further analogue paper logs of the drilling archive at the Austrian Geological Survey. The horizon Base of Pleistocene is further constrained by resistivity data (Berger, 1989), which image the horizon due to the high resistivity contrast between fine-grained Upper Miocene strata and Pleistocene unconsolidated fluvial gravels.

Geomorphologic features related to faults are analysed using a digital terrain model with 10 m ground resolution (by courtesy of the Government of Lower Austria). Analyses focused on evidences for active surface-breaking faults such as fault scarps and offset Quaternary river terraces, as well as on drainage patterns and alluvial fan geometries indicative for active vertical motions (Silva et al., 1992). Analyses also include previous studies on tectonic geomorphology of the Vienna Basin and adjacent areas (Zamolyi et al., in press). Structural information was further gained from field work (outcrops).

5. Gravity data from the southern and central Vienna Basin

5.1. The Bouguer Anomaly

The Bouguer anomaly map of the Southern and Central Vienna Basin shows a southwest to northeast elongated zone with a clear density deficit of more than - 40 mgal in contrast to the surrounding Alps (Fig. 3). The gravity low in the southern Vienna Basin roughly coincides with the Mitterndorf Pleistocene Basin, which is separated from the gravity low in the central Vienna Basin by a region with higher Bouguer anomalies (approx. - 20 mgal).

The high Bouguer anomaly deficit of the Vienna Basin primarily represents the ~ 1000 - 2500 m thick Neogene sediments of the basin, which contrast from the underlying pre-Neogene Alpine units with a much higher mean density. The density of Neogene Units depends very much on the diagenesis of the sediments. Density values obtained from available drill cores vary between a minimum recorded value of only 2.55 g/cm³ at a

depth of c. 1550 m (marine sediments) and the highest value derive from a fluvial conglomerate (2.78 g/cm^3) at a depth of more than 2700 m. Densities from Alpine Units below the Neogene Sediments range from 2.65 g/cm^3 (cellular dolomite, Northern Calcareous Alps) to 2.909 g/cm^3 (Anhydrites from the Northern Calcareous Alps). Data are mean values, obtained from numerous core samples. Measurements from Pleistocene gravels at 40 m give densities of c. 2.30 g/cm^3 . Bouguer anomaly data was used to calculate derivatives of gravity (horizontal and vertical gradient; Fig. 3). Both derivatives act as high pass filters and amplify near-surface density contrasts, especially where density differences are high. Strong density differences of the fluvial Mitterndorf Basin fill and the underlying Neogene sediments generate strong amplitudes of both derivatives at faults with vertical offset.

5.2. Fault mapping from high-pass filter derivatives of the Bouguer anomaly (horizontal and vertical gradient)

The vertical gradient (VG) highlights maximum and minimum values of Bouguer anomaly data. Normal faults displacing sediments of different density produce a maximum at, or close to the footwall cutoff and a minimum at the hangingwall cutoff. In contrast, the maximum amplitude of horizontal gradients (HG) is located over the centre of the fault heave, i.e., between the maximum and minimum of the vertical gradient. The width of a horizontal gradient anomaly depends mainly on the dip and the vertical offset of a fault. Differences in the location of the maximum value of the vertical gradient with respect to the maximum of the horizontal gradient allow assessing the dip (steep vs. shallow) and dip direction of the fault. For near-vertical faults both maxima almost coincide, whereas both maxima are markedly offset for shallow-dipping faults. Anomaly characteristics also allow distinguishing between near-surface faults and structures near the base of the Neogene basin. Near-surface faults have higher amplitude depending on density contrast and offset, whereas deep-seated faults show blurred weak anomalies. Steep faults producing anomalies with short wavelengths are common in the Mitterndorf Basin. These faults are sub-vertical strike-slip faults combining to the negative flower structure underlying the Pleistocene basin. HG and VG signals are almost superimposed (Fig. 3 b, c). In contrast, the rather shallow E-dipping Leopoldsdorf normal fault produces a very broad maximum of the horizontal gradient, which is markedly offset and from the maximum of the vertical gradient occurring further east (Fig. 3 b, c). For the mathematic details, high pass filter techniques and modelled anomaly characteristics see Appendix 1.

5.3. Structural patterns of the southern and central Vienna Basin inferred from gravity derivatives

Anomalies derived from VG and HG points to 3 dominant anomaly systems in the south and central Vienna Basin (Fig. 3). A north to south trending anomaly produces a wide and very strong anomaly with a length of about 20 km in the north of the study area. This signal can be attributed to the Miocene Leopoldsdorfer fault (LF; Fig. 3).

The second group includes short northwest - southeast trending anomalies which do not exceed 10 km length. Amplitudes of these structures are rather weak. The features abound in the Rauchenwarth Plateau and the Arbesthal Hills, which are separated by a very prominent NE-trending anomaly corresponding to the Vienna Basin Transfer Fault (VBTF).

The third system of northeast - southwest trending anomalies is most prominent along the VBTF and its associated Pleistocene Basins. This trend is marked by strong anomalies along the limits of the Mitterndorf and Lasseebasin. Faults within the basins have commonly lower vertical offsets and produce rather lower density contrasts. These faults are related to weaker anomalies.

6. Correlation of gravity anomalies with near-surface faults

Fault mapping from Bouguer gravity derivatives was constrained and validated by industry 2D and 3D seismic, well log, geoelectric (Prohaska, 1983; Berger, 1989) and outcrop data.

6.1. Pleistocene Mitterndorf Basin

Gravity anomalies (HG, VG) produced by density contrasts of the fluvial basin fill and underlying Neogene sediments follow the northeast to southwest trend of the basin. Available high quality seismic data in the north of the basin show that the anomalies do exactly coincide with normal faults mapped in the Neogene strata (Fig. 4 II). The coincidence of gravity anomalies with faults can be particularly demonstrated in the southern Mitterndorf Basin parts where a dense grid of well data allows an exact determination of Quaternary fault locations. Faults are mapped from the offset Top Neogene and correlated marker horizons (Fig. 6). Faults with more than 10 m vertical offsets were mapped from some 30 cross sections (Fig. 5).

The geoelectric surveys (Berger, 1989) as well as drillings demonstrate the existence of 3 major depocenters within the Mitterndorf Basin. The larger, elongated northern one reaches a maximum depth of more than 170 m, the two smaller one in the south up c. 115 and ~ 100 m, respectively (Fig. 7). The depocenters are separated by a continuous gravity anomaly which is traced over a length of more than 40 km and referred to as a cross basin fault. The absence of anomalies (Fig. 3), undisturbed lithological sequences as well as geoelectric data indicate that the central parts of the Mitterndorf basin is not affected by faulting (Fig. 6). This is also confirmed by seismic data which show that the strata in the centre of the negative flower structure below the Mitterndorf Basin appear almost undisturbed (Fig. 4, II).

However, the inferred fault pattern of the Mitterndorf Basin suggests that there is no continuous normal fault which sharply delimits the Mitterndorf Basin. The SE basin margin is characterized by a series of sub-parallel NNW-striking faults. Fault segments are arranged in a right stepping pattern and converge with the cross-basin fault. Individual faults terminate along-strike within a distance from the centre of the basin. Faults are separated by relay ramps, which are shown by the gradual increase of Pleistocene sediment thicknesses (Fig. 7). The geometry of the described faults, which may be interpreted as Riedel shears of the central basin fault, is compatible with sinistral strike-slip.

6.2. Neogene hills along the Danube in the Vienna Basin

2D seismic cross sections through the northern part of the southern Vienna Basin image the major normal fault of the Miocene Leopoldsdorf fault (Fig. 4 I) and the negative flower structure at the VBTF strike-slip fault (Fig. 4 II; Brix and Schultz, 1993). High-pass filtered gravity data highlight both faults (VG, HG; Fig. 3).

The tilt of the Rauchenwarth Plateau towards west (Fig. 9, section 3) demonstrates active normal faulting of the Leopoldsdorf Fault, which delimits the plateau to the west (Hinsch et al., 2005). However, the most prominent morphologic features of the plateau are NW striking grabens, asymmetric valleys and gullies (Fig. 9, section 1, Fig. 11). High pass filtered gravity data show a coincidence of grabens scarps and over large parts with asymmetric valleys and gullies. Anomalies appear rather weak compared to the Leopoldsdorf fault and the Vienna Basin Transfer Fault. 2D seismic sections (Fig. 4, section I) and 3D inlines demonstrate that these northwest-southeast trending scarps are related to conjugate sets of normal faults developing east of the Leopoldsdorf fault. Vertical offsets of the faults imaged in seismic are low and in the range of only 15 m. Comparisons of fault locations derived from seismic and gravity indicates that faults with even less offset may be imaged by the gravity derivatives. Density contrasts causing these anomalies may derive from lithological differences of Pannonian delta gravels and marine

fine-grained clastics (Salcher, 2008; cf. Harzhauser, 2004b). Graben systems of the Rauchenwarth Plateau develop in a complex system between the major Leopoldsdorf fault and the active, NE trending negative flower structure (Fig. 9).

Similar NW-trending gravity anomalies paralleling discontinuous (dry) valleys also occur in the Arbesthal Hills east of the VBTF (Fig. 9, Fig. 11). There, structural data indicate that these features parallel the strike of conjugate normal faults.

In sum, both seismic and structural data strongly indicate that NW-striking grabens and asymmetric valleys are fault-controlled morphologies. Fault ages are only constrained to post-Pannonian times as new evidence from drillings and heavy mineral data indicate that fluvial Pleistocene sediments are missing both at the Rauchenwarth Plateau and in the Arbesthal Hills. Recent normal fault activity is suggested by steep and distinct scarps occurring at some faults. The very minor fluvial activity in the Rauchenwarth Plateau and the Arbesthal Hills, in contrast to basin flats of the southern Vienna Basin, preserved the forms from fluvial erosion.

6.3. Eisenstadt Basin

The density of well information and the quality of seismic in the Eisenstadt Basin (EB) is not comparable to the high quality data which is available in the southern Vienna Basin to evaluate fault locations. Assessment of gravity derived fault locations is mainly based on geomorphology, outcrop data and geological maps.

However, NW- and NE-directed normal faulting is also evident from the EB. Gravity anomalies (HG, VG) coincide with some of small and several kilometres long NW striking asymmetric valleys (Fig. 3, 8). The asymmetric valley shape might be the consequence of normal faulting and half graben formation causing minor fluvial erosion of the hanging wall (Schumm and Holbrook, 1999; Fig. 9).

NW striking faults in the western parts EB are cut by NE striking faults of the Mitterndorf Basin. To the East, gravity anomalies show tectonic features striking sub-parallel to the VBTF. Gravity anomalies partly follow the drainage pattern (Wulka River, largest creek of the Eisenstadt Basin; Fuchs and Grill, 1984) and the eastern mountain front of the Leitha Mountains (Fig. 7). The eastern border of the EB to the Pannonian Basin is marked by a N- to NNE-striking gravity anomaly related to a W-directed normal fault (Rust Hills, Fig. 2, Fig. 3).

7. Active tectonics and geomorphology in the southern and central Vienna Basin

7.1. The Quaternary evolution of the Mitterndorf Basin

The fault map synthesized from high pass gravity derivatives, drillings and seismic gives a very detailed picture highlighting Quaternary and active faults in the Mitterndorf Basin and the adjacent areas (Fig. 7). Tectonic landscape evolution and its effects on geomorphology could be linked to distinct faults. The high resolution fault map available from the MB allows for a detailed analysis of basin kinematics. Faults delimiting the Quaternary basin outline a narrow and elongated basin, which is 10 km wide and 50 km long (Fig. 7). Both the NW and SE basin margins are characterized by arrays of right-stepping en-echelon faults with intervening relay ramps. Data do not support the presence of continuous basin boundary faults as previously proposed by Hinsch et al. (2005). The basin is cut by a major cross-basin fault (CBF, Fig. 7), which is traced throughout the basin along strike. The cross-basin fault and sub-parallel faults divide the basin into parts with different sediment thickness. The basin model obtained from well data (inverse-distance algorithm, Fig. 7) confirms the dip direction of faults inferred from gravity analyses. The impact of active tectonics on Quaternary landscape evolution is particularly evident from the northern part of the Mitterndorf Basin where it is delimited by a steep and straight fault scarp from the Rauchenwarth Plateau. The scarp is linked to a major fault of the Miocene negative flower structure (Hinsch et al., 2005; Fig. 4). Along this fault the MB has its highest subsidence rates causing highest sediment thicknesses

(Fig. 7) and faults with Quaternary offsets larger than 100 m. The formation of this sag pond is associated with the extensive formation of peat (cf. Havinga, 1972). Active faulting along this segment of the Vienna Basin Transfer Fault is associated with moderate seismicity ($M_{\max} = 5.2$, $I_0 = 8$; Fig. 2). Even though comparable seismic activity with earthquake magnitudes up to $M_{\max} = 4.6$ ($I_0 = 7$) is evident for the southern part of the VBTF (ZAMG, 2008), fault scarps are less prominent in the southern part of the Mitterndorfer Basin. The basin is wider and shallower in the south and it is not delimited by a single straight fault. Gravity derivatives and drillings demonstrate that the number of faults increase and the vertical offset distance per fault decreases. Instead of a single straight fault the Mitterndorf Basin is delimited by left steeping segments, or by normal faults in en-echelon alignment (Fig. 7). Normal fault displacements of the en-echelon faults increase continuously towards the basin centre.

The absence of fault scarps from the floodplain of the Mitterndorf Basin may be related to the high fluvial activity. Fault scarps, however, are also not evident from the Pleistocene alluvial fans, which became inactive between about 14 ka and the end of the Younger Dryas (about 11 ka; Salcher and Wagreich, 2008). The absence of scarps from this paleo-surface may be related to the rather low subsidence rate of approximately 0.2 – 0.5 mm/a in the southern Mitterndorf Basin. Subsidence is distributed over several faults resulting in very low vertical displacement rates for each individual fault, which may therefore be too low to exceed erosional scarp degradation. Strong anthropogenic overprint on the basin plays a further major role in scarp degradation.

Definite evidences of active fault scarping in the south are therefore rare. A straight topographic scarp (6 km in length), which coincides with a normal fault east of the Mitterndorf cross basin fault (Fig. 7; Fig. 8) delimits the Piesting River alluvial fan to the east. This normal fault, however, dips to the NW, i.e. opposite to the scarp. The morphological scarp is therefore interpreted to result from fluvial axial erosion by the Fische creek (Fig. 8, Fig. 11). NW lateral erosion of this creek is a consequence of channel migration (avulsion) towards the depocenter of the Mitterndorf Basin forcing the tributary to erode the fan surface. Channel migration and tilting of the floodplain demonstrates the higher subsidence in the basin centre.

Effects of the subsidence in the south-central Mitterndorf Basin can also be observed from the Danube's largest tributary in the southern Vienna Basin, the Leitha River. Along the low swell, which separates the southern Vienna Basin from the Pannonian Basin (Fig. 7; Fig. 8) gravity anomalies (VG, HG) highlight NE striking normal faults, which forced the Leitha River to migrate away from the Leitha and Rosalia Mountains. A consequence was the formation of low terrace scarps and abandoned meander loops reflecting river shifting towards the zone of highest subsidence (Fig. 11). Meander loops of former Leitha courses are well detectable in aerial images (Zamolyi et al., in press). These meanders postdate the Younger Dryas (Salcher and Wagreich, 2008). Terraces scarps have no direct tectonic origin as they do not coincide with faults. They mark a continuous shift of the river forced by the increase of subsidence towards the depocenter of the basin. Although a tendency of migration towards the maximum subsidence area is evident from cut off meanders and terraces, the river changes its course in its northern part leaving the MB. This changing river course is related to the confinement of the Leitha to an incised valley east of the MB (Sadezky-Kardoss, 1937).

Subsidence of the Mitterndorf Basin also has major impacts on the geometry and topographic evolution of the Piesting and Schwarza River alluvial fans. Quaternary subsidence of the southern depocenter of the MB, which coincides with the Schwarza River alluvial fan causes subsidence induced alteration of the fan surface. This is demonstrated by the flattening of the fan's contour lines around the depocenter. The generally tight, NE striking basin results in an elliptical form of the Piesting River alluvial fan. Subsidence is demonstrated by growth strata and the preservation of extensive paleosols and overbank fines (Fig. 6).

7.2. NW striking grabens and asymmetric valleys

NW striking normal faults and grabens are the most prominent morphological and tectonic features mapped in the Rauchenwarth Plateau and the Arbesthal Hills. Drillings, seismic and outcrop data show that the youngest fluvial sediments offset by these faults are of Late Pannonian age providing a maximum fault age. The structures are correlated to grabens with similar orientation in the northern Vienna Basin and the Molasse Unit (Decker et al., 2005), which partly are dated to the Early Pleistocene (Havlicek et al., 1998). NW-striking post-Miocene normal faults are also evident from the Little Carpathians (Mahel, 1972). NW striking terrestrial graben systems cross-cutting the Vienna Basin transfer fault in Moravia are dated as Plio- to Pleistocene (Knobloch, 1963; Hrubes, 1994; Hrubes and Ctyroka, 1998). The main activity of NW striking, terrestrial graben can therefore be well attributed to NE-SW-directed extension during the Plio- to Pleistocene. Seismotectonic analyses from the eastern margin of the Vienna Basin point to present activity of some of these faults (Schenkova et al., 1995).

The strong morphological impact on the Rauchenwarth Plateau and Arbesthaler Hills (Fig. 11) demonstrates that the effects of Vienna Basin's Plio- Pleistocene extensional kinematics have been widely underestimated. Other tectonic and geomorphologic features, which might be related to the same deformation, are the dominant NW-directed drainage system and caves in the Leitha Mountains (Plan et al., 2006).

8. Conclusions:

The application of the vertical and horizontal gradient of Bouguer anomaly in normal fault settings to high pass gravity data has been proven very suitable to detect surface near faults. Drillings, seismic data and the geomorphologic features have been confirmed to coincide with faults. However, principle knowledge on the basin history is necessary, additional geophysical and geological information must be used to correctly evaluate anomaly signals. Gravity derivatives highlight three dominant surface-near structural fault systems within the southern and central Vienna Basin. NE striking segments associated with the active Vienna Basin Transfer Fault along the Mitterndorf and Lasse Basin (Fig. 3, Fig. 10), short NW striking extensional faults associated with the Plio- to Pleistocene extension (Fig. 9) of the Vienna Basin (Decker et al. 1996) and a north striking system which is associated with the reactivated Miocene Leopoldsdorf fault (Fig. 3). Geomorphological features like asymmetric valleys, grabens, gullies, tectonic and fluvial scarps were found to be importantly influenced by (active) faulting (Fig. 11).

Appendix 1:

Gravity map gridding

The Bouguer gravity data is distributed very irregularly over the study area with strongly varying station intervals in different sub-regions. The average station interval is about 470 m. Therefore the grid spacing for data interpolation has been selected by 300 m. Interpolation has been performed by applying a kriging procedure.

Vertical and horizontal gradient determination for fault enhancement

It is well known that first and higher order vertical derivatives enhance anomaly features caused by shallow structures (e.g. Blakely, 1995).

This can be done efficiently by potential field transformation in the frequency domain applying FFT techniques. The transformed field quantity h can be derived by evaluating the inverse Fourier integral, where in the integral kernel appears the Fourier transform S of the Bouguer gravity g_3 multiplied by the filter operator $F(k_1, k_2)$:

$$h(x_1, x_2) = \frac{1}{4\pi^2} \int_{-\infty}^{\infty} \int_{-\infty}^{\infty} F(k_1, k_2) S(k_1, k_2) e^{i(k_1 x_1 + k_2 x_2)} dk_1 dk_2 \quad (\text{A1})$$

In eq. (A1) k_1 and k_2 denote the components of the wave number vector. Following filter operators have to be used for calculating the first spatial derivatives of the Bouguer gravity:

$$\begin{aligned} \frac{\partial g_3}{\partial x_1} : F(k_1, k_2) &= i k_1 \\ \frac{\partial g_3}{\partial x_2} : F(k_1, k_2) &= i k_2 \\ \frac{\partial g_3}{\partial x_3} : F(k_1, k_2) &= -\sqrt{k_1^2 + k_2^2} \quad \text{vertical gradient (VG)} \end{aligned} \quad (\text{A2})$$

The total horizontal gradient (HG) of the Bouguer anomaly then is calculated by eq. (A3):

$$HG = \sqrt{\left(\frac{\partial g_3}{\partial x_1}\right)^2 + \left(\frac{\partial g_3}{\partial x_2}\right)^2} \quad \text{total horizontal gradient (HG)} \quad (\text{A3})$$

First order derivatives are especially suited to enhance the anomaly features of shallow faults. This is demonstrated by Fig. A1, which displays the gravity effect of successive, vertical normal faults with different separation from each other and its first order derivatives. They were calculated by applying closed formulas for 2D fault structures (e.g. Militzer and Weber 1984, Jung 1961):

$$\begin{aligned} HG(x) &= 2G\Delta\rho \ln\left(\frac{r_u}{r_l}\right) \\ VG(x) &= 2G\Delta\rho(\varphi_u - \varphi_l) \end{aligned} \quad (\text{A4})$$

where G denotes the gravitational constant, $\Delta\rho$ is the density contrast. r_u and r_l represent the distances between gravity station and the cut off points of the hanging wall and footwall respectively. φ_u and φ_l are the angles between the positive x -axis and the corresponding cut off points (see Fig. A1).

When successive, vertical normal faults are well separated, each fault is clearly associated by a HG maximum, while the VG shows a coupled maximum-minimum feature close to the cut off points of hanging wall and footwall respectively (Fig. A1, top left panel). The signal amplitudes decrease with the depth of the fault structure. The shallower the structure, the smaller is the lateral separation of the VG extremes, which coincide if the fault extends to the surface. If the lateral fault separation is small, Bouguer gravity and its first derivatives are almost identical with the anomalies caused by one single, large fault (Fig. A1, right panels). Fig. A1 displays the situation for continuous gravity observations across the fault structure. In practise, HG and VG amplitudes are smaller due to sampling effects depending on the station interval. If the normal fault is vertical, then the VG and HG anomalies are symmetrical as can easily seen from eq. (A4). Otherwise their symmetry gets slightly broken. Nevertheless, the HG maximum remains located between the VG extremes. The position of the HG to the VG maxima can be used to evaluate the dip direction of fault (cf. Fig. A1 and A2).

Figures

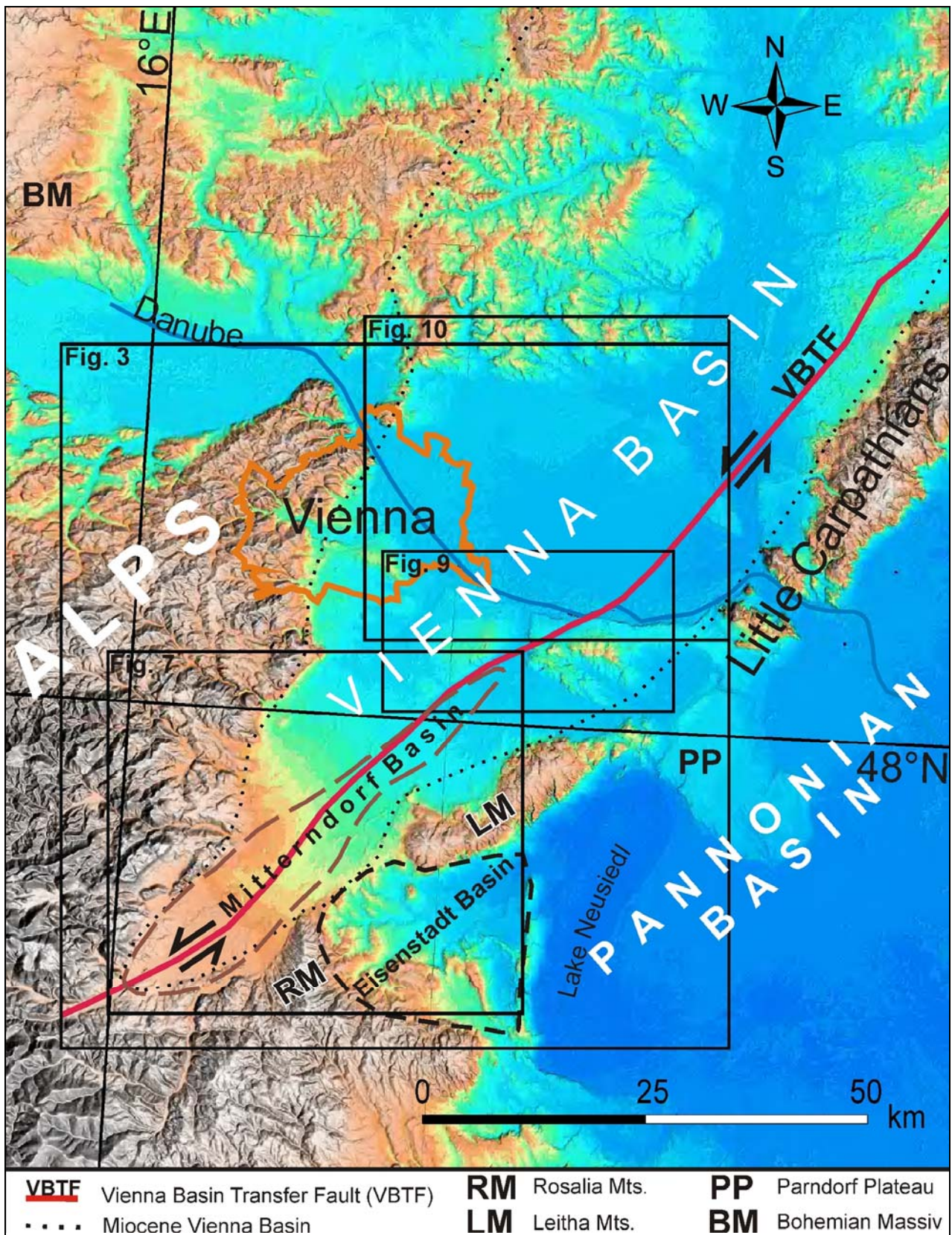


Fig. 1: Shaded DEM of the Vienna Basin and its surroundings. Boxes refer to the location of detailed maps in Figs. 3, 7, 9 and 10.

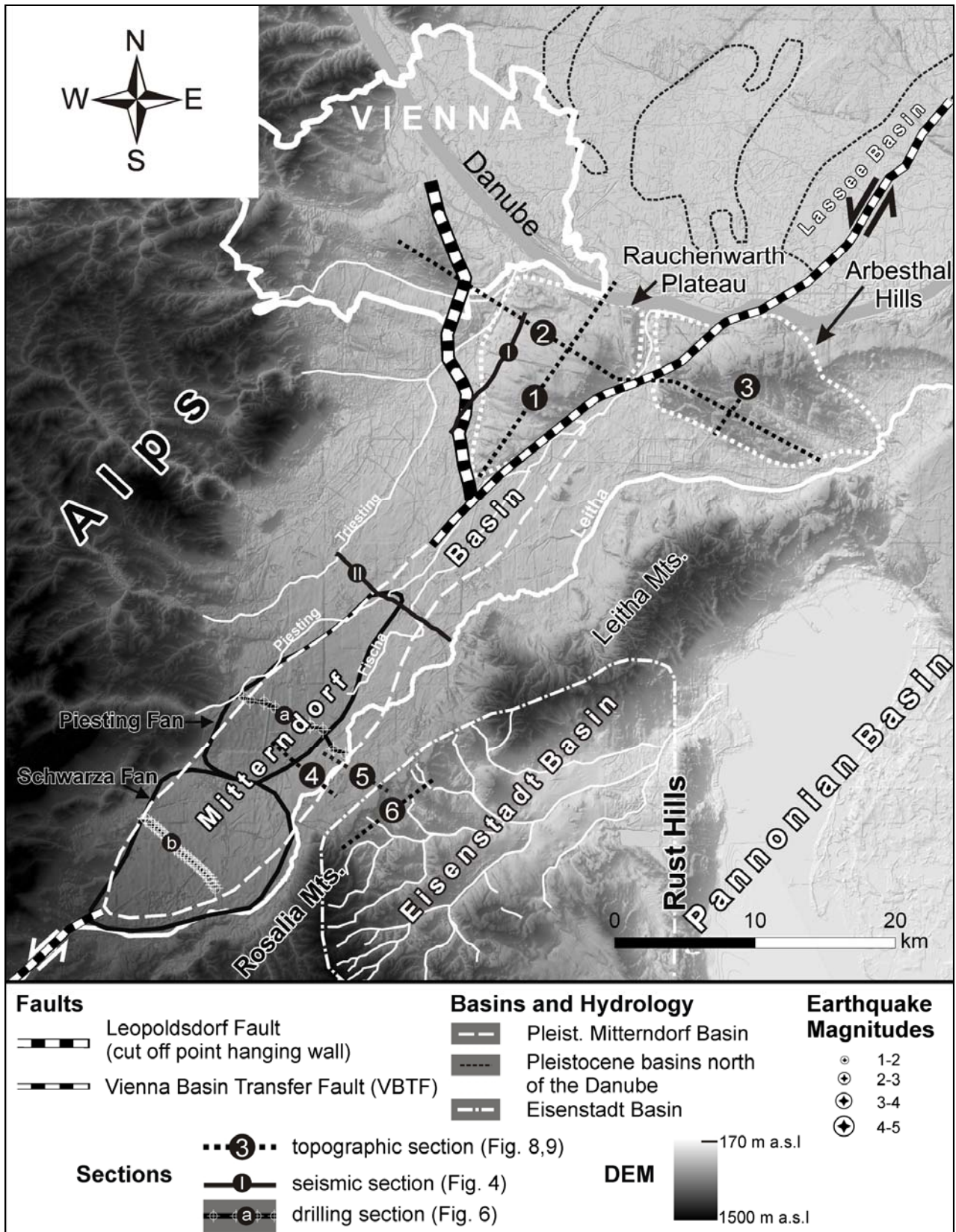


Fig. 2: Overview of the study area showing Pleistocene Basins and seismicity of the southern and central Vienna Basin. The strongest earthquakes occur along the Vienna Basin Transfer Fault (VBTF) in the Southern Vienna Basin. The Mitterndorf pull apart basin is related to a releasing band of the VBTF. Mitterndorf Basin alluvial fans formed during cold periods and are presently inactive. The Neogene hills along the Danube (Rauchenwarth Plateau and Arbesthal Hills) divide the Vienna Basin into a southern and central part. The map shows the location of topographic, seismic and well sections data.

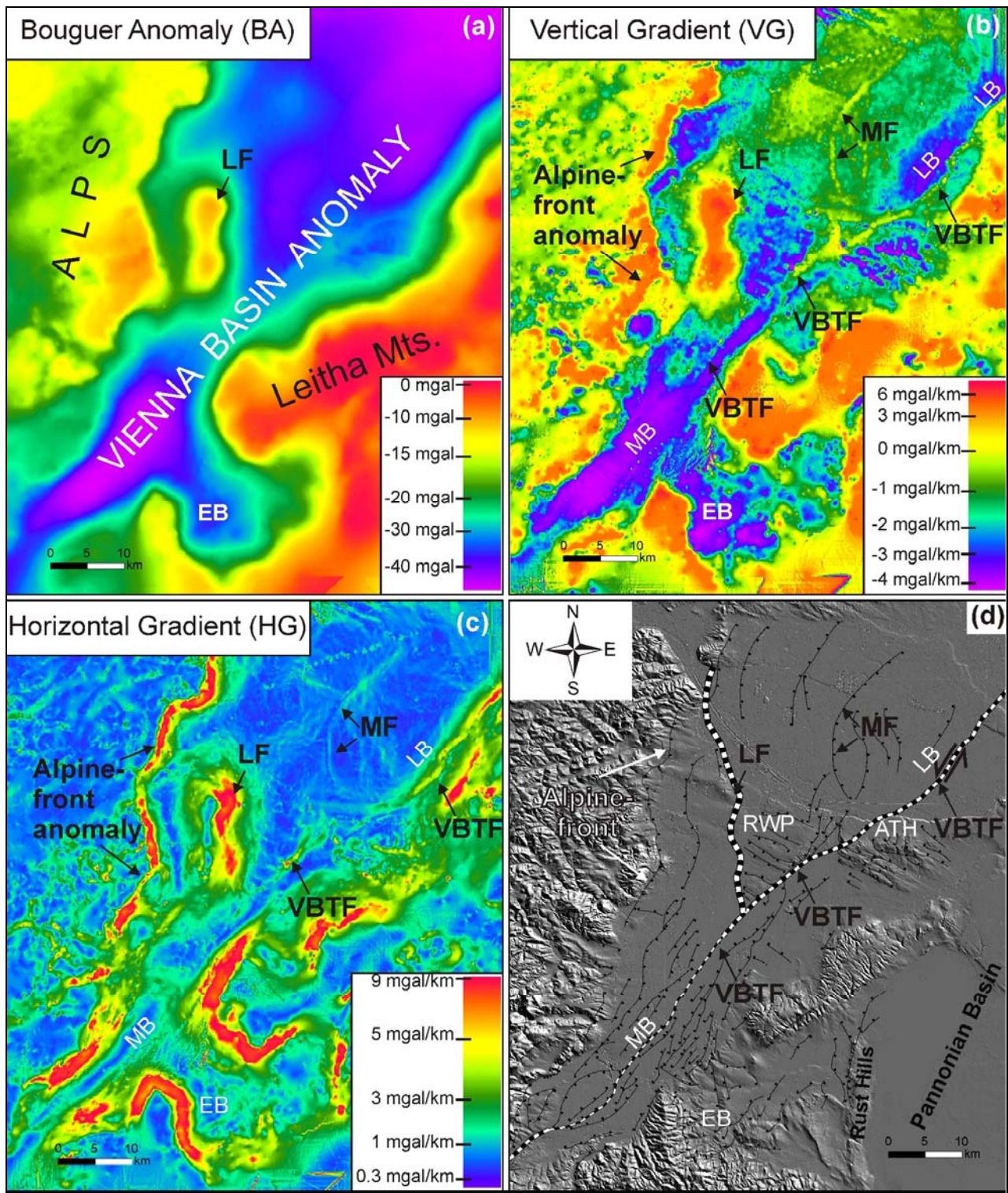


Fig. 3: Overview of the study area showing Pleistocene Basins and seismicity of the southern and central Vienna Basin. The strongest earthquakes occur along the Vienna Basin Transfer Fault (VBTF) in the Southern Vienna Basin. The Mitterndorf pull apart basin is related to a releasing band of the VBTF. The Mitterndorf Basin alluvial fans formed during cold periods and are presently inactive. The Neogene hills along the Danube (Rauchenwarth Plateau and Arbesthal Hills) divide the Vienna Basin into a southern and central part. The map shows the location of topographic, seismic and well sections.

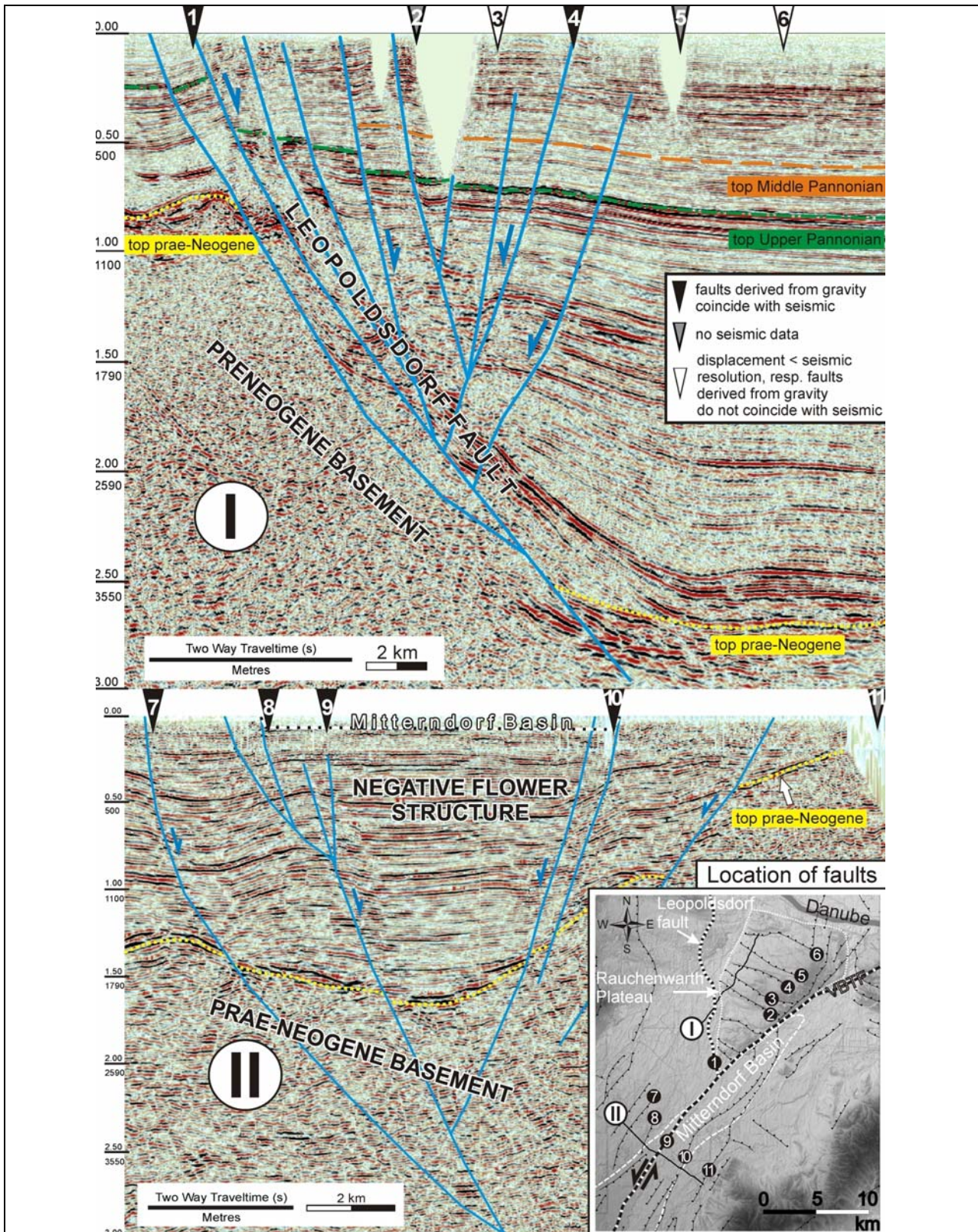


Fig. 4: Seismic sections showing the coincidence of faults derived from maximum values of the vertical gradient anomalies. (I) NE striking synthetic and antithetic faults between the Leopoldsdorf fault and the Vienna Basin Transfer Fault (VBTF). The NE striking faults reflect the dominant extensional kinematics of the Vienna Basin during the transition from Plio- to the Pleistocene. Geomorphology demonstrates the strong impact of faulting (Rauchenwarth Plateau and Arbenthal Hills, see also Fig. 8, 9, 11). (II) Synthetic and antithetic faults of the negative flower structure below the Mitterndorf Basin. Active faults are reactivated Miocene ones.

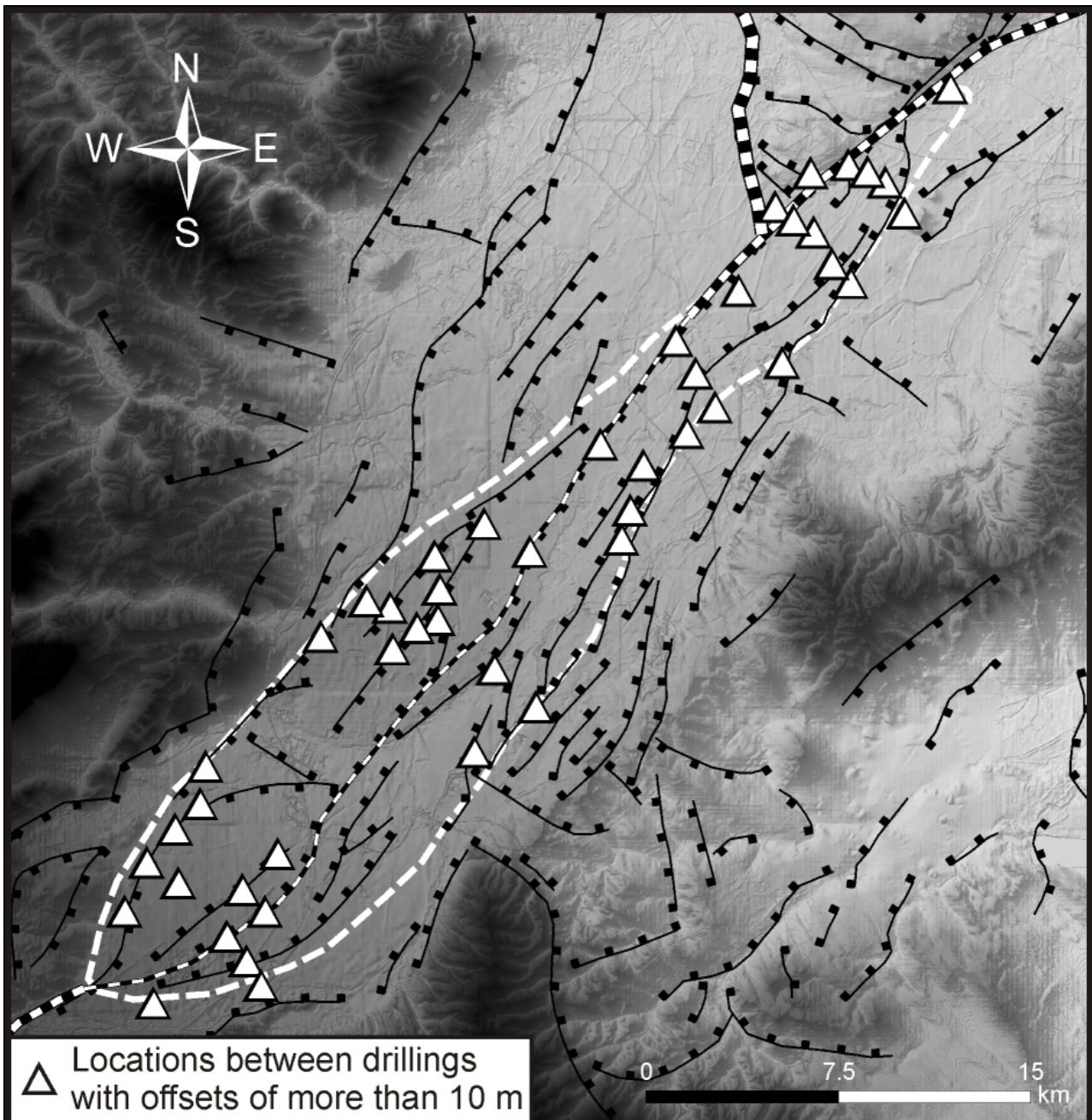


FIG 5: Fault locations in the Mitterndorf Basin obtained from the analysis of drillings (c. 300 wells). Triangles show locations of faults with vertical offsets of more than 10 m. Note the excellent correlation of faults inferred from well data with faults derived from gravity (black lines). The accuracy of the exact fault position increases with decreasing distance between drillings. Highest drilling density and highest coincidence is given in the southern part of the Mitterndorf Basin (see also Fig. 6).

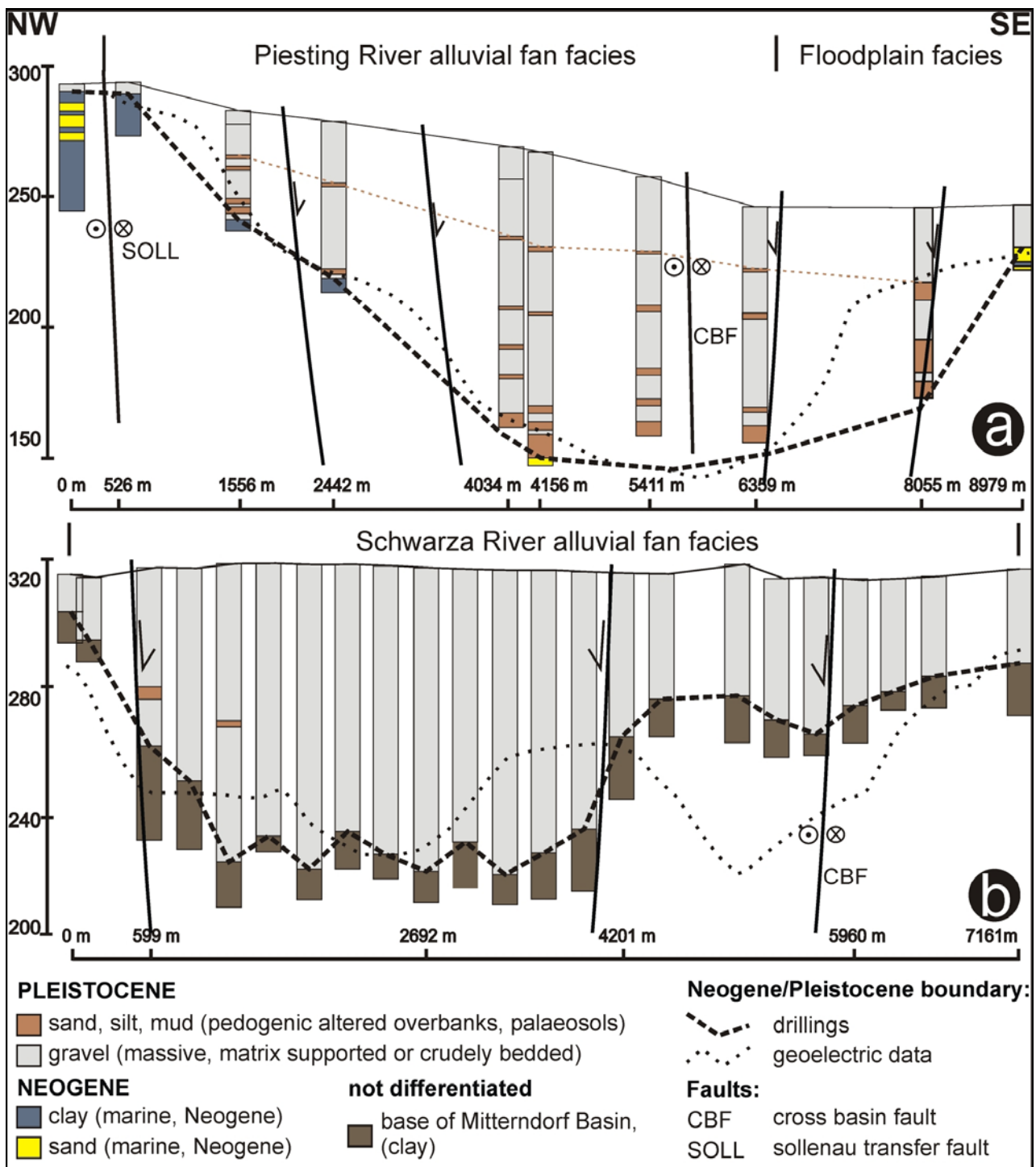


Fig. 6: Cross sections through the Piesting river alluvial fan (a) and the Schwarza river alluvial fan (b) derived from drilling. Sections show Pleistocene growth strata thickening towards the centre of the Mitterndorf Basin. Preserved overbank fines are pedogenic altered and deposited during rather warm periods, while thick gravel units reflect sheet flow dominated events during cold periods. Overbanks in Schwarza river fan were disregarded in driller's logs. Plotted fault locations are vertical gradient (VG) anomalies, demonstrating the suitability of VG data for precise fault constraint.

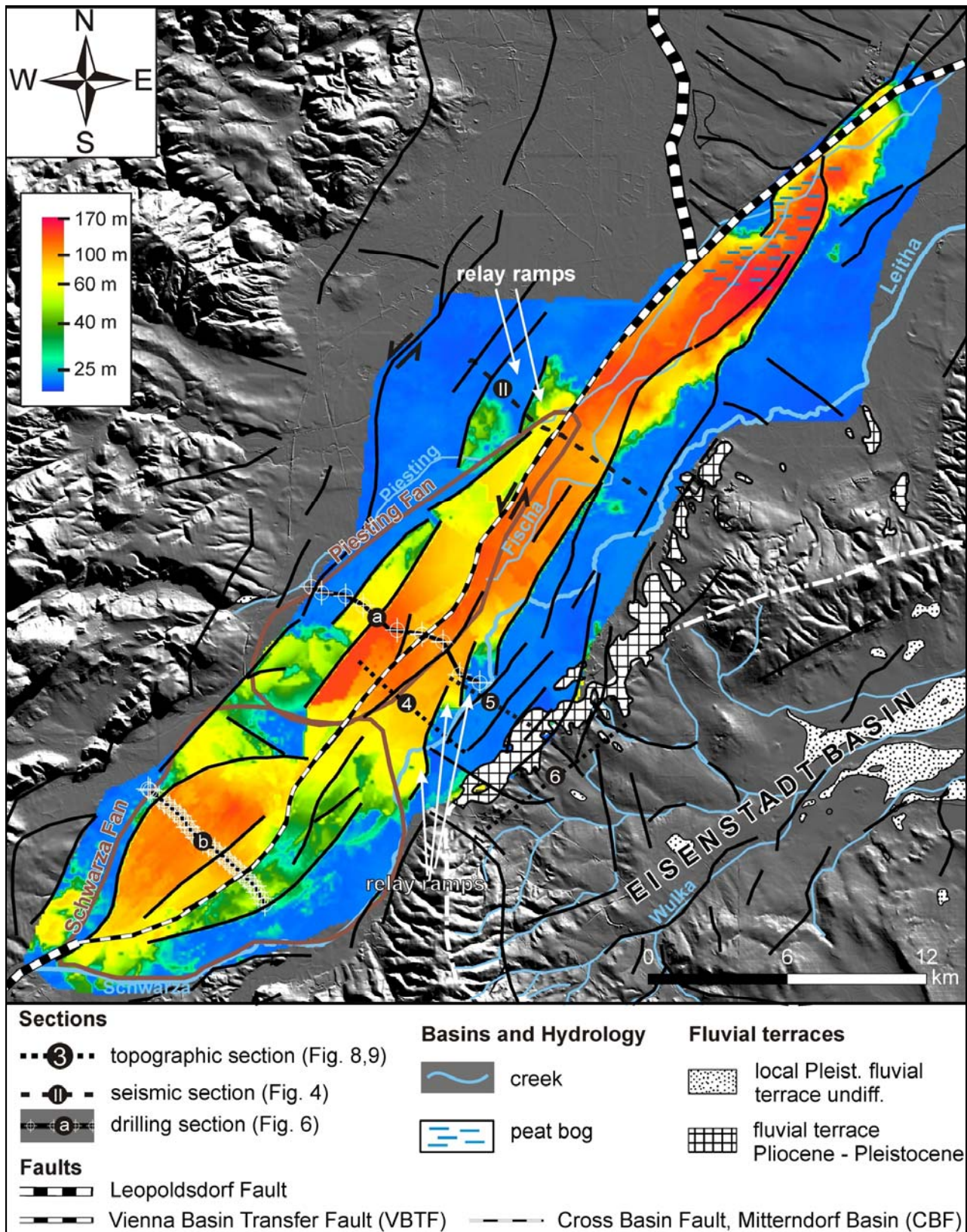


Fig. 7: Thickness map of the Pleistocene sediments in the Mitterndorf Basin calculated from c. 2000 drillings. The cross basin fault (CBF) delimits three depocenters in the NE, central and SW part of the basin. Thickness map gives an indication for the activity of the reactivated Neogene faults. Left stepping segments of the cross basin fault and left stepping relay ramps along the limit of the basin in an en echelon alignment are indicative for sinistral slip along the VBTF.

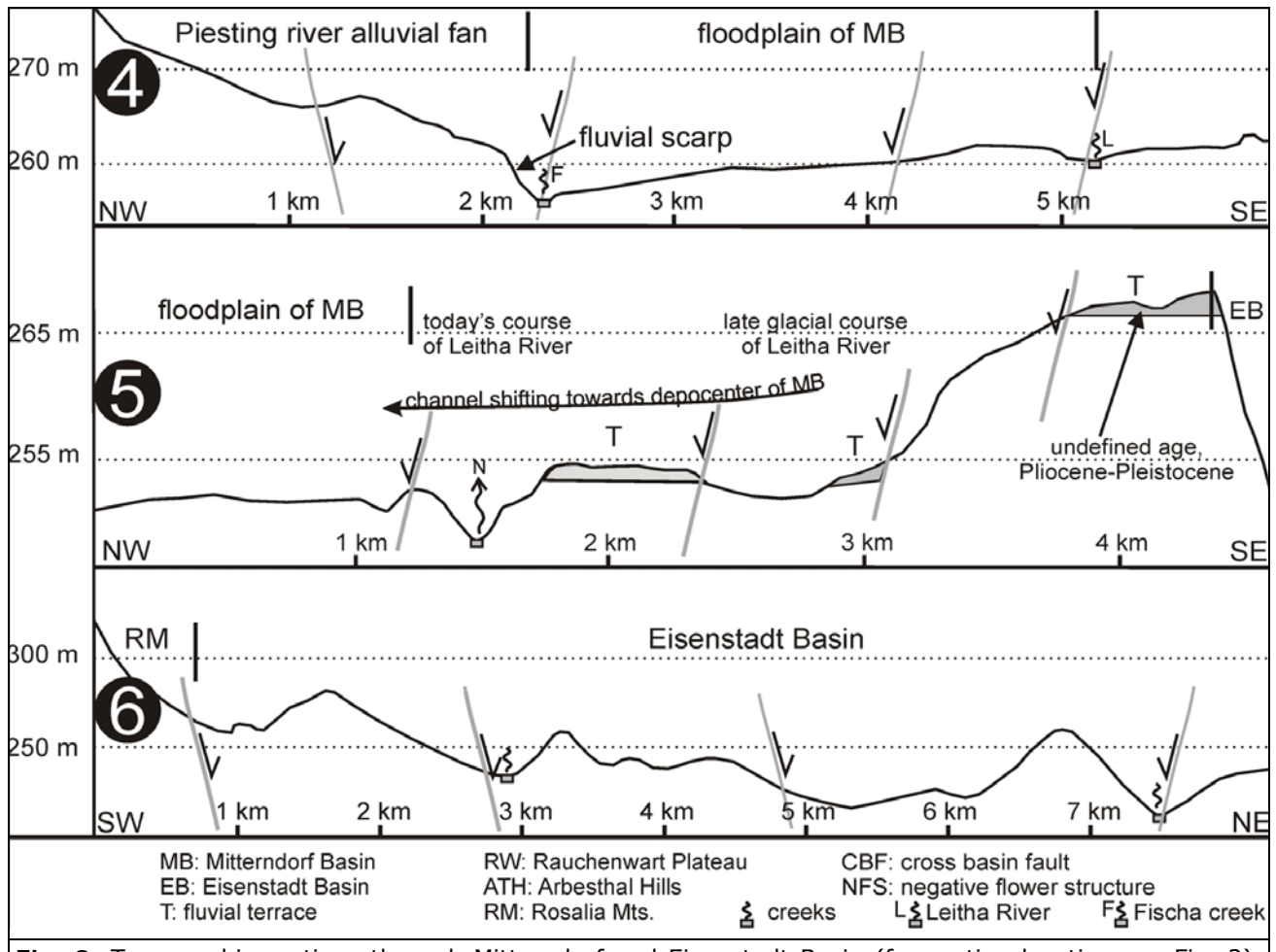


Fig. 8: Topographic sections through Mitterndorf and Eisenstadt Basin (for section location see Fig. 2). Plotted faults derive from vertical gradient maps. (4) Degradation of the Piesting River surface through normal faulting processes. Tilted floodplain of the Mitterndorf Basin forces rivers to shift towards the subsiding Mitterndorf Basin. The Piesting fan surface is limited by a fault. Erosion along this fault is the consequence of tilting. (5) Avulsion of the river Leitha (westward shift of the river channel) left terrace scarps. Clearly elevated fluvial terraces along the eastern basin limit, point to a much higher position of palaeo-rivers in the Southern Vienna Basin. (6) Coincidence of gravity derived faults with asymmetric valleys in the Eisenstadt Basin.

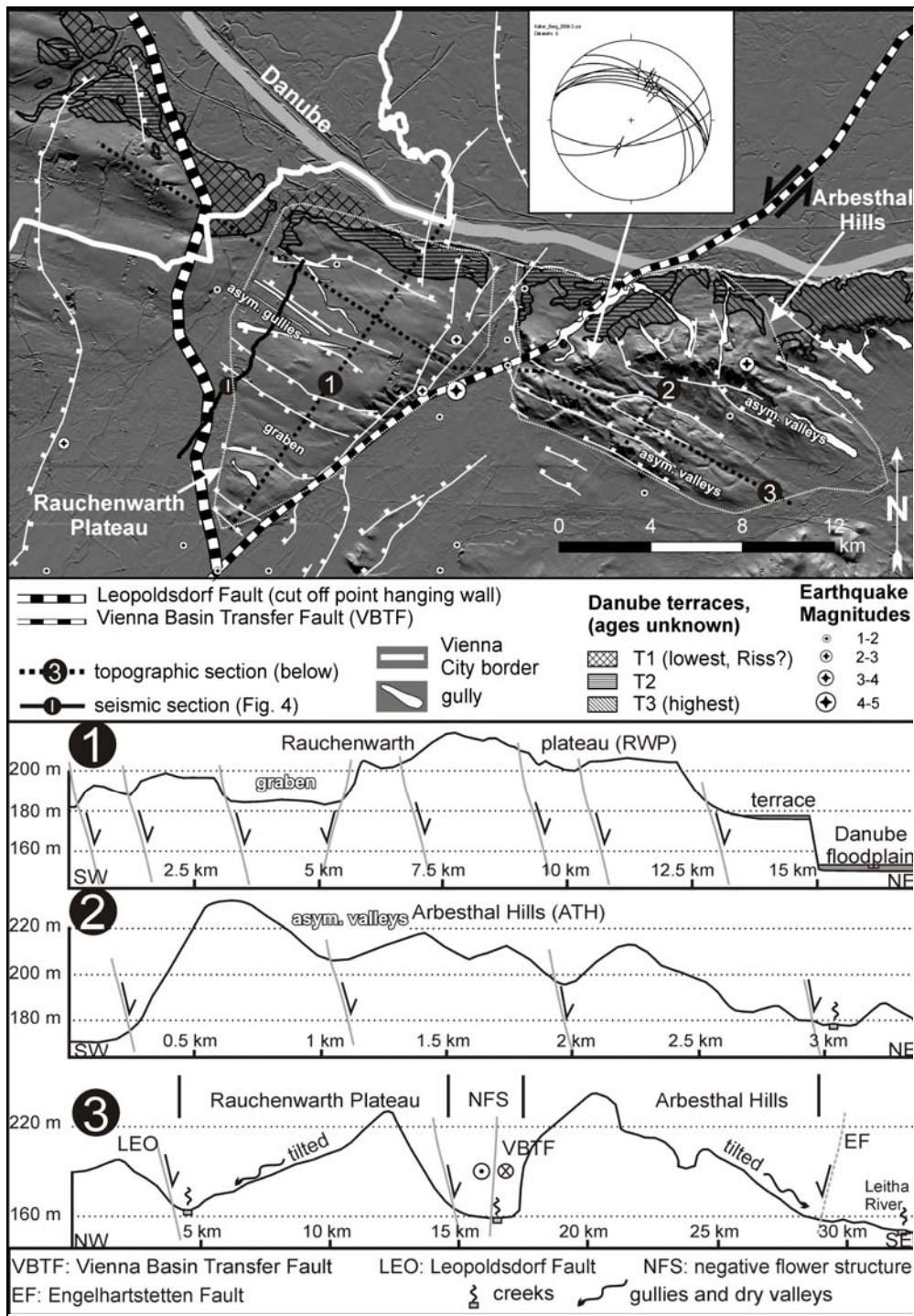


Fig. 9: Miocene (Upper Pannonian) hills along the Danube. NW striking valleys and grabens at the Rauchenwarth Plateau and in the Arbesthal Hills coincide with normal faults (1), (2). Discontinuous or dry valleys and gullies form along the faults. Fluvial overprint is marginal through very small drainage areas. The strong impact on the post Pannonian geomorphology is in accordance with the Plio-/ Pleistocene NE-SW extension kinematics of the Vienna Basin as shown by fault slip data from the Arbesthal hills (Schmidt's net lower hemisphere projection). (3) Active faulting is evident from the Leopoldsdorf fault causing westward tilting and drainage to NW. Arbesthal hills tilt to southeast caused by the activity of the Engelhardtstetten fault systems limiting the basin from the Leitha Mts. and little Carpathians. Inaccuracies due to the density interval of gauging station interval are in the range of up to max. 300 m.

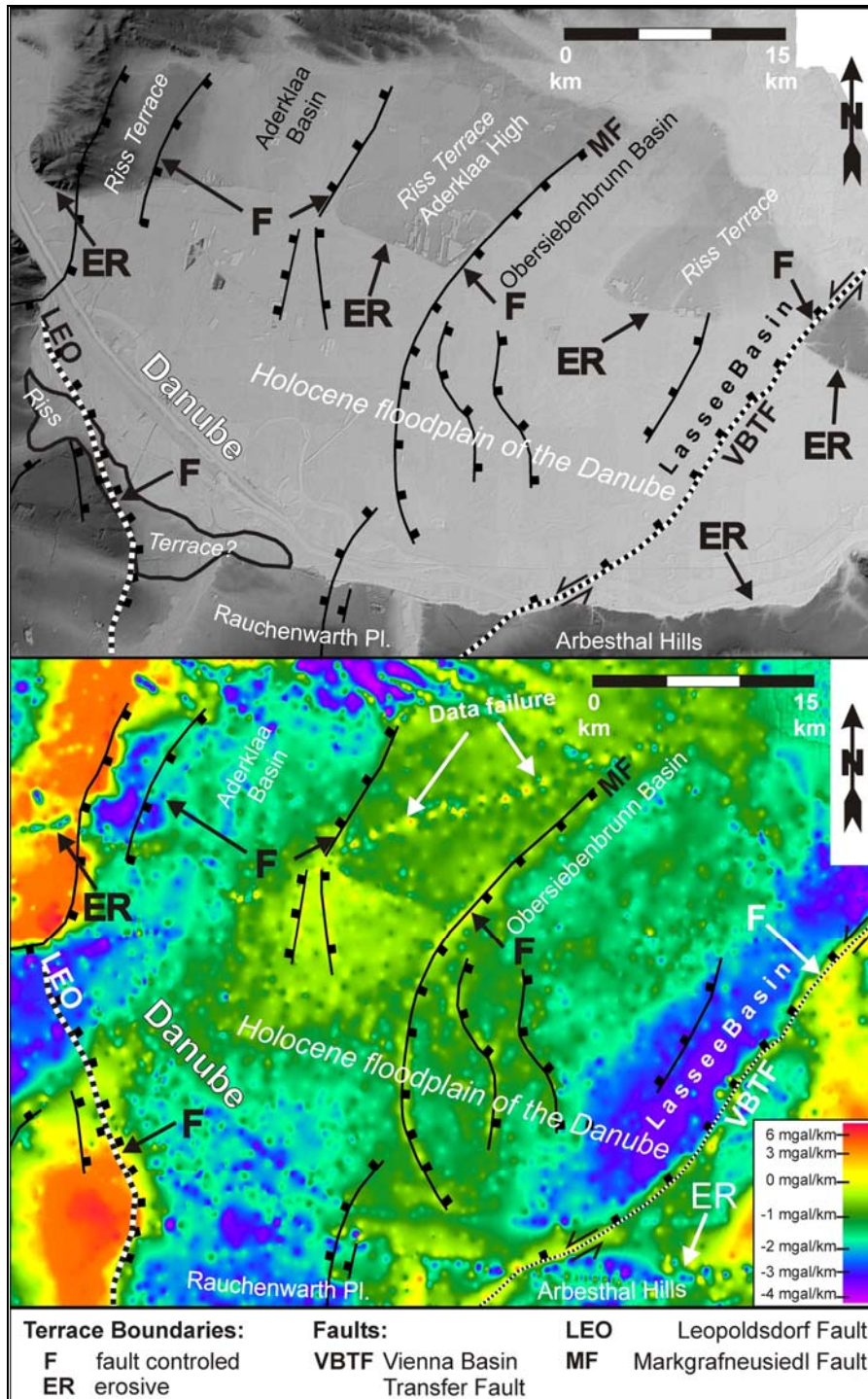
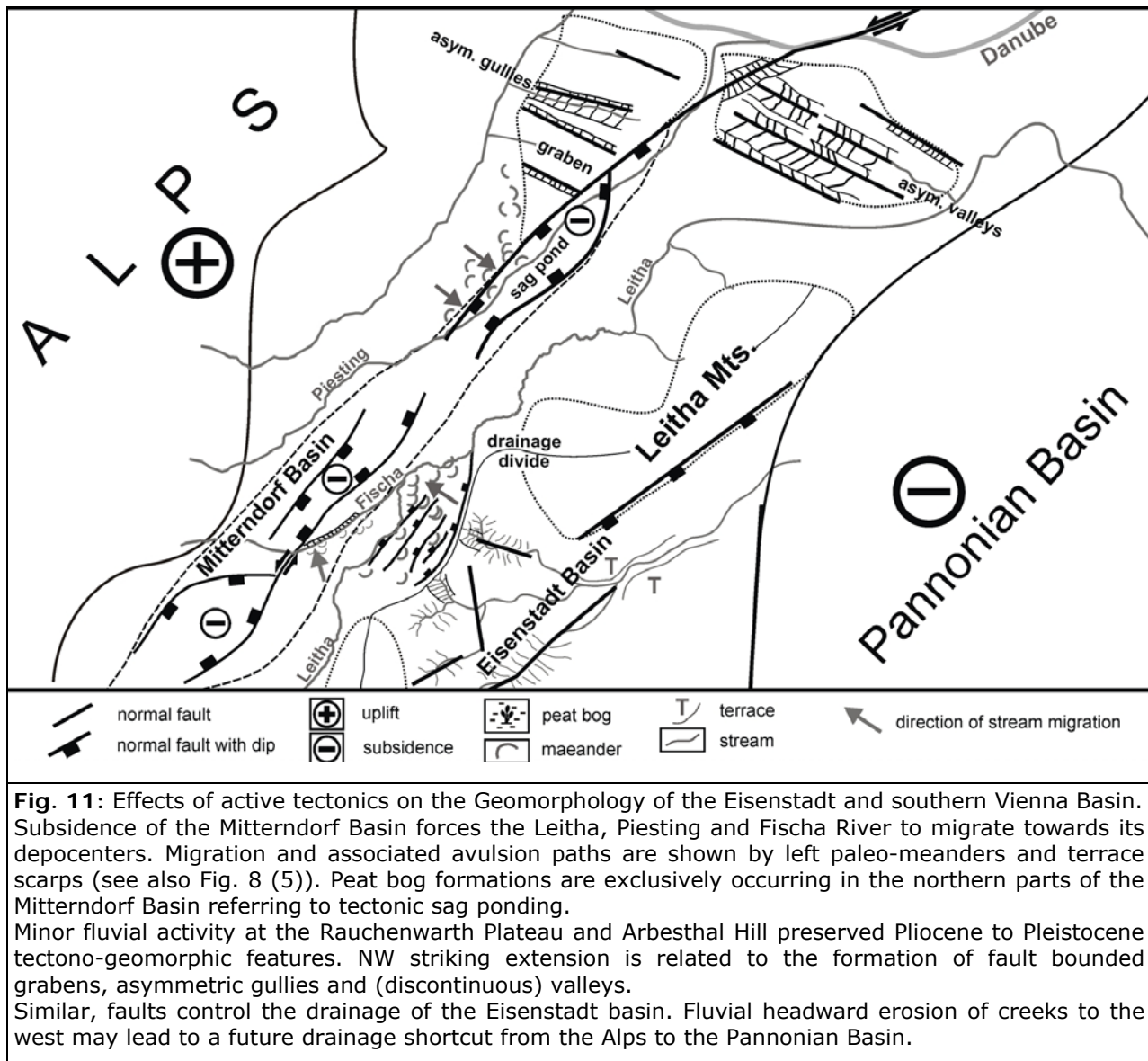


Fig. 10: Pleistocene Basins north of the Danube. Plotted gravity derived faults (F) coincide exactly with north and northeast striking terrace scarps north of the Danube supporting their tectonic origin. Terrace boundaries along the Leopoldsdorf fault south of the Danube suggest ongoing normal faulting. The fluvial activity of the Danube eroded large parts of the terraces leaving erosive scarps (ER). Below: Anomalies of the vertical gradient (VG). Subsidence of Pleistocene Basins and their "light" fluvial infillings in contrast to the underlying compacted, Neogene strata produce strong differences in density (e.g. Markgrafneusiedl fault, modified after Decker et. al. 2005). Note the strong anomaly of the up to c. 100 m deep Lassee Pleistocene Basin along the Vienna Basin Transfer Fault (VBTF) which extends into the Slovakian Republic (Zohor graben).



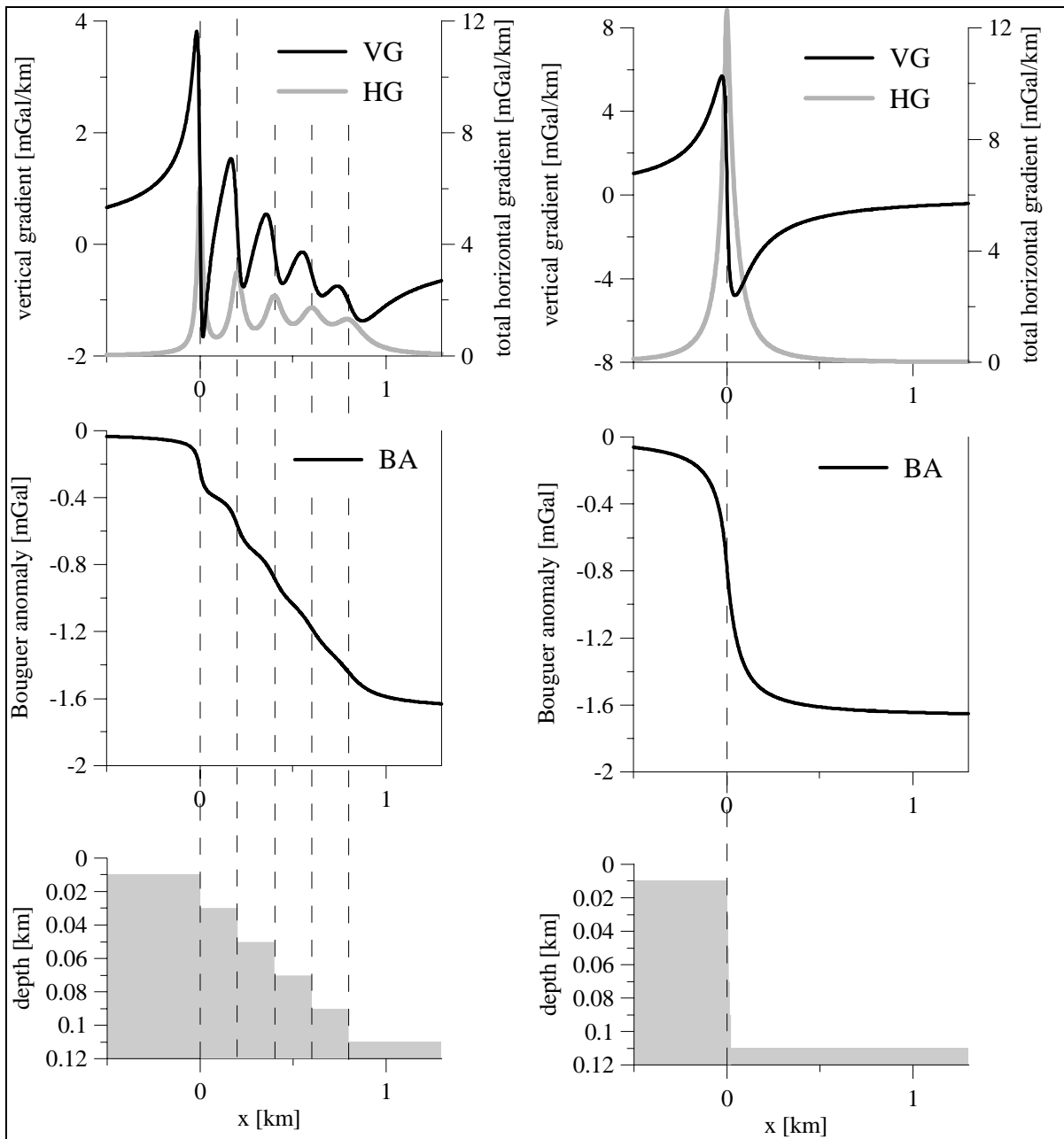


Fig. A1: Synthetic case study showing successive, vertical normal faults (bottom panels, note vertical exaggeration) and their images in Bouguer gravity (middle panels) and in the vertical (VG) and total horizontal (HG) gradients (top panels) at the 0 m level. The density contrast is -400 kg/m^3 . See text for explanation.

Numerical modeling of factors controlling sequence development of Pleistocene alluvial fans, Vienna Basin, eastern Austria.**Abstract:**

Tectonic, climate and base-level related factors are the main controlling factors on alluvial fan development and evolution. In this study a numerical model approach was used to investigate climate induced aggradation and degradation cycles, the influence of tectonic subsidence, and the impact of an axial main river on Austria's largest Pleistocene alluvial fan setting, the Mitterndorf Basin in the southern Vienna Basin, eastern Austria. A simulation time frame of 25 ka was applied. Climatic variations were mainly modeled through variations in sediment supply, whereas the impact of subsidence was modeled through variations in slip rates along faults. Incision and aggradation tendencies of the axial main river were modeled by a lowering of the water level.

Sequence development and geometry of the two modeled alluvial fans are mainly controlled by Pleistocene climate oscillations but also by subsidence and changing level of the axial main river. Cold periods generally led to a decrease in vegetation cover and to an increase of periglacial weathering processes causing abundant sediment supply and aggradation on fan surface. In contrast, decreasing sediment supply and increasing precipitation during warmer periods led to fan incision, to a decrease in accumulation space and to changes in river pattern. Our models show that adjustments in sediment supply mainly impact alluvial fans evolution. Climate is found to be the main control factor on the alluvial fan development. The impact of subsidence and influence of the axial main river becomes important during simulated warm periods.

Keywords: alluvial fan, climate, Pleistocene, subsidence, numerical modeling

1. Introduction

Tectonic, climate and base-level related factors are generally assumed to act as main influencing factors on alluvial fan development (Bull, 1977). Climatic factors control sediment supply and runoff power from the catchment. Therefore, the discharge to sediment supply ratio influences whether fans undergo aggradation or degradation (Wells and Harvey 1987). Similarly, if fans toe out on unstable base levels, response may cause incision or fan aggradation.

Climatic induced sediment supply is supposed to be the primary control on alluvial fan sequence development (e.g. Harvey 2002a, Harvey 2002b, Harvey 1999a), especially during the Pleistocene where distinct oscillations have a large and fast influence on sediment supply to discharge ratio (e.g. Vandenberghe; 2008, Bogaart, 2003; Vandenberghe 2002, Van Husen, 2000). The significant impact of Quaternary glacial-interglacial cycles on alluvial sequence development in a basin-scale has been described by Shanley and McCabe (1994), Weissmann et al. (2005). A depositional model for Austria's largest Pleistocene basin at the time span between MIS 3 to MIS 1 has been presented by Salcher and Wagreich (2008).

However, during warmer periods when base level and tectonic changes relatively increase their influence on the system; mutual interactions of all controlling factors are complex. To better understand these interactions we choose a numerical model approach which was used to simulate the landscape evolution during the last glacial/interglacial cycle.

Multi-process landscape models which consider two or more mutually interacting geomorphic processes have a widespread application in literature covering processes like fluvial transport of sediment, weathering or landsliding (e.g. Tucker and Slingerland, 1997; Willgoose et al., 1991). Numerical models which focus on the morphologic or sedimentologic evolution of alluvial fans in time were carried out e.g. by De Chant et al. (1999) and Allen and Densmore (2002), respectively.

In our study a numerical model approach was chosen to simulate the relevance of Quaternary climate fluctuations, subsidence and base level change on two stream

dominated mountain front fans, which are linked to Austria's largest Pleistocene Basin. The principle knowledge on the regional climate and basin evolution (Salcher and Wagreich, 2008; Salcher et al. 2008) better helped to calibrate a reference model from which alterations in sediment supply, subsidence and elevation change of the axial main river were observed. A series of numerical experiments simulate fan build up, the mutual interaction of fans and their degradation in time.

Numerical experiments covered a time frame of 25 ka. Decrease in vegetation density and increase in weathering was modelled through an increase of sediment release to the basin, causing fan aggradation (cf. Leeder et al., 1998; Bull, 1996; Bull, 1991). In contrast warmer periods are associated with increased precipitation, reduced weathering and a higher vegetation density around the study area (Van Husen, 2000). This scenario was modelled through a continuous reduction in sediment supply leading to higher discharge to sediment supply ratios and associated stream incision and fan abundance. Consequences of subsidence on fan development during times were simulated via changing slip rates along faults. The role of Austria's largest river, the Danube, as base level for all tributaries of the study area was modelled via simulation of a low and a high water level.

2. Regional Settings

The Vienna Basin Transform fault is an active fault system extending from the Eastern Alps through the Vienna Basin into the West Carpathians. The rhomb-shaped, SW-NE trending Miocene Vienna Basin extends about 200 km. The Danube River divides the basin into a northern and southern part, which are further divided into several Quaternary sub-basins. Active deformation is related to these sub-basins (Fink, 1955) of which the largest is the Mitterndorf Basin. This sub-basin is supposed to be a strike-slip duplex (Decker, 2005) which evolved since early to middle Middle Pleistocene. The Mitterndorf Basin has a maximum width of not more than 15 km and a length of about 60 km (Fig 1). The northern part of the basin is very narrow (< 2 km) and filled with fluvial gravels up to 170 m. Two mountain front alluvial fans are filling the southern Mitterndorf Basin with up to 110 m of massive gravels. Both fans are stream dominated and comprise mainly sandy, coarse fluvial gravels largely comparable to the Scott-type braided river model (Miall, 1977). These gravels are related to aggradational responses associated with cold periods (Küpper, 1950) due to a significant decline in vegetation cover. Paleosols encountered in numerous drillings are indicating periods of undisturbed soil development on fan surfaces during warm periods. The youngest aggradational event on both alluvial fans could be constraint to the MIS 2 cold period (Salcher and Wagreich, 2008). Aggradation ended around c. 12 ka. Currently no active deposition occurs on both fan surfaces. The Piesting River alluvial fan (Piesting fan), at the western margin of the basin sizes about 88 km², the adjacent, southern Schwarza River alluvial fan sizes (Schwarza fan) about 120 km². Schwarza fan is confined filling the southern part of Mitterndorf Basin. The drainage area of the Piesting fan covers approx. 280 km², with highest elevation of 1723 m above sea level and elevation of fan apex of 310 m above sea level, median gradient is 0.28°. The drainage area of the Schwarza fan covers about 670 km², with highest elevation of 2076 m above sea level and fan apex of about 370 m above sea level. Weak glaciation (several sq km) of highest points during Pleniglacial is evident in the Schwarza drainage basin (Van Husen, 1987).

3. Modeling Software (WinGeol/SedTec) and data preparation

WinGeol/SedTec is a finite difference code based on WinGeol (TerraMath 2001-2008). The software was firstly presented on the ENTEC (Environmental Tectonics) spring workshop 2002 (cf. Faber and Wagreich, 2005) There is no connection to the SedTec Modeling Group (Royal Holloway University, UK) and the software SedTec2000, which was published in 2002 (Boylan et al. 2002). For this study WinGeol/SedTec version 1.2x was used.

The primary application of the multi-process landscape stratigraphic forward modeling software WinGeol/SedTec is focused on erosion / transport and sedimentation of clastic material in a basin wide scale including the sediment source area in dependency of climatic changes and vertical tectonic movements (cf. Slingerland et al. 1994). Temporal changes of environmental conditions are supported using time tables, which store changes of sediment supply, precipitation, base level and vertical tectonic displacement. The modeled stratigraphic record is saved at the end of each time step. Erosion rates are user defined and can be set for each individual rock type. Initially a rock is defined as a rigid block which becomes partially scattered by weathering processes. As soon as the components are loose, it is possible to transport them. The transport distance within a certain time (dt) depends on the local situation (composition, slope, friction, presence of a fluid). As this approach supports different speeds of transportation, the transport path within dt can be considerable longer than just to the next neighboring cells of the grid based surface.

In WinGeol/SedTec a strict separation of data structures / associated methods and modeling functions/methods is given. This is necessary to shorten debugging times, readability of code and allow later integration of functional extensions.

The software support 3 D visualizing of all model results together with a wide range of geological data like well logs (stratigraphy, geophysical), digital elevation models, geological maps, vector data (river networks, triangulated faults) and dip maps. For documentation purposes virtual wells can be created and during the simulation the development can be monitored using user defined control points, where the fitting to log data is continuously reported.

3.1. Definitions

Source cell

A Grid cell from which material is taken.

Target cell

A grid cell which receives material from a source cell.

Time step

A time step represents a number of calculation cycles after which the actual state of the simulation is saved. In the presented study all time steps have identical durations (3125 years). After the end of a time step new sediments are stored within a new grid layer.

Calculating cycle

Each time step consists of numerous calculation cycles. During a calculating cycle all cells of a model are processed at least one time.

Process sequence order

Defines the sequence in which the single cells of the model are processed (for explanations see section 3.2.1).

3.1. Data structure

WinGeol/SedTec models are derived from grid data and is therefore based on equal spaced cells in x and y direction whereas z dimension is variable. The smallest unit of a model is called a cell. A cell itself is defined as a volume with no internal structure. The number of cells is given by the number of rows and columns and multiplied with the number of time steps. Additionally, a further layer is used as temporary storage for not yet deposited material. Every cell stores a number of variables which are divided into two groups:

- Condition: State variables like local flow, vertical tectonic offset, cumulative erosion and sedimentation, local temperature
- Material content (grouped by material and grain size (if a grain size reduction algorithm is used), water is stored as solid or fluid without further separation)

All values are stored internally as 4 byte floating point values.

The structure was chosen because of its simplicity, good performance and because most of the input data is derived from grid based data, which simplifies data handling.

Important consequences of the data structure for the simulation are:

- Each cell has 8 neighbors on the topographic surface and just 8 possible directions where a material flow can be directed to. WinGeol/SedTec distributes sediment to the two grid cells which are closest to the maximum dipping direction (section 3.2.3.1 Determining transport direction)
- A fixed minimum resolution in x and y direction: Transport distances are always a multiple of the cell size (the sediments might be distributed on several targets cell proportional to the transport distance)
- Tectonic is limited to a 90° vertical displacement as cells are fixed to their x and y position.

3.2. Data structure related methods

These methods are functions which help to administrate the model. Low level functions are necessary for the basic management like initialization, resetting, scaling or splitting of cells. Medium level functions retrieve or set values which describe the relationship between two or more cells (e.g. calculation of difference matrices, finding the lowest neighboring cell, retrieving the status of a neighbor). Functions which affect more cells than the direct neighbors (like path of transport) are the high level functions of this library.

These functions do not decide if / where and how much is eroded / moved or deposited – this is the task of the algorithms introduced in section 3.3. Nevertheless, these functions have a direct influence on the results and should be mentioned therefore.

3.2.1. Process sequence calculation

Processes in nature are occurring more or less parallel with or without dependency to each other. As long as processes do not interact (spatial or temporal separation) there is no conflict. If interaction is needed, a ranking method is needed to determine which cell will be processed first (process sequence sorting): Cells might be sorted by their topographic elevation, by slope – assuming that movement will start in the steepest areas first - or by using a random sequence. Simulations in this study used sorting by topographic elevation algorithm.

3.2.2 Determining the transport target

Transport direction is determined by (a) the evaluation of the neighborhood matrix and calculation of the dipping direction and (b) by adding a movement vector from prior calculation cycles.

Based on the elevation matrix of the nearest neighbors the direction of steepest dipping is calculated. The lowest neighbor cell and its direct neighbors are evaluated, whereby it is assumed that the dipping direction is located between the steepest the lowest cell and its lower neighbor. As the grid allows just discrete positions the dipping vector (Fig. 2: black vector) is split up into 2 components pointing to the nearest 2 grid cells (Fig. 2: Target 1: lowest neighbor, target 2: lower neighbor of target 1). In case that from a previous calculation step a movement vector has to be considered, this vector is added to the dipping vector before the resulting vector is split up into its components. The lengths of the single vectors are calculated by algorithms introduced in 3.3.3 (Transport distance and speed).

3.2.3 Support for velocity modeling - Out of Order Processing

During a calculation cycle, each cell of the model is processed one time. During this operation the cell is allowed to shift a certain amount of material to one (or more) of the

neighboring cells. Even if the used transport equation returns different volumes depending on the situation, the speed of transport stays constant. To model different velocities, a target cell has to become itself a start cell just after receiving material from the previous cell. The cycle will be repeated until a certain amount of time is consumed (e.g. end of processing time) or the speed drops under a minimum value. As these cycles are not in the sequence of the normal processing it is called "out of order processing". It can be assumed that material from a source cell will be moved to all lower cells. However, WinGeol/SedTec supports only one target cell per move (the second ranked target cell will be processed the next time the cell is accessed). Multiple target cells would lead to a huge increase of calculation time as every cell has 8 direct neighbors. In average 4 of them will be of lower elevation. Processing time would increase approx. with the factor 4^n , where n is the average transport distance (unit is cell size; Fig. 3).

3.2.4 Transport path

The used transport equation (section 3.3.3) is solved by approximation for a given distance (average distance to the neighboring cell center). In case that the required time is smaller than a processing time step, the operation is repeated until the whole processing time duration is consumed. If the time interval is too short to move the transported mass to the target cell, it is split into two fractions ($f_{\text{source}} = \text{distance}/\text{distance_to_target}$; $f_{\text{target}} = 1 - f_{\text{source}}$).

3.2.5 No data areas and model boundaries

No data areas and model boundaries are treated in the same way. In both cases no information about elevation and material is available. WinGeol/SedTec estimates the local slope to the no data area by extrapolating the slope from the opposite neighbor to the central cell to avoid unrealistic effects like incision or damming at the model boundary.

3.2.8 Time dependent behavior

WinGeol/SedTec supports time dependent environmental changes like sediment supply factor, precipitation, tectonic (vertical) movement and base level fluctuations. The values are read from ASCII tables (separate one for tectonic) and are interpolated linear.

3.3 Algorithms

3.3.1 Regolith production

Regolith production is mainly controlled by climate and the production rate decays exponentially with regolith thickness, as the lower lying material is more and more covered by the overlying fresh regolith. According to Anderson and Humphrey (1990) the following equation was used:

$$E_w = k_w e^{(-R/R_0)} \quad (1)$$

E_w	rate of descent
k_w	original bedrock weathering rate (at surface)
R_0	thickness of regolith where weathering rate is equal to $1/e k_w$
R	regolith thickness

Weathering rates for different rocks are given for example in Allen and Allen (2005).

3.3.2. Erosion

In WinGeol/SedTec erosion is modeled using two different approaches. Hill slope erosion is implemented using the diffusion equation. Fluvial bed rock incision is processed by using the stream power approach.

3.3.2.1. Diffusion

From observation it is known that erosion is proportional to local slope – steep mountains erode much faster than plateaus (Culling, 1960; Andrews and Buckham, 1987). To describe this observation the diffusion equation can be used (Allen and Allen, 2005):

$$\frac{\delta q}{\delta x} = -\rho_b \frac{\delta z}{\delta t} \quad (2)$$

$$q = -k \frac{\delta z}{\delta x} \quad (3)$$

q	mass flow (discharge of mass per unit width)
ρ_b	bulk density of moved regolith
k	transport coefficient
δz	elevation difference
δx	horizontal distance
δt	time interval

Combining formula (1) and (2) mass diffusion is written as:

$$\frac{\delta z}{\delta t} = \kappa \frac{\delta^2 z}{\delta x^2} \quad (4)$$

$$\kappa = k / \rho_b \quad (5)$$

κ diffusivity

The transport coefficient is material dependent, in case of bedrock material, whereas for material in state of transport it is calculated from the volume ratio fluid to solid components (as a rough estimation).

$$k = m(V_{fl} / V_{sol})^n$$

Denudation rates for European river basins were estimated to be in the range of 20 to 100mm / ka for the last 10 ka (Schaller et al., 2001). These values may be used for estimating the diffusion rate D.

3.3.2.2. Bedrock incision, stream power rule

Stream power can be calculated using following approach (Allen and Allen, 2005):

$$P / dx = \rho g Q dz/dx \quad (6)$$

$$Q = C_r AR \quad (7)$$

P/dx	stream power per length of channel
Q	discharge
ρ	density
C_r	run off coefficient
A	drainage area
R	precipitation

The stream power is proportional to slope and discharge. Bedrock incision was included in the form of a power law of equation 6:

$$\frac{\delta z}{\delta t} = -c_b Q^m S^n \quad (8)$$

S slope

c_b bedrock incision coefficient
 m, n empirical coefficients

According to Stock and Montgomery (1999), reasonable values for c_b are:

Mudstone 0.007
 Granite 0.000006

In our models m and n were set to 1. Incision is therefore linear, proportional to stream power. Q is the product of drainage area size & Precipitation. WinGeol/SedTec stores the current discharge value in every cell. It is updated every time the cell is affected by a transport process.

3.3.3. Transport distance and velocity

The velocity of the mass flow is essential for calculating time of deposition: Flow rate Q and the height of the sediment stream h , together with processing time step length Δt can be used to calculate the transport velocity.

$$v = Q / (h \Delta t) \quad (9)$$

In case that we assume that the transport velocity depends on:

v_0 initial velocity
 a acceleration (due to gravity)
 F friction

The velocity of the sediment stream can be written as:

$$v = v_0 + a \Delta t - F \Delta t / m \quad (10)$$

To model friction, two formulas are used: F_S (sliding friction) and F_K (kinetic friction - Stokes law is used as rather low velocities can be expected)

$$\begin{aligned} F &= F_S + F_K \\ F_S &= F_N \mu \\ F_K &= 6\pi\eta r v \end{aligned}$$

$F_N = m g \cos \alpha$
 μ friction coefficient
 m mass
 η dynamic viscosity
 g gravity constant
 r particle radius
 α slope

F_S is velocity independent, whereas F_K is velocity dependent. As shown by Amy et al. (2005) and Krieger and Dougherty (1959) the viscosity of fluid particle mixtures depends to a great extent on the ratio between the volume of the particles and the volume of the fluid. At low concentrations of particles the viscosity increases very minor and approximately linear (Fig. 4):

$$\begin{aligned} \text{visc} &= c (\text{visc}_{\text{Wat}} V_{\text{Wat}} + \text{visc}_{\text{Sed}} V_{\text{Sed}}) / (V_{\text{Wat}} + V_{\text{Sed}}) \\ c &\text{ correction factor in dependency of particle concentration} \end{aligned} \quad (11)$$

The viscosity is increasing very fast in a non linear way at particle concentrations greater than 60 vol %, (exponential, $\text{visc} = (V_{\text{Sed}}/100)^{10}$).

In the present study, WinGeol/SedTec was forced to deposit all transported material at the end of the transport path.

3.3.4 Time dependent environmental parameters

Several environmental parameters were altered in dependency of time during the process of simulation:

3.3.4.1. Precipitation

The amount of available water influences the simulation in different ways:

- Increasing stream power (see 3.3.2.2.)
- Ratio between transported sediment and water influences the transport speed and sedimentation. (3.3.3.)

In our models, discharge is held constant at simulated cold and warm periods. Low discharge at simulated cold periods would lead to unrealistic low transport not emulating strong (glacio-) nival regimes with peak runoff conditions during glacial periods (Van Husen, 2000). High discharge during warm periods may lead to unrealistic high transport capacities or channel incision. Climate is simulated via a changing sediment supply to the model.

3.3.4.2. Sediment supply factor

The sediment supply factor controls how much sediment is available in a certain time step to be transported into the drainage area. Sediment supply is not connected to a certain chemical, biological or physical process. In the presented work this factor was used to model environmental changes due to climatic changes and related processes such as change in vegetation coverage or change in weathering.

3.3.4.3. Tectonism

Tectonism in WinGeol/SedTec is treated as a passive process. Rates are read from a separate (time) table, which is linked by an object id with a polygon element. Each element may have different rates and be activated as often as needed.

4. Methodology

4.1. Reference model

Numerical models were validated against real world conditions to better compare all simulated alterations in climate, tectonic and base-level on our models. We calibrated a reference model (1a, 2a, 3a) which fits best to the present fan geometry and produces comparable thicknesses since the last maximum glaciation (c. 25 ka, Fig. 6; cf. Salcher and Wagreich, 2008). The reference model helped to better interpret modelled scenarios.

4.2. Modelled time span, calibration to climate, tectonic and base level

Our numerical experiments cover the last glacial to interglacial cycle from - 25 ka B.P. to 0 ka. In the study area, times around the last glacial maximum are related to a periglacial climate associated with a low vegetation density, strong weathering and low precipitation values. Absence of vegetation and glaciation during the MIS 2 caused large quantities of debris in the alpine hinterland (congelifraction, Van Husen, 2000). Such a period was modelled via high sediment supply and reduced discharge values. In contrast warmer periods are associated with increased precipitation, reduced weathering and a higher vegetation density around the study area (Van Husen, 2000). This scenario was modelled through a decline in sediment supply and increase in precipitation causing

stream incision and fan abundance. The switch from aggradation to fan incision happened somewhere between 14 ka and 9 ka B.P (Salcher and Wagreich, 2008, cf. Van Husen, 2000). In the following model series, the change in sediment supply was constrained to after the Younger Dryas at ca. 11.5 ka. The continuous decline reflects the continuous climatic recovery since that the time (cf. Oldfield, 2005).

In the presented study, the precipitation factor is not changed between individual models with low values up to 11.5 ka (time step 5) and increasing values towards present time.

Consequences of subsidence on fan development were simulated via different slip rates (low at the basin's edge, high in basin's depocenters) and via changing total slip rates between models (experiment 2).

The role of Austria's largest river (Danube) as base level for all tributaries of the study area was modelled via simulation of a low and a high water level.

In our study case the individual model time steps were set to 8 cycles, à 3125 years. (Fig. 5).

4.3. Initial model preparation

Landscape evolution models which simulate changes in a geologic time scale and large areas have to be simplified due to limited computation power and limited information of relevant processes of the investigation area. Therefore, the initial models have to be optimized and simplified (e.g. Cowie et. al 2006, Clevis 2003, Allen and Densmore 2000). Model resolution was down sampled from 10 x 10 m to 150 x 150 m or 200 x 200 m. The model combines natural elevation data of mountain catchments with a virtual basin surface grid. The virtual surface represents a tilted plane simulating the mean dip ($\sim 0.1^\circ$) of the southern Vienna Basin (including Mitterndorf Basin). It offers the opportunity to evaluate fan and basin development without an anthropogenic overprint on the basin grid. Morphological structures like alluvial fan surfaces, incised streams, gullies, depressions or anthropogenic alterations caused mainly by dams, railroad tracks, highways and gravel pits would strongly influence simulation. Furthermore, the slope of the present day basin surface is not supposed to be realistic for an initial model. Present fan surfaces are supposed to approach to rather lower slope angles towards the next aggradational event where slope will be increased again. Simulated fan growth and sequence development is therefore not affected by the present day surface of the alluvial fans but rather by a flat tilted basin which better allows the fans to evolve with the set frame work conditions.

4.4. Local depression handling

In every digital elevation model (DEM) some cells may appear as local depressions (e.g. narrow valleys where resolution is larger than width). We used a cycle prior the simulations to fill up artificial local depressions of the elevation model. Results of these cycles were analyzed to be sure that geometrical alterations stay minor.

5. Results

In this study we generated 12 model runs to investigate the effects of different combinations of input variables (see table 1).

At proximal fan areas sequence aggradation on fan surfaces is immoderate (artificially) large during time step 1, reflecting the small transition gap from the "natural" DEM of the Alpine Hinterland to the artificial flat plan of the basin (4.1.). This effect is not realized at distal areas.

5.1. Experiment 1 - responses to climate change

In order to evaluate influence of different sediment supply and precipitation rates on fan evolution, we created models that simulated the consequences of strong climate change during 25 ka by tuning discharge/sediment ratios.

The models of experiment one are simulated via changing sediment supply affected by colder (more sediment input, model 1c and 1d) and warmer climate (less sediment input, model 1b) than the reference model. Values are allowed to develop with sediment supply rates transporting - 50 % (1b), + 100 % (1c) and + 400% (1d) of the reference model (1a). Tectonic slip rates were held constant and the influence of neighbouring axial river (Danube) on base level were censored.

In model 1b, our results showed that the decreased availability of sediment leads to increased stream power per unit bed width (higher discharge/sediment supply ratios), causing both, high sediment conveyance capacity and high rates of bed rock erosion (Fig. 6). At proximal fan areas, model 1b was not even accumulating to end of simulated full glacial up to time step 5.

Lower availability of sediment was found to be associated with lower sequence thickness, lower channel activity on fan surface and a higher sensitivity on subsidence. Models with low sediment availability are not effectively able to balance progressive formation of accumulation space through subsidence. Main channels are deflecting towards highest subsidence areas in the centre of the basin, controlling active deposition area.

Low sediment supply at model 1b allows only very minor deposition at the upper fan. Little sediment is preferentially stored in the distal fan areas (Fig. 8). The decreased sediment supply rates are associated with high rates of stream incision, which is even more increased towards the end of the model runs, where sediment/discharge relations are lowered (Fig. 5, 6, 7). The "active depositional lobe" in the model is shifting towards distal areas during the simulation, reflecting decreasing accumulation space. Loss of accumulation space is associated with (interfan) channel incision (Fig. 6, 7). Progressive incision at the lower fan parts and active deposition at lower fan parts can be equated with intersection point shifting towards distal areas.

In the models 1c and 1d the higher availability of sediment was found to cause higher sequence thicknesses, some higher fan progradation distances, an increasing number of channels on fan surface, different runoff patterns and less influence of basin's subsidence.

In models with abundant sediment supply subsidence is balanced more effectively, resulting in a different flow pattern which is rather straight to the model's edge than to the highest subsidence areas. Aggradation behaviour on fan surfaces during the simulation is similar at models 1c and 1d. Up to time step 4, aggradation occurs on the upper fan positions. With time step 5 (lowering of sediment supply) aggradation is preferentially occurring at outer fan positions. Models with less sediment are forced to fill the high subsidence areas at distal positions. Models with abundant sediment supply lead to multiple channel development with restrained incision.

In all models the southern Schwarza fan is affected by a larger number of channels which is especially obvious in model 1b (low sediment). This corresponds very much to the real world where the Schwarza fan is incised by more, commonly dry channels in contrast to the Piesting fan which is completely abandoned by channels. In summary, climate induced variations of sediment supply have a strong impact on fan aggradation and morphology. Abundant sediment supply allows thicker sequences to develop, resulting in a larger fan and valley backfilling which corresponds to a fan apex at higher elevations. Models with high sediment supply show lower bedrock incision, numerous but shallow channels and low sensitivity on subsidence. Low sediment supply produces some smaller fans, allows higher bedrock incision, resulting in fewer but deeper channel systems and results in a higher sensitivity to tectonic subsidence. In our models a higher channel density reflects active fan surface or active depositional lobes showing reduced incision and a higher avulsion tendency (Fig. 6, 7). High channel density on lower fan parts can be equated with intersection point shifting to lower fan parts and loss of accumulation space relating to low sediment supply rates. High channel density on extensive areas of

the fan can be equated with intersection point closer to the apex and high accumulation space (open fan deposition) relating to abundant sediment supply rates. Active depositional lobes are represented by high-slope areas, because numerous flow (transport) events produce numerous channels with relative steep banks. These channel banks are showing a high contrast, which is visible in a slope distribution map (Fig 7). High slope areas on fan surfaces are also developing in our models, e.g. through distally eroding or confining processes (erosive scarps). Low slope areas on fan surface show sediment congestion (laterally fan confinement, e.g. at the Alpine front) or an abandoned fan surface (no channel development). The tendency of interfan channels at the Piesting fan to deflect towards NE is an effect of the overall basin slope

5.2. Experiment 2 - responses to changes in fault slip rates

In order to better understand the consequences of developing accumulation space on alluvial in the Mitterndorf Basin, we created models with different subsidence rates. The elongated basin sizes about $\sim 270 \text{ km}^2$ and trends to SW-NE. Precise levelling data indicate continuous subsidence (Höggerl, 1980) ranging around 1 mm/a which was set as maximum slip rate (subsidence area I, Fig.1) of the reference model 2a. Sequence thicknesses are declining from North to South, and from the mountain front in the West to the East, showing some asymmetry in basin form (Fig.1, schematic cross section). Therefore, maximum slip rates can be assumed in the East and North of Basin. Within the model this difference is included by a defined faults map (via a set of polygons) attributed with different subsidence rates (Fig. 1). This situation is simulated via a set of polygons with lowest slip rates in the West close to the mountain front and maximum rates in the East of the Basin.

In experiment 2, the ratios of precipitation and sediment supply are held constant, whereas fault slip rates vary: Model 2a serves as reference model. Model 2b is characterized by tectonic quiescence (0 mm/a), model 2c develops with low subsidence (max. rates are 0.3 mm/a), model 2d with medium subsidence (max. rates are 0.6 mm/a) and model 2e with fast subsidence (max. rates are 2.4 mm/a; e.g. Decker et al., 2005). For further simplification, we did not take strike slip movement into account:

In model 2b, the Piesting fan builds a radial form, only confined in the southeast by the prograding Schwarza river fan (Fig. 9). Large subsidence values lead to minor sequence development during the simulation. Although, aggradation at proximal positions is something higher than on models with high subsidence rates (Fig. 9) missing subsidence does not force channels to incise and aggradation is not drawn to these areas. Progradation is then just an effect of critical slope. Aggradation decreases uniformly at distal and proximal fan locations. Effects of sediment lowering with time step 5 lead to a complete interfan channel incision and to the abandonment of the fan surface. Interfan main channels of low (2c) or no tectonic model (2b) series are levelling in N-S direction (along the Alpine front), with increasing time and decreasing sediment supply. This might be due to flow characteristics preferring shortest distance and steepest slope (= highest energy) to model edge. The resulting abandoned fan surface during warm periods of the Piesting fan appears very large and is not at all comparable to today's geometry.

In model 2e, the response of the catchment fan system to the increase in fault activity is reflected by tracking the mean sequence thicknesses, fan geometry and drainages of fan channels (Fig. 9). During periods of fan build up, extreme subsidence rates in 2e produce conspicuous fan forms, which are elongated towards the maximum subsidence area. Progradation distance and geometry is therefore shown to be directly in dependence of the tectonically created accommodation space. Main interfan channels are clearly controlled by subsidence and get deflected to a West – East direction towards high subsidence areas. Already with time step 4, most sediment is accumulated at high subsidence areas at the distal fan locations. With beginning low supply (time step 5) the constantly high vertical slip rates lead to fan incision and to channel confinement. Low supply naturally amplifies the influence of tectonism as sediment is forced to move into these subsiding areas (Fig. 8, Fig. 9).

Fans affected by low or no tectonic activity create less accumulation space than fans affected by high subsidence rates. As a consequence, the fan systems of these models are characterized by thinner sequence thicknesses during build up. Thickening at the proximal areas is minor, but somehow longer active within models affected by lower activity. Nevertheless, incision starts later, and is only triggered by climate and not by subsidence as in the models with exaggerated vertical slip rates.

Models with high subsidence rates are progressively filling subsidence areas, causing an earlier levelling of main channels towards maximum slip rates (Fig. 9). This effect is amplifying as sediment supply decreases and accumulation is deflected to the depocenter of the basin. In contrast, main channels of low or no tectonic model series are levelling in N-S direction (along the Alpine front), with increasing time and decreasing sediment supply. This might be also an artificial effect of flow which prefers shortest distance to model edge.

Again, like in the experiment 1, the channel number is clearly higher on the southern Schwarza fan preventing an abandoned fan surface to develop.

5.3 Experiment 3 – river level fluctuations of the main axial river (Danube)

The investigated fans toe out onto the subsiding Mitterndorf Basin. Streams of the Mitterndorf Basin are also influenced by the level of the axial Danube River to which all streams are tributary. The level of the Danube River may alter due to fluvial incision or accumulation. The Danube River acts as a conveyor belt which gathers all sediments from Vienna Basin tributaries. Therefore, the water level is climatically influenced.

In experiment 3, the impact of a main river onto local base level and thus fan development during the sequence of 25 ka is observed. Streams are allowed to drain to different elevation levels at the model's edge, simulating the effect of incision of the Danube River. Within this experiment sediment supply and subsidence rates are held constant (values correspond to reference model). Reference model is 3a. Average distances to base level is changed to – 15 m in model 3 b. For simplification base-level variations within model runs held constant.

In model 3b the water level of the main river is set to lower positions (some 15 m below the present Danube level) resulting in strong incision (Fig. 10) and suppression of fan development. At proximal fan areas, aggradation occurs up to time step 2 at the Piesting fan, but almost completely ends at time step 3 (Fig. 8). A wave of dissection which progrades upstream reaches the fans and lead to total fanhead trenching, and prevents accumulation on upper fan position, which are then completely abandoned. However, if accommodation to that baselevel is finished, models allow a constant aggradation on the distal fan parts even when sediment supply decreases with time step 5.

6. Discussion

We studied the relative impact of climate change, tectonics and the influence of a neighbouring axial river system on the development of two mountain front alluvial fans in eastern Austria by a numerical model approach. The evolution time frame was 25 ka, in which a main oscillation from a glacial to an interglacial occurred.

In accordance with regional studies (Salcher and Wagneich, 2008; Küpper, 1950) and other studies on mountain front fan systems (e.g. Harvey 2002, Harvey, 1999a), climatic induced variation in sediment supply is the primary control on the sequence development of fans in such a setting. This assumption is especially valid during Pleistocene (Weissmann et al., 2005; Weissmann et al., 2002; Roberts, 1995; Frostick and Reid, 1989) where strong oscillation of climate with clear aggradation and degradation processes were present around the modelled area (Van Husen, 2000; Fink, 1977). The influence of climate on transport capacity is comparable fast (cf. Allen and Densmore 2000). Shifts to low ratios of sediment supply to discharge, starting with time step 5, lead commonly to channel incision. The important role of climate on fan geometry (Nemec and Postma, 1993; Ritter et al. 1995) is shown in the experimental series 1.

Second, fan geometry depends strongly on tectonic influence (e.g. Silva et al., 1992). In accordance with other numerical model studies (Allen and Densmore, 2000; Clevis et al., 2003) our models show a rather long term, constant effect on tectonics (subsidence) provided by the increasing accumulation space. The developing accumulation space, particularly in high subsidence areas, was found to have a strong influence on runoff pattern, especially during periods of low sediment supply (Fig. 9). The largest abandoned fan surface was produced during the simulation without vertical slip (2b). These streams were then not forced to destroy the fan. Incision (lowering) of the axial main river causes incision and upstream dissection through tributaries in our models.

In experiment 1 our results showed that abundant sediment supply produces larger fans and restrains influence of subsidence. In contrast, decreased availability of sediment leads to higher rates of bed rock erosion, to lower sequence thickness and to a higher sensitivity on subsidence. The large drainage area of the Schwarza fan and its laterally confinement through the Alps (Fig. 1) cause higher sequence thicknesses during the first time steps. In turn, confinement leads to the development of more channels which are incising, in contrast to the Piesting fan where drainage can evolve without confinement. Model results converge with results from the natural system, where a higher fluvial activity of streams and some lower subsidence rates caused lower preservation chance of soils in the stratigraphic record of the Schwarza Fan (Salcher and Wagneich, 2008).

The abandonment of the Piesting fan during sediment shift to lower values at time step 5 lead to widespread fan exposure. The occurrence of continuous, widespread paleosols in the stratigraphic record of the Piesting fan shows the importance of fan exposure for their formation. Models do also stress the long term evolution of the Piesting River drainage which is mainly controlled by subsidence and basin slope.

Experiment 2 shows that an increase in subsidence affects fan form and size: Higher subsidence allows higher sequence thicknesses at distal areas and allows elongation of the fans towards the maximum subsidence area (Fig. 9, TS 5).

The role of subsidence becomes more important at the end of model runs where simulated warm periods cause fan degradation. Then, alluvial fan drainage is influenced significantly if slip rates are high or low, determining whether trenching is directed towards subsidence area or towards a possible short distance (=highest slope) to the model's edge. Models with high vertical slip rates are progressively filling these areas. The tendency is amplified as sediment supply decreases. In the study area, incipient distal headcut development at the Piesting fan towards the area of highest subsidence is evident (Salcher and Wagneich, 2008). Subsidence may trigger or enforce distal fan incision and lead to total trough trenching (Harvey, 2002; Harvey, 1996; Harvey, 1987, Fig. 9 if subsidence remains higher than aggradation rates.

Absence of subsidence leads to clear reduction in thickness (reduction in sequence preservation, Fig. 8) and to exaggerated large fan surface. Streams do accommodate to the model's edge and not to subsidence areas, which would force them to erode the fan surfaces. However, different subsidence rates control the chance of sequence preservation to move them below possible depths of incision and degradation (cf. Blum and Törnqvist, 2000). The impact of different subsidence rates is clearly visible in preserved sequence thicknesses (growth strata, Fig. 8).

In all tectonic models (2 a, c, d and e) in that fans are affected by lowering through subsidence, progressive creation of accumulation space causes burial of old fan sequences, developed during times of abundant sediment supply. Lowering of fan areas due to subsidence enables (axial) streams to reoccupy these areas and force streams to fill the space. The higher the vertical slip rates (2 d and 2 e) the more sediment is delivered to the maximum subsidence area, and the higher is the tendency for streams to aggrade and fill these areas. The large amount of accumulated sediment in these high subsidence areas is reflecting very minor erosion which can be associated with high sequence preservation potential. In the study area this subsidence effect is characterised by the occurrence of paleosols, which are thicker and more frequent in the basin centre (Salcher and Wagneich 2008; Küpper, 1950,).

The influence on base level by a neighbouring main river (Danube) is computed in experiment 3. Responses to a base level fall are fast, causing a wave of dissection which

progrades from the main river to upper basin parts. Fan development is suppressed but depends on the amount of main river incision and on sediment supply. Similar to experiment 2 abundant sediment supply suppresses trenching tendencies, while decreasing sediment supply values towards the end of the simulation result in formation of deep fan trenches. Nevertheless, in the natural course, strong base level alterations of the kind simulated in this model are unlikely, as within this specific time frame water level can be assumed relatively stable. Fluctuations in elevations of Danube River are very minor (Fink, 1955). Elevation of terraces of the late Middle Pleistocene (MIS 6, Riß, some 130 ka) above the contemporary floodplain of the Danube is not exceeding c. 15 m, demonstrating generally very low incision. Therefore, experiment 3 is of rather hypothetical interest and results can only be applied with caution.

6.1. Strength and limitations of simulated landscape models

The used program code was sensitive enough to explain a geomorphic evolution of our study area. We were able to generate realistic fan geometries and drainages and could detect the most probable factors controlling Mitterndorf alluvial fan evolution. Landscape evolution models which simulate changes in a geologic time scale and large areas have to be simplified due to limited computation power and limited information on relevant processes of the investigated area (e.g. Cowie et Al., 2006; Clevis 2003). Naturally, models are only a simplification compared to the complex natural system. Because of limited computation power we did not include very short climatic oscillations (climate oscillations around the Younger Dryas event). Furthermore, initial models were down sampled from 10 x 10 m (DEM) to 150 x 150 m or 200 x 200 m and were connected to a virtual drainage basin representing a tilted plane with mean dip of the southern Vienna Basin. Environmental parameters such as weathering and grain size reduction were excluded.

6. Conclusion

Fan development is primarily controlled by climate induced release of sediment to drainage basin. A glacial/interglacial cycle produces clear aggradation and degradation of fan surfaces, reactions on the system can therefore assumed to be relatively fast. Tectonic control is secondary and the impact is long term increasing with higher slip rates or decrease of sediment supply. Furthermore, tectonic has a major influence on the evolution of axial drainage pattern and therefore a strong impact on erosion of fan surfaces. Development of main interfan channel is controlled by fan geometry (thus also depended on confinement) and tectonics. Variations in elevation of an axial main river have a strong and fast effect on all tributaries of drainage basin. Consequently, incision of the main river causes incision of tributaries and suppresses fan built up at simulated cold periods. Our results generally converge with literature.

Acknowledgments

This project was founded by the Austrian Science Foundation (FWF Project AP18203). We thank Dr. Belinda Plattner for help with the manuscript write-up.

Table

Reference model	time (ka)	sediment supply	precipit.	subsid., area V, distal: (m/ka)	subsid., area I, proximal: (m/ka)	time step
1 a, 2 a, 3 a	25 - 11.5	0.3	0.15	0.075	1.2	1-4
	11.5 - 0	0.1	0.5	0.075	1.2	5-8

Tab. 1: Parameters used in the reference model. Changes in sediment supply and precipitation are not abrupt but increase linear. For location of subsidence areas see Fig.1.

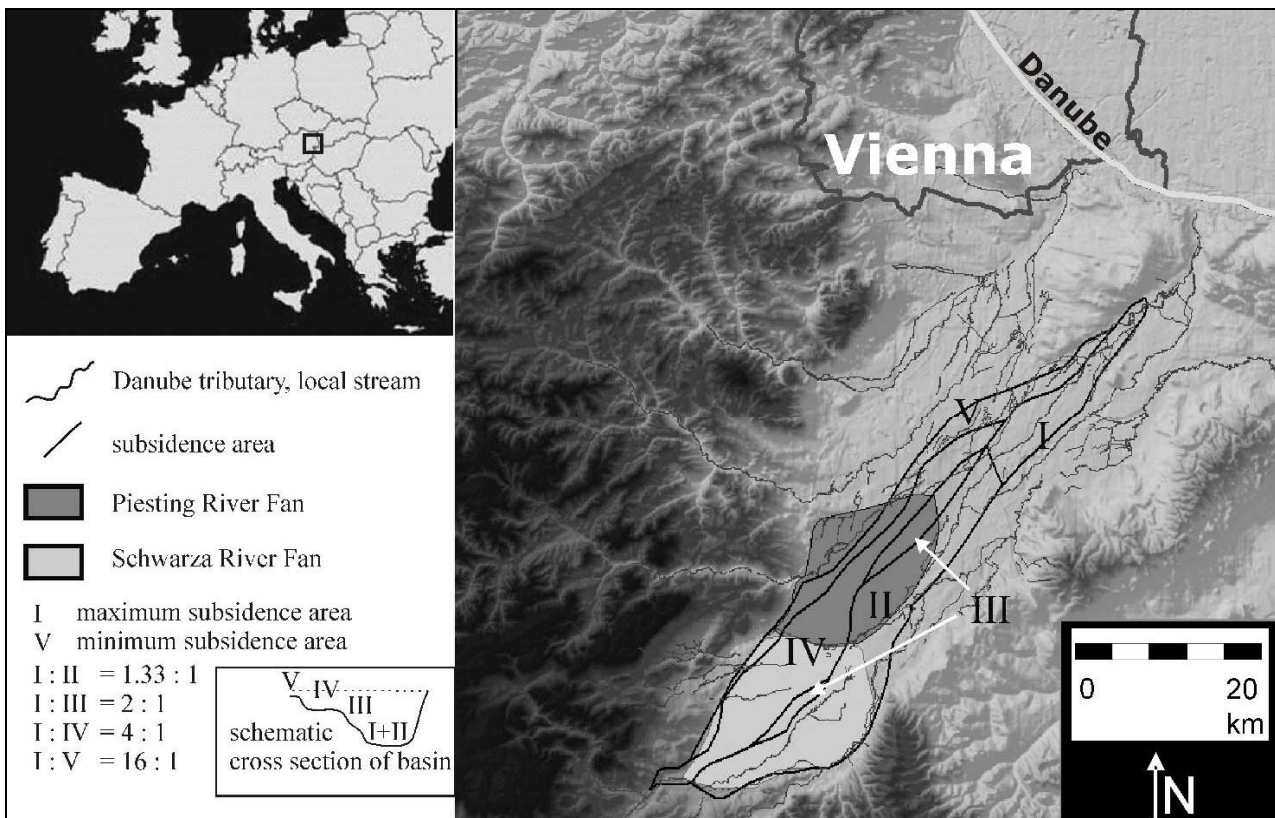
Figures

Fig. 1: Shaded DEM of the southern part of the Vienna Basin. The Mitterndorf basin area is shown by the outline of the subsidence map created based on log, seismic and gravity data.

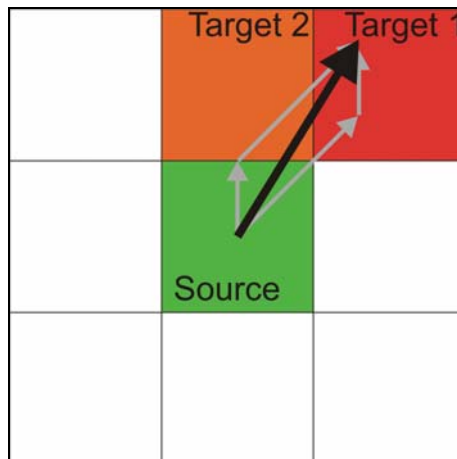


Fig. 2: Wingeol/Sedtec Modelling: Determining transport targets: The lengths of the light grey vectors represent the fractions the target cells will receive. The black vector represents the calculated movement vector.

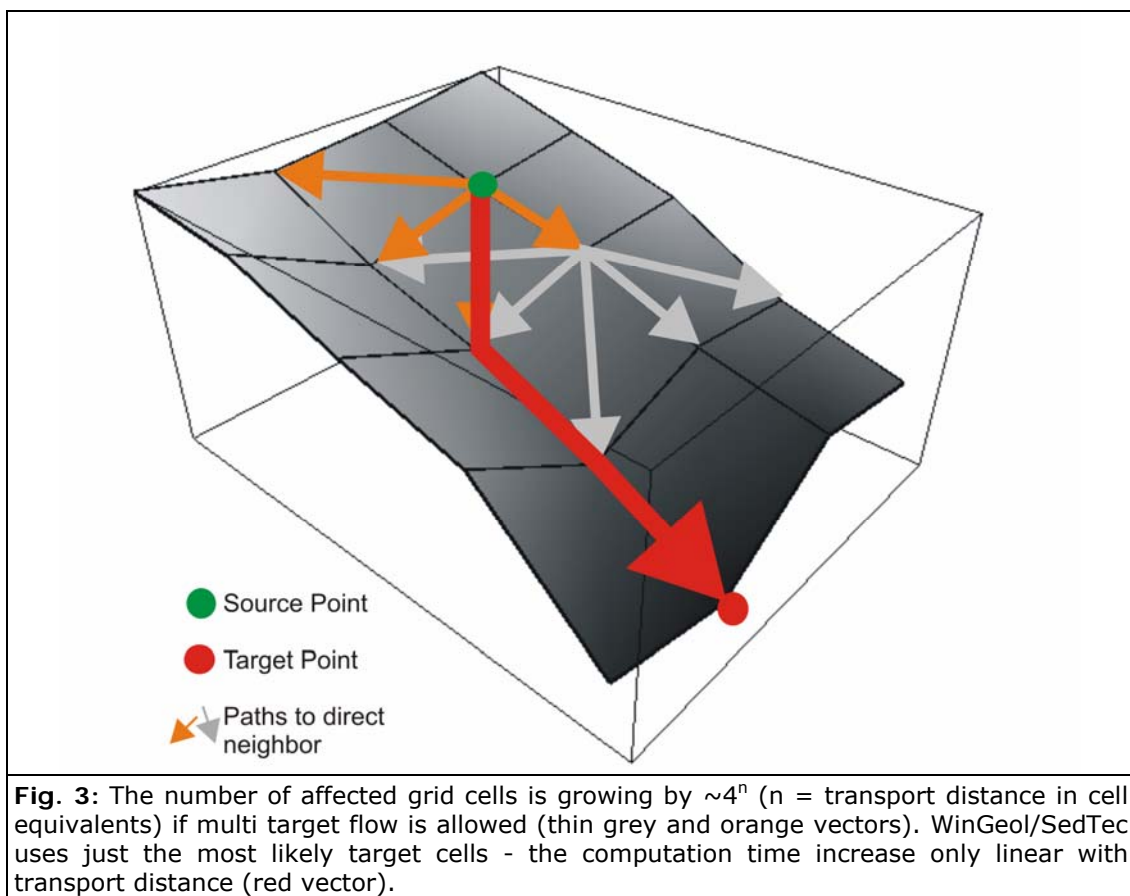


Fig. 3: The number of affected grid cells is growing by $\sim 4^n$ (n = transport distance in cell equivalents) if multi target flow is allowed (thin grey and orange vectors). WinGeol/SedTec uses just the most likely target cells - the computation time increase only linear with transport distance (red vector).

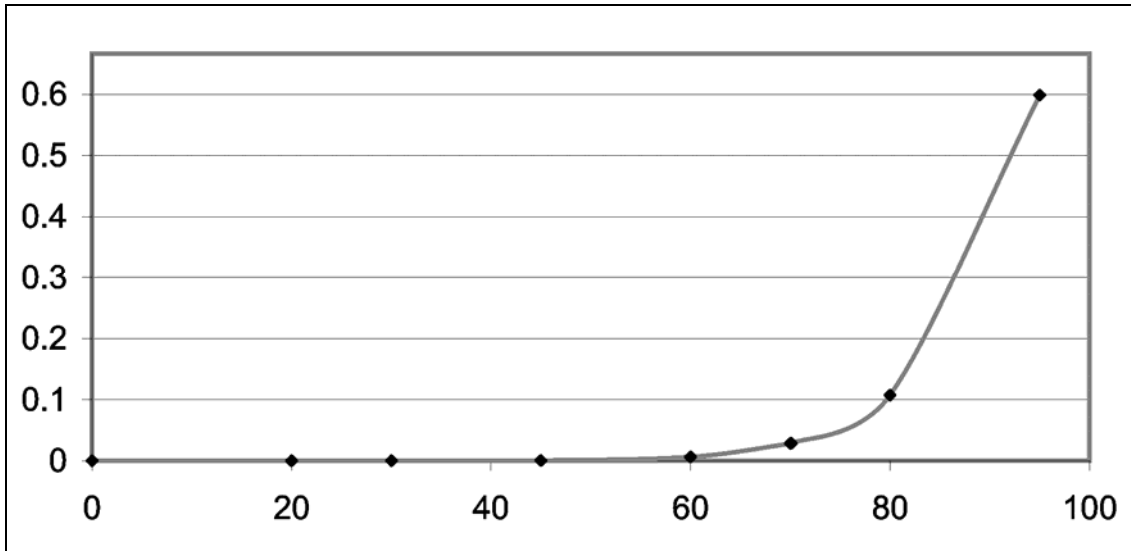


Fig. 4: Viscosity of mixture fluid and cohesionless particles (Krieger and Dougherty, 1959), fluid viscosity is set to 0.001, "viscosity" of particles is set to 1.

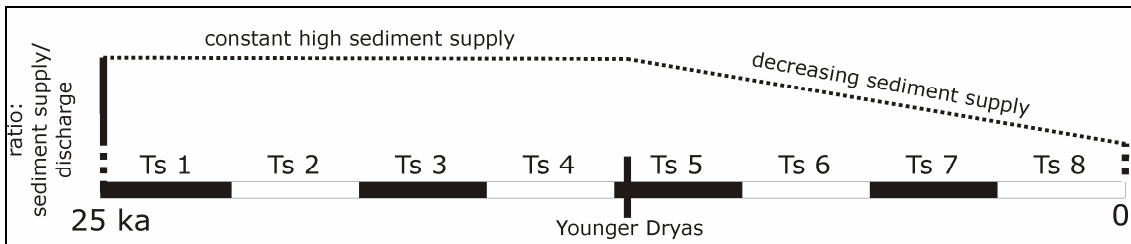


Fig. 5: Simulated time span of 25 ka, 8 time steps. Applied curve of sediment supply as a ratio of sediment supply divided by discharge.

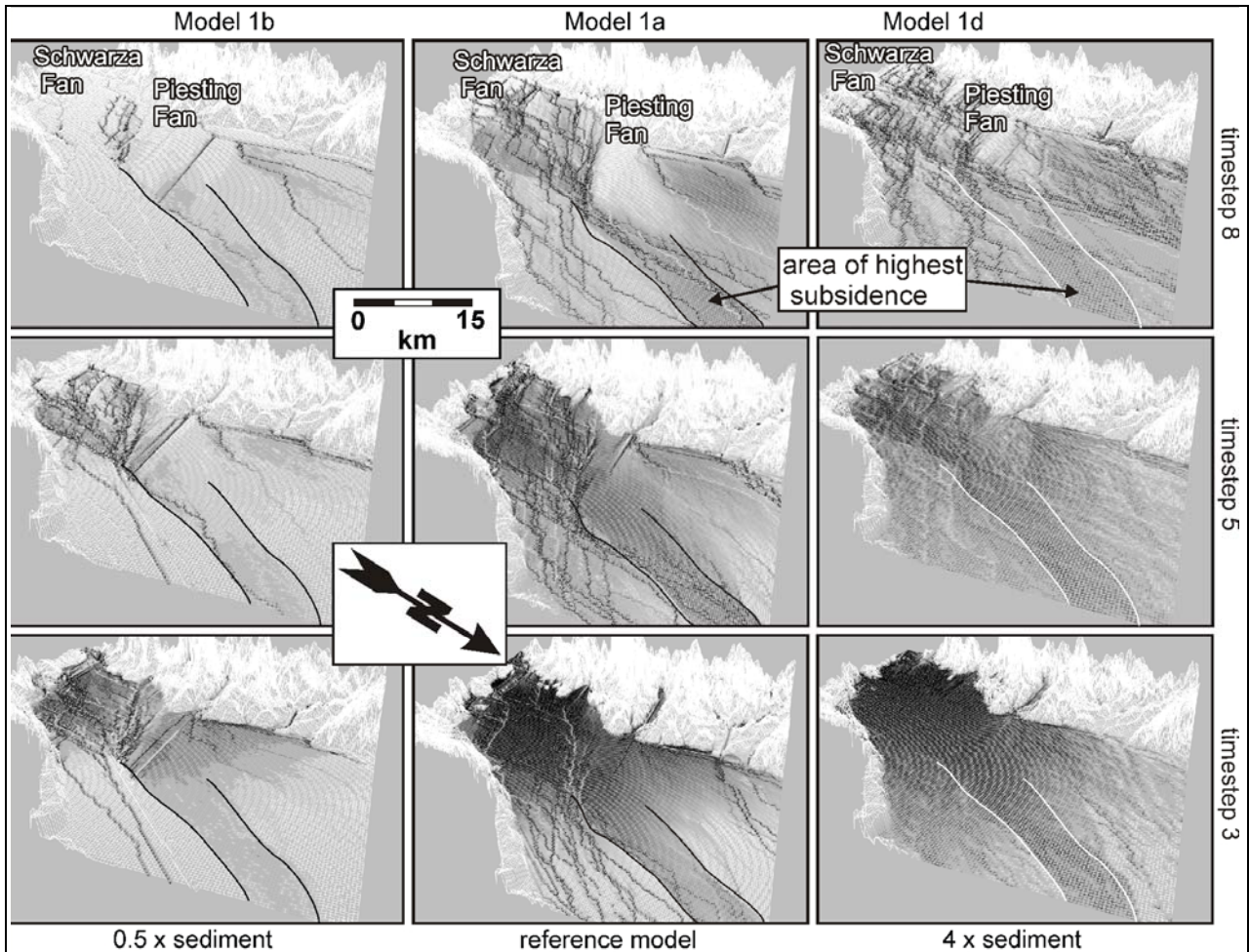


Fig. 6: Influence of sediment supply variability on study area. Low supply models (1b) are strongly influenced by the basin's high subsidence areas in the central parts. Channels are able to incise deeply, especially during simulated warm periods, leaving large abandoned fan surfaces at the end of model runs (time step 8). High sediment supply (1d) causes large aggradation on fan surfaces during the first time steps, weak tectonic influence and a multiple network with shallow channel. All models show the difference in aggradation, Schwarza to Piesting Fan. The southern Schwarza Fan is affected by higher aggradation but also by stronger degradation. Reference model (1a) show a, compared to the nature, realistic drainage network evolving and realistic fan area sizes during the end of model run. Black colour represents thicknesses of more than 10 m; white colour represents no accumulation on cell. Black and white lines frame areas of highest subsidence. Grid space is 200 m, vertical exaggeration is 20 times.

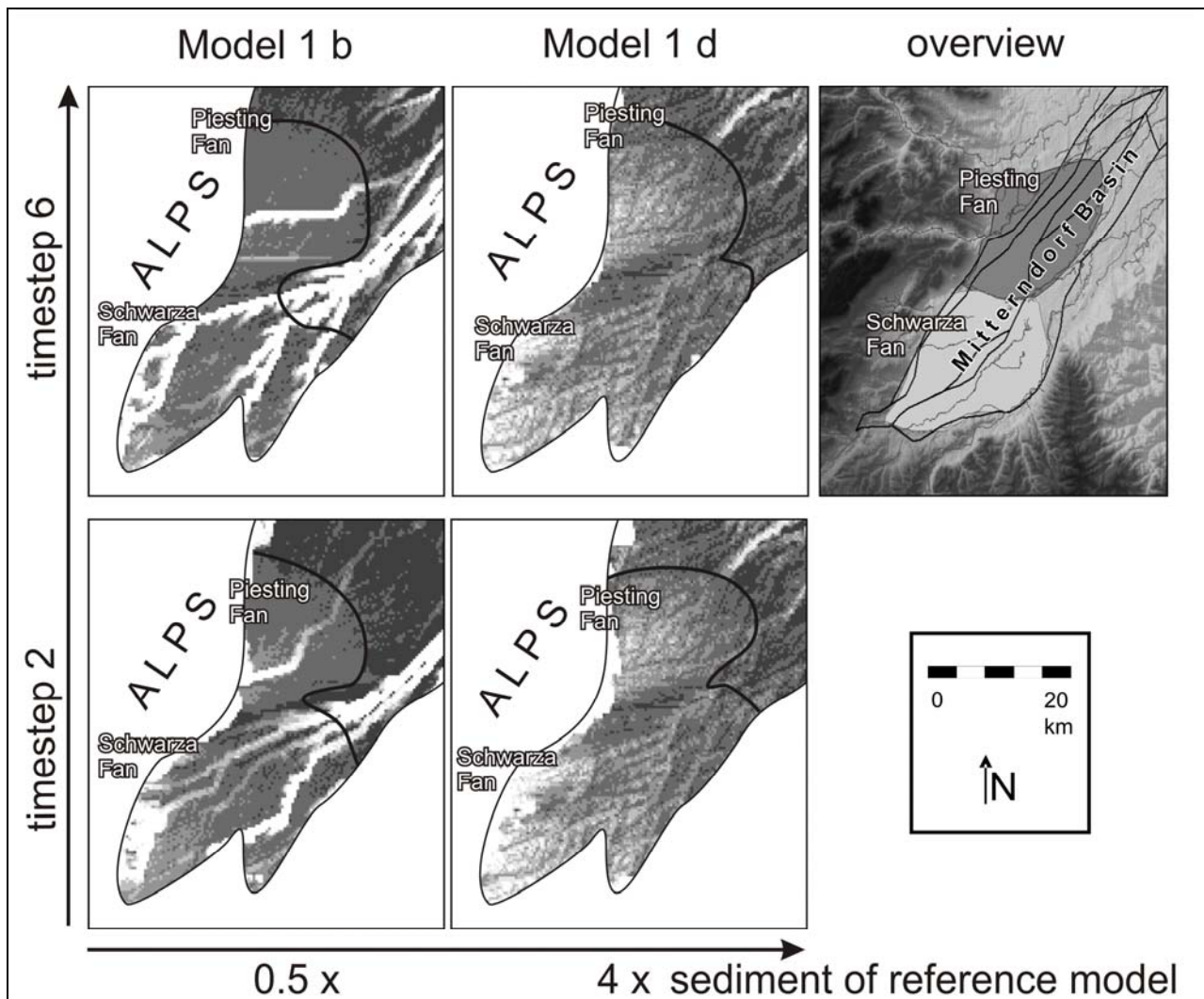


Fig. 7: Slope map of model 1b and model 1d, showing the impact of low and high sediment supply on models. White colour indicates high slope ($> 1^\circ$, deep incised channels), black indicates low slope (0°). Low sediment transport to the basin (1b) cause strong incision into fan surface producing steep channel banks. Models with high sediment supply have to disperse their sediment on the surface creating abundant but less deep channels.

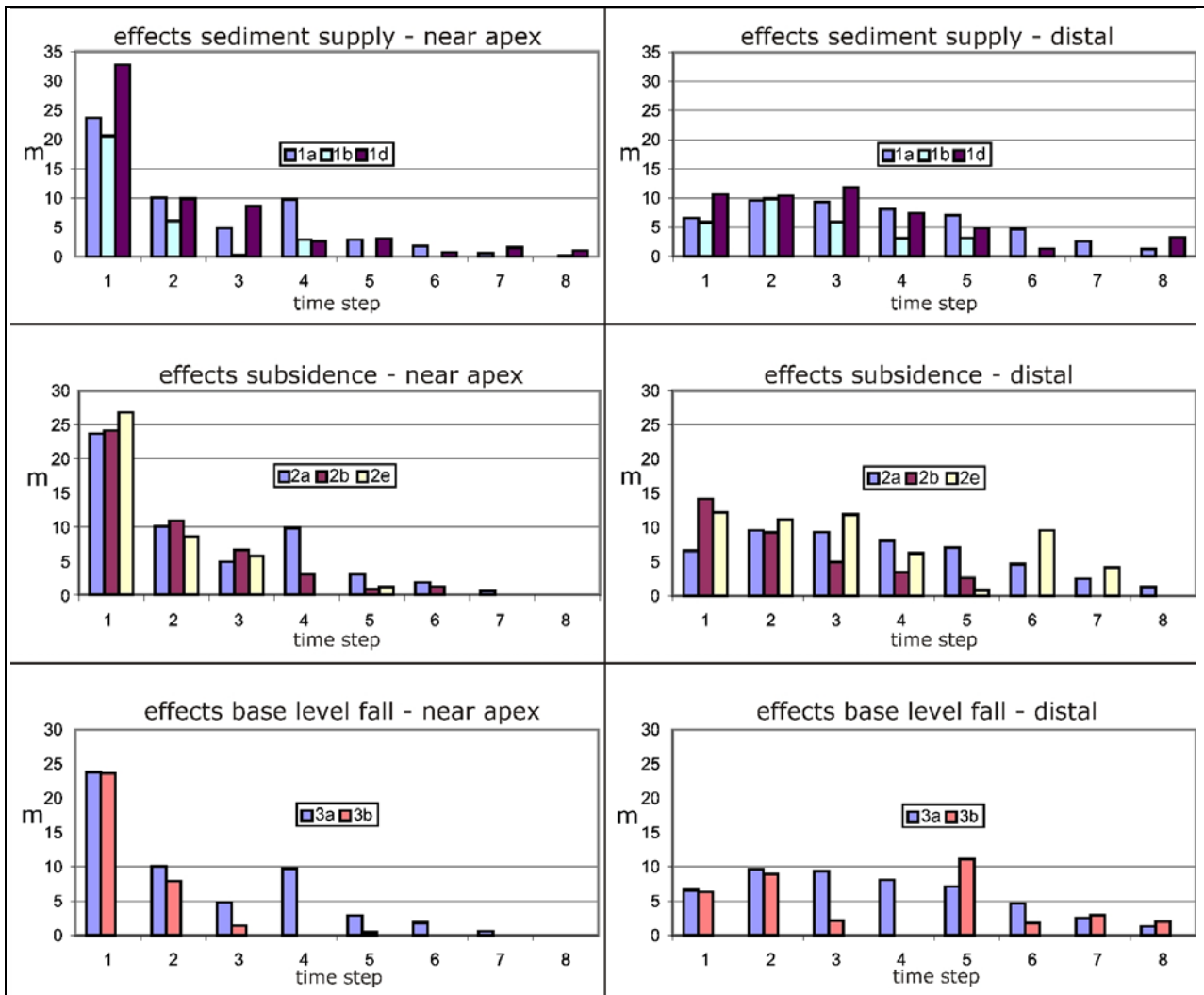


Fig. 8: Virtual wells show the amount of aggradation (in m) on Piesting fan near the apex and on a distal position at the end of a simulation (showing the remained sediment after each time step). At proximal positions, strong aggradation during time step is a filling effect at the transition natural DEM Alps to virtual Vienna basin DEM (see 4.3.). Model 1 series show the effects of sediment availability. Model 2 series show the preservation potential between no, normal and high subsidence rates. Model 3 series show the effects of a lowered base – level. All model show the clear decline at time step 5 at simulated warm periods (increasing discharge/sediment supply values). See text for details.

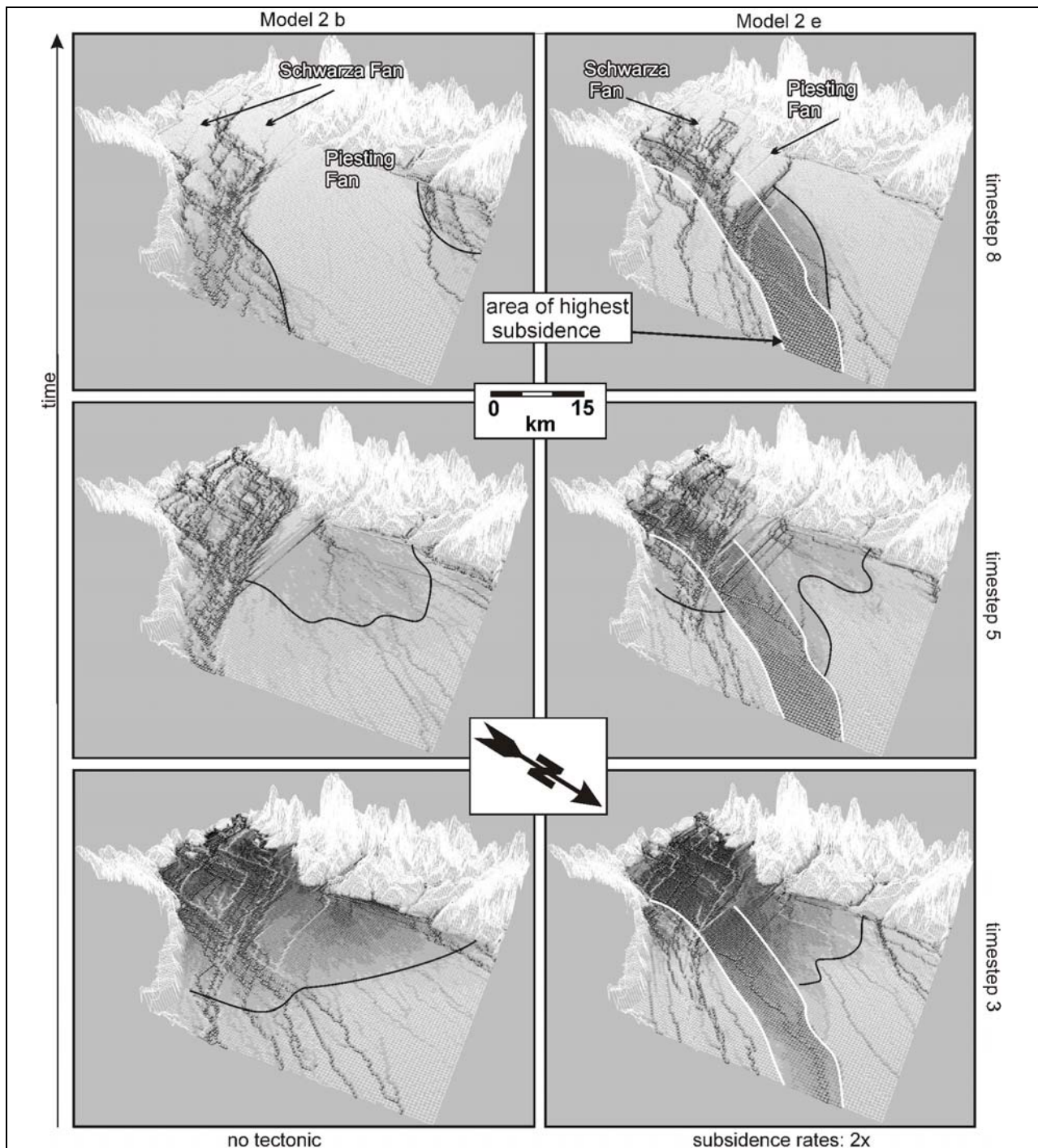


Fig. 9: Influence of strong basin subsidence (model 2e) and tectonic quiescence (model 2b) on fan evolution, showing stream pattern development. Black colour represents thicknesses of more than 10 m; white colour represents no accumulation on cell. Channels appear often dark, showing a high amount of sediment passing individual cells per time step (high sediment flux). Note the progressive filling of high subsidence areas. Grid space is 200 m, vertical exaggeration is 20 times.

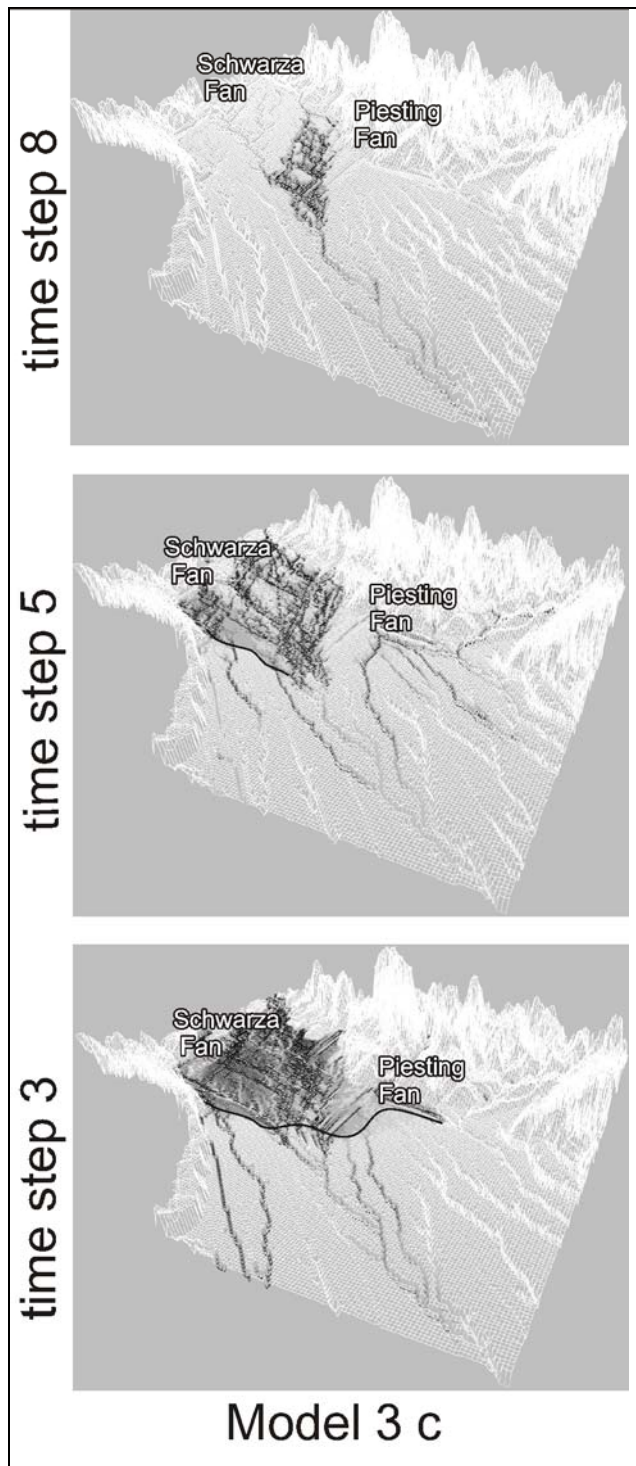


Fig. 10: Extreme lowering of base level in model 3c shows the strong incision of Danube River tributaries into bedrock and the suppression of fan progradation. Black colour represents thicknesses of more than 10 m; white colour represents no accumulation on cell. Grid space is 200 m, vertical exaggeration is 20 times.

Appendix Tab. app. 1, Sample list outcrops

add. samples	location name	sample discription	pos. x	pos. y	pos. z	14C age B.P.	sample for
1	Bad Fischau pit	from cryoturbated area	737618	297528	~276.5		indefinite
1a	Bad Fischau pit	spherical charcoal piece (~1.5 cm), within fluvial gravels - some 1 m below surface	737615	297521	~281	> 45000 (S9)	14C
2	neben Fischadep pit	7-10m below surface	745675	302775	~~260		indefinite
3	neben Fischadep pit	7-10m below surface	745675	302775	~~261		indefinite
4	neben Loidl pit	red palaeosol	741516	302572	~286		indefinite
5	Tattendorf pit	overbanks in channel	748428	311605	~228		indefinite
6	Tattendorf pit	overbanks in channel	748269	311721	~228		indefinite
7	Neurißhof pit	overbanks at the top	749095	310414	~225.5		indefinite
8	Hitzehammer 1 pit	palaeosol remnants	748822	310743	~223		indefinite
9	Hitzehammer 1 pit	top overbanks	748762	310807	~228		indefinite
10	Hitzehammer 2 pit	sand, 1-2 m below surface	748221	310965	~228		indefinite
11	Neurißhof pit	sample from open-framework gravels with balck crusts, Mn	749101	310397	~224.5		indefinite
12	Neurißhof pit	top overbanks	749101	310397	~225.5		indefinite
13	Neurißhof pit	palaeosol? sample location as 49	749059	310464	~220		pollen
14	Hitzehammer 1 pit	palaeosol remnants	748639	310973	~223		pollen
15	Hitzehammer 2 pit	finer sediments from cryoturbated areas	748208	310980	~224		pollen
16	Tattendorf pit	gravels with calcite crusts at its underside	748304	311624	no point		indefinite
17	Neurißhof pit	top overbanks	748438	311634	~225.5		pollen
18	Wopfinger pit	overbanks	746062	303883	~261		pollen
19	neben Loidl pit	red palaeosol	746062	303883	~286		pollen
20_1	Neurißhof pit	soil at the transition from brown to yellow or gray gravels (cryoturbated)	749067.65	310459.809	229.827		pollen
20_1	Neurißhof pit	soil at the transition from brown to yellow or gray gravels (cryoturbated)	749067.65	310459.809	229.827		freshwater molluscs
20_2	Neurißhof pit	soil cm to dm below tiefer als 20_1	749067.65	310459.809	~228.5		pollen
20_3	Neurißhof pit	sand lense at the base of the pit	749064.16	310464.146	221.184		heavy minerals
20_4	Neurißhof pit	sand lense at the top of the pit	749073.11	310438.577	223.248		heavy minerals
21	Hitzehammer 1 pit	paleosol sample 14 taking at 11082006	748711.81	310905.021	225.795		pollen
21_1	Hitzehammer 1 pit	overbanks close to the top	748691.21	310923.643	222.582		pollen

sample Nr.	add. samples	location name	sample discription	pos. x	pos. y	pos. z	14C age B.P.	sample for
22_1		Hitzehammer 2 pit	limit fresh to brown gravels, strong cryoturbation, no sample only dgps measurement	748367.47	311018.943	225.86		indefinite
22_2		Hitzehammer 2 pit	sand lense close to the bottom of the pit	748214.57	310985.535	226.729		heavy minerals
22_3		Hitzehammer 2 pit	overbanks	748219.83	310979.982	230.154		heavy minerals
22_4		Hitzehammer 2 pit	sand lense at top area	748215.1	310986.345	229.238		heavy minerals
23_1		Tattendorf pit	sand lense next to the "ice wegde" (overbank fines in channel)	748323.32	311642.078	227.369		heavy minerals
23_2		Tattendorf pit	sand, gravel lense close to the bottom of the pit	748378.34	311657.436	224.096		heavy minerals
24_1		Theresienfeld pit	paleosol some 10 m below surface	745541.56	305156.209	252.8		pollen
24_1		Theresienfeld pit	paleosol some 10 m below surface	745541.56	305156.209	252.8		freshwater molluscs
25_1		neben Fischadep pit	Reiterer pit, sand lense, somewhere at top area	745898.54	303379.51	254.959		heavy minerals
25_2		neben Fischadep pit	Reiterer pit, sand lense, somewhere at top area, only dgps measurement	745897.66	303357.895	255.592		indefinite
26_1		neben Loidl pit	red palaeosol	741531.6611	302532.7688	284.195		pollen
27_1		Bad Fischau pit	sand lense close to the top , at charcoal sample loaction 1a	737635.0179	297517.165	282.035		heavy minerals
27_2		Bad Fischau pit	sand lense at the croturbation area, very weak pedogenic altered sediment	737660.675	297530.657	276.651		heavy minerals
27_3		Bad Fischau pit	sandlense at the croturbation area, very weak pedogenic altered sediment (some 20 cm above 27_2)	737669.553	297539.429	276.651		heavy minerals
27		Hitzehammer 1 pit	overbanks	748789.6363	310821.0207	227.667		indefinite
28		Hitzehammer 2 pit	pedogenic altered sediment below croturbation area, base of the pit	748278.3888	311065.0415	224.223		freshwater molluscs
28		Hitzehammer 2 pit	pedogenic altered sediment below croturbation area, base of the pit	748278.3888	311065.0415	224.223		pollen
29		neben Loidl pit	red palaeosol, measurement at its top	741530.4039	302534.1185	286.28		freshwater molluscs
30		Bad Fischau pit	very weak pedogenic altered sediment from the croturbation area	737669.553	297539.429	~276.5		freshwater molluscs
31		pit 3, street Weik_Neunk	sand lense	733234.675	291934.4396	326.737		heavy minerals

sample Nr.	add. samples	location name	sample discription	pos. x	pos. y	pos. z	14C age B.P.	sample for
32		Cemex pit (at highway A2), section Kaiser	sand lense top of the pit	739550	295900	no point		heavy minerals
33		Breitenau 4 pit	sand lense at basis of the pit	735657.816	289382.675	318.25		heavy minerals
34		Breitenau 4 pit	sand lense top of the pit	735677.0968	289355.5927	330.874		heavy minerals
35		neben Loidl pit	sand lense top of the pit	741541.8556	302485.355	285.184		heavy minerals
36		neben Loidl pit	sand lense at basis of the pit	741579.6438	302660.717	282.54		pollen
36		neben Loidl pit	sand lense at basis of the pit	741579.6438	302660.717	282.54		heavy minerals
37		Hitzehammer 2 pit	palaeosol, some 2.5m above pit's basis	748204.2767	310997.8398	228.73		indefinite
38		Mahrersdorf pit	RBK, infilling	729085.84	287870.338	390.167		freshwater molluscs
38		Mahrersdorf pit	RBK, infilling	729085.84	287870.338	390.167		pollen
39		Mahrersdorf pit	RBK, infilling, top of the wedge structure	729085.21	287871.823	393.41		freshwater molluscs
40		Mahrersdorf pit	RBK, infilling, top of the wedge structure	729085.21	287871.823	392.41		freshwater molluscs
40		Mahrersdorf pit	RBK, infilling, middle position of the wedge structure	729085.21	287871.823	392.41		pollen
41		Mahrersdorf pit	RBK, infilling	729085.05	287888.958	393.98		freshwater molluscs
41		Mahrersdorf pit	RBK, infilling	729085.06	287888.958	393.98		pollen
42		Cemex pit (at highway A2)	3 horizons at the base of the pit, just above the thick, 1. base horizon (740020.63	294841.094	274.288		heavy minerals
43		Cemex pit (at highway A2)	3 horizons at the base of the pit, top of the thick, 1. base horizon	740020.63	294841.094	274		pollen
43		Cemex pit (at highway A2)	3 horizons at the base of the pit, top of the thick, 1. base horizon	740020.63	294841.094	274		freshwater molluscs
43		Cemex pit (at highway A2)	3 horizons at the base of the pit, top of the thick, 1. base horizon	740020.63	294841.094	274		heavy minerals
44		Cemex pit (at highway A2)	3 horizons at the base of the pit, top of the 3. top horizon	740017.95	294872.571	274.113		pollen
44		Cemex pit (at highway A2)	3 horizons at the base of the pit, top of the 3. top horizon	740017.95	294872.571	274.113		freshwater molluscs
44		Cemex pit (at highway A2)	3 horizons at the base of the pit, top of the 3. top horizon	740017.95	294872.571	274.113		freshwater molluscs
45A		Cemex pit (at highway A2)	sandlense above the toppest overbank horizon of the pit	740038.54	294541.323	274.575		heavy minerals

sample Nr.	add. samples	location name	sample discription	pos. x	pos. y	pos. z	14C age B.P.	sample for
45B		Cemex pit (at highway A2)	overbank remnant (erosive lense) above the toppest overbank horizon of the pit	740038.54	294541.323	274.575		freshwater molluscs
45B		Cemex pit (at highway A2)	overbank remnant (erosive lense) above the toppest overbank horizon of the pit	740038.54	294541.323	274.575		pollen
46		pit NK (east)	sand lense, hard	733018.04	288082.472	345.903		heavy minerals
46	Fr. 9	pit NK (east)	sand lense, hard	733018.04	288082.472	345.903		freshwater molluscs
47		Neurißhof pit	overbanks, at the top	749169.75	310334.066	225.735		heavy minerals
47		Neurißhof pit	overbanks, at the top	749169.75	310334.066	225.735		freshwater molluscs
48	Fr. 7	Neurißhof pit	"brown palaeosol" 0.5 m below overbanks, upper palaeosol	749169.75	310334.066	225.2	8999 ± 65 (S7)	freshwater molluscs
48		Neurißhof pit	"brown palaeosol" 0.5 m below overbanks, upper palaeosol	749169.75	310334.066	225.2		pollen
49	Fr. 8	Neurißhof pit	lower palaeosol horizon, same like sample 13 but some darker	310460.314	749059.74	219.929		freshwater molluscs
49		Neurißhof pit	lower palaeosol horizon, same like sample 13 but some darker	310460.314	749059.74	219.929		pollen
50		HS2 Pannon pit	sample at the border: Pannonian sands and overlying gravels (Pannonian sands)	306239.991	743041.19	225.232		heavy minerals
51		HS2 Pannon pit	sample from the overlying gravels	306239.991	743041.19	225.7		heavy minerals
51		HS2 Pannon pit	sample from the overlying gravels	306239.991	743041.19	225.7		freshwater molluscs
52		Tattendorf pit	overbanks some 1 m below surface	311718.3	748258.24	229.238		indefinite
53		Tattendorf pit	sand some 2 m below surface	311718	748258	228		heavy minerals
54		Tattendorf pit	top overbanks	311815	748170	239		freshwater molluscs
55		Hitzehammer 1 pit	palaeosol remnants, close to the base	748712	310905	225.795		freshwater molluscs
56		Hitzehammer 2 pit	palaeosol, pedogenic altered overbank at the base	748246.611	311080.78	226.989		freshwater molluscs
56		Hitzehammer 2 pit	palaeosol, pedogenic altered overbank at the base	748246.611	311080.78	226.989		pollen
57		Hitzehammer 2 pit	overbank at the base	748246	311080	226		indefinite
58	Fr. 6	gegenüber Wopfinger pit	overbanks some 20-30cm below the gravel/overbank limit, 2-3 m below surface	746231.51	304043.454	259.792		freshwater molluscs
58		gegenüber Wopfinger pit	overbanks some 20-30cm below the gravel/overbank limit, 2-3 m below surface	746231.51	304043.454	259.792		pollen

sample Nr.	add. samples	location name	sample discription	pos. x	pos. y	pos. z	14C age B.P.	sample for
59		Wopfinger pit	some 3 m below top, top overbank	746064.731	303887.246	261		indefinite
59		Wopfinger pit	some 3 m below top, top overbank	746064.731	303887.246	261		pollen
60		Wopfinger pit	sample of the base overbank	746064.731	303887.246	256.684		heavy minerals
60		Wopfinger pit	sample of the base overbank	746064.731	303887.246	256.684		pollen
61		Cemex pit (at highway A2)	sample of topmost overbank horizon	740083.616	294517.896	281.905	40460 ± 650 (S1)	freshwater molluscs
61	Fr. 5	Cemex pit (at highway A2)	sample of topmost overbank horizon	740083.616	294517.896	281.905	47766 ± 1400 (S2)	freshwater molluscs
62		Cemex pit (at highway A2)	some 1 m below 61	740083.616	294517.896	~280		indefinite
63		pit 2 street Weik_Neunk	sandlense at the base	734075	293025	324		heavy minerals
64		pit 2 street Weik_Neunk	sandlense at the top	734125	292995	330		heavy minerals
65		Rauchenwarth 1 pit	sandlense at the basis	765868.117	326712.806	216.663		heavy minerals
66		Rauchenwarth 1 pit	clay, silt, palaeochannel, at the bottom	765828.956	326651.61	221		indefinite
66		Rauchenwarth 1 pit	clay, silt, palaeochannel, at the bottom	765828.956	326651.61	221		pollen
67		Rauchenwarth 1 pit	clay, silt, palaeochannel, at the middle	765828.956	326651.61	221.26		indefinite
67		Rauchenwarth 1 pit	clay, silt, palaeochannel, at the middle	765828.956	326651.61	221.26		pollen
68		Rauchenwarth 1 pit	clay, silt, palaeochannel, at the top	765828.956	326651.61	221.5		indefinite
68		Rauchenwarth 1 pit	clay, silt, palaeochannel, at the top	765828.956	326651.61	221.5		pollen
69		Rauchenwarth 2 pit	sandlense from gravels some dm above stratified sands , close to top of pit	765521.114	326228.536	216.028		heavy minerals
70		Rauchenwarth 2 pit	stratified sands	765517.592	326206.53	211.356		heavy minerals
71		Rauchenwarth 3 pit	clay, silt, palaeochannel	765762	325946	226		indefinite
72		Schwalbeninsel, Danube, at Stopfenreuth village	overbank silt, sand, present day deposits	790530	332770	142		heavy minerals
73		Rauchenwarth 2 pit	stratified sands, at the base	765445	326205	208		heavy minerals
74		Rauchenwarth 3 pit	clay, palaeochannel	765762.01	325946.34	225.645		freshwater molluscs
74		Rauchenwarth 3 pit	clay, palaeochannel	765762.01	325946.34	225.645		pollen
75		Rauchenwarth 3 pit	sand lense below palaeochannel	765757.011	325954.78	222.47		heavy minerals
76		Rauchenwarth 3 pit	clays from the top area	765762	325946	226.5		indefinite
77		Schlossofer Platte, near Breitensee	sandlense at the bottom	791200	344724	157		heavy minerals
78		Schlossofer Platte, near Breitensee	sandlense closer to the top	791200	344724	159		heavy minerals
79		Kottingbrunn graveyard	unknown, Pr. Nr. Kü 4856/II/38 (Geol, survey of Austria, Dr. Küpper)	742373	313176	251		freshwater molluscs

sample Nr.	add. samples	location name	sample discription	pos. x	pos. y	pos. z	14C age B.P.	sample for
80		Frohsdorf, archaeologic site	archaeologic site, Dr. E. Draganits, Tu Wien	744003	290003	~~293		freshwater molluscs
81	Fr. 1	neben Loidl pit	red palaeosol	741530.4039	302534.1185	~286		freshwater molluscs
82	Fr. 2	neben Loidl pit	sand lense at the base of the pit	741530.4039	302534.1185	~282.5		freshwater molluscs
83	Fr. 3	Hitzehammer 2 pit	palaeosol close to the bottom of the pit	748246.611	311080.78	~227		freshwater molluscs
84	Fr. 4	Tattendorf pit	top overbanks	311815	748170	239		freshwater molluscs
85		neben Loidl pit	red palaeosol, at a distal position	741531.6611	302532.7688	284.195		soil
86	Fr. 10	Hitzehammer 2 pit	palaeosol close to the bottom of the pit	748246.611	311080.78	~227		freshwater molluscs
87		neben Loidl pit	red piece of gravel, from central section of the red palaeosol	741531.6611	302532.7688	284.195		soil
88	Fr. 11	Bad Fischau pit	sand lense at the cryoturbation area	737669.553	297539.429	~276.5		freshwater molluscs
89	Fr. 12	Cemex pit (at highway A2)	toppest overbank horizon of the pit, toppest position of that horizon	740083.616	294517.896	~281		freshwater molluscs
90	Fr. 13	Cemex pit (at highway A2)	toppest overbank horizon of the pit, middle position of that horizon	740083.616	294517.896	~281		freshwater molluscs
91	Fr. 14	Cemex pit (at highway A2)	toppest overbank horizon of the pit, lowest position of that horizon	740083.616	294517.896	~280		freshwater molluscs
92	Fr. 15	Cemex pit (at highway A2)	toppest overbank horizon of the pit, below lowest position (sand)	740083.616	294517.896	~280		freshwater molluscs
93	Fr. 16	Cemex pit (at highway A2)	3 horizons at the base of the pit, top of the 1. base horizon	740017.95	294872.571	~274		freshwater molluscs
94	Fr. 17	Cemex pit (at highway A2)	3 horizons at the base of the pit, top of the 2. middle horizon	740017.95	294872.571	~275		freshwater molluscs
95	Fr. 18	Cemex pit (at highway A2)	3 horizons at the base of the pit, top of the 3. top horizon	740017.95	294872.571	~277		freshwater molluscs
96	Fr. 19	Cemex pit (at highway A2)	overbank horizon somewhere at the middle of pit below the "Cemex label", height = somewhere beteen top and base horizons	740000	294700	~~278		freshwater molluscs
97	Fr. 20	Cemex pit (at highway A2)	lense in braided sediments above horizon of the top area (once sampled)	740038.54	294541.323	~281		freshwater molluscs
98	Fr. 21	Wopfinger pit	overbank top horizon (only some few dm thick)	746231.51	304043.454	261		freshwater molluscs
99	Fr. 22	Wopfinger pit	overbank base horizon (only some few dm thick)	746231.51	304043.454	256.684		freshwater molluscs

sample Nr.	add. samples	location name	sample discription	pos. x	pos. y	pos. z	14C age B.P.	sample for
100	Fr. 23	gegenüber Wopfinger pit	overbank horizon, at the top	746231.51	304043.454	~260		freshwater molluscs
101	Fr. 24	gegenüber Wopfinger pit	overbank horizon, at the base	746231.51	304043.454	~259		freshwater molluscs
102	Fr. 25	neben Loidl pit	sand lense from the base (somewhere at the boulder lag)	743185	303563	~283.5		freshwater molluscs
103	Fr. 26	Cemex pit (at highway A2)	3 horizons at the base of the pit, between the 1. top and the 2. middle horizon	743185	303563	283.5		freshwater molluscs
104	Fr. 27	Cemex pit (at highway A2)	sand somewhere at the middle of pit below the "Cemex label", height = somewhere beteen top and base horizons	743185	303563	283.5	45672 ± 1000 (S3)	freshwater molluscs
105		remnants, core material drilling THER-SCI-1	remnants through casing procedure, rough depth: 33 - 34.5 m below surface (core is listed seperatly)	743171	303555	283		indefinite
106		remnants, core material drilling THER-SCI-1	remnants through casing procedure, rough depth: 33 - 34.5 m below surface (core is listed seperatly)	743171	303555	283		indefinite
107		remnants, core material drilling THER-SCI-1	remnants through casing procedure, rough depth: 34.9 - 36 m below surface (core is listed seperatly)	743171	303555	283		indefinite
108		roter Boden	red palaeosol, at a distal position	741531.6611	302532.7688	284.195		C14
109	Fr.28	Theresienfeld_große Grube_liegender Bodenhorizont	same like 24_1, some 10 m below surfcae, base of 2 fine grained horizons	745541.56	305156.209	~253		freshwater molluscs
110	Fr.29	Theresienfeld_große Grube_hangender Bodenhorizont	same like 24_1, some 10m below surfcae, top of 2 fine grained horizons	745541.56	305156.209	~253		freshwater molluscs
111		Tattendorf pit	overbanks top	748269	311721	239		14C
112		Tattendorf pit	overbank filling in channel	748269	311721	239		14C
113		Neurißhof pit	overbank close to the base, source for the palaeosol (sample 49) at the bottom?	310460.314	749059.74	~225	40785 ± 1000 (S8)	C14, freshwater molluscs
114		gegenüber Wopfinger pit	overbank horizon, at the top	746231.51	304043.454	~260	43326 ± 1000 (S5)	14C
115		gegenüber Wopfinger pit	overbank horizon, at the bottom	746231.51	304043.454	~259	35884 ± 600 (S6)	14C
116		pit NK (east)	sand lense, somewhere close to the base	732770	288820	~343	> 45000 (S9)	14C

sample Nr.	add. samples	location name	sample discription	pos. x	pos. y	pos. z	14C age B.P.	sample for
117		Triesting river at Guenselsdorf	sand, river bank	744565	312174	no point		heavy minerals
118		Piesting river at Neuribhof	sand, river bank	749889	310846	no point		heavy minerals
119		Leitha river at Zillingdorf	sand, river bank	749355	302517	no point		heavy minerals
120		Leitha spring at nature trail	sand, river bank	741725	289000	no point		heavy minerals
121		Warme Fische river in Bad Fischau	sand	737923	299783	no point		heavy minerals
122		Kalter Berg pit	clay, many faults	774350	327350	~227		heavy minerals
123		Kalter Berg pit	sands and gravels from the top	774500	327450	~230		heavy minerals
124		Cemex pit (at highway A2)	root, in situ, at the some 10 m	740017	294451	~~274	> 46000 (S4)	14C
125		Haslau pit	sand from Danube gravels some 2 m below surface close to an ice wedge cast	780854	330381	~189		heavy minerals

Appendix Tab. app. 2, Sample list drilling core SCI-THER-1

to (m)	thickness (m)	colour	lithofacies interpret.	Strat. interpret	subsidence rate	OSL age, feldspar	heavy mineral assemblage
0.53	0.53	brown	soil	Holocene	fast		
2.00	1.47	yellow brown	massive gravels	MIS 2/ full glacial	fast		
8.00	6.00	yellow brown	massive gravels	MIS 2/ full glacial	fast		
14.00	6.00	flushed section	gravels	Würm glacial	fast		
15.50	1.50	light brown	massive gravels	Würm glacial	fast		
15.60	0.10	brown	massive gravels	Würm glacial	fast		
15.72	0.12	grey	channel sediments	Riß/Würm interglacial	fast		
16.00	0.28	brown	paleosol, medium alteration	Riß/Würm interglacial	fast		K21
16.05	0.05	brown	channel sediments	Riß/Würm interglacial	fast		
16.17	0.12	brown	channel sediments	Riß/Würm interglacial	fast	135+-9 ka	
16.25	0.08	brown	channel sediments	Riß/Würm interglacial	fast		
17.00	0.75	grey	channel sediments	Riß/Würm interglacial	fast	134+-10 ka	
17.50	0.50	grey brown	massive gravels	Riß full glacial	fast		
18.00	0.50	brown	massive gravels	Riß full glacial	fast		
18.50	0.50	whitish grey	massive gravels	Riß full glacial	fast		
19.30	0.80	hellbraungrau	massive gravels	Riß full glacial	fast		
20.00	0.70	light brown grey	massive gravels	Riß full glacial	fast		
20.20	0.20	light brown grey	massive gravels	Riß full glacial	fast		
20.45	0.25	light brown grey	massive gravels	Riß full glacial	fast		
20.80	0.35	very light brown	massive gravels	Riß full glacial	fast		
21.00	0.20	darker brown	paleosol, medium alteration	Riß-interstadial	fast		K20
21.70	0.70	brown	massive gravels	Riß glacial	fast		
22.08	0.38	hellbraeunlichgrau	massive gravels	Riß glacial	fast		
22.20	0.12	light brown	massive gravels	Riß glacial	fast		
22.80	0.60	hellbraeunlichgrau	massive gravels	Riß glacial	fast		K26
25.78	2.98	hellbraeunlichgrau	massive gravels	Riß glacial	fast		
25.83	0.05	red	massive gravels, remnants of paleosol?	Riß glacial	fast		
27.50	1.67	whitish grey	massive gravels	Riß glacial	fast		
27.67	0.17	brown	channel sediments		fast		
32.50	6.83	whitish grey	massive gravels		fast		
32.58	0.08	yellow light brown	overbanks, not pedogenic altered	interstadial/interglacial	transition		

33.00	0.42	brown	overbanks, light pedogenic altered	interstadial/interglacial	transition		K18
33.50	0.50	darker brown	paleosol, medium alteration	interstadial/interglacial	transition		K4
33.56	0.06	dark brown	paleosol, strong alteration	interstadial/interglacial	transition		K1
33.82	0.26	dark brown	paleosol, strong alteration	interstadial/interglacial	transition		
34.25	0.43	dark brown, to top lighter	paleosol, medium alteration	interstadial/interglacial	transition		K19
34.30	0.05	grey	channel sediments		low		
34.55	0.25	grey brown	channel sediments		low		
35.50	0.95	whitish grey brown	massive gravels		low		
35.90	0.40	brown	paleosol, medium alteration	interstadial/interglacial	low		K13
36.00	0.10	light brown	overbanks	interstadial/interglacial	low		K15
36.50	0.37	brown	channel sediments	interstadial/interglacial	low		
37.00	0.50	light grey	massive gravels		low		
37.50	0.50	lighter brown	overbanks	interstadial/interglacial	low	246+-24 ka	K28
37.62	0.12	brown	overbanks	interstadial/interglacial	low		
37.80	0.18	brown	channel sediments		low		
38.00	0.20	brown	channel sediments		low		
38.18	0.18	brown	channel sediments		low		
38.23	0.05	grey	channel sediments		low		
38.28	0.05	grey brown	paleosol remnants	interstadial/interglacial	low		
38.30	0.02	brown	channel sediments		low		
39.00	0.70	grey brown	massive gravels		low		
39.15	0.15	grey	overbanks		low		
40.50	1.35	grey brown	massive gravels		low		

Appendix Tab. app. 3, Heavy mineral assemblages

sample Nr.	sample location (details append. XX)	source area	Zirkon	Turmalin	Rutil	Apatit	Granat	Chloritoid	Staurolith	Epidot	grüne Hornbl.	Klinozoisit	Chromspinell	Sillimanit	Glauko- phan	Disthen	Monazit?	farbl. Hbl.	Andalusit	sum
Rauchenwart Plateau, Arbesthal Hills, Danube																				
65	Rauchenwarth 1 pit	Pannonian Danube	4.6	3.3	3.0	5.3	29.7	0.3	26.4	18.1	1.7	5.0	0.3	0.3	0.0	1.7	0.0	0.3	0.3	303
75	Rauchenwarth 3 pit	Pannonian Danube	1.8	1.2	1.8	5.0	29.7	0.0	24.9	28.2	3.0	1.2	0.0	0.9	0.0	1.8	0.0	0.6	0.0	337
69	Rauchenwarth 2 pit	Pannonian Danube	2.2	2.6	1.9	1.5	30.6	0.0	12.7	37.3	3.0	0.7	0.0	3.0	0.0	2.2	0.0	2.2	0.0	268
123	Kalter Berg pit	Pannonian Danube	0.8	1.5	1.9	1.9	42.0	1.1	18.7	10.7	15.3	0.4	0.0	3.8	0.0	1.9	0.0	0.0	0.0	262
70	Rauchenwarth 2 pit	Vienna Basin	1.2	2.4	2.0	2.8	56.8	0.0	8.0	20.0	2.8	0.0	0.0	1.2	0.0	2.4	0.0	0.0	0.4	250
73	Rauchenwarth 2 pit	Vienna Basin	1.1	0.7	1.4	0.7	50.2	0.7	10.8	22.9	5.7	0.0	0.0	0.7	0.0	2.9	0.0	1.4	0.7	279
122	Kalter Berg pit	Vienna Basin	3.5	5.4	0.4	23.3	14.3	2.7	24.0	24.0	0.8	0.4	0.0	0.8	0.0	0.4	0.0	0.0	0.0	258
125	Haslau pit	Pleistocene Danube	8.8	2.6	3.6	1.8	29.2	0.4	20.8	25.5	4.7	1.1	0.0	1.1	0.0	0.4	0.0	0.0	0.0	274
77	Schlosshofer Platte, near Breitensee	Pleistocene Danube	1.5	6.8	1.9	4.5	56.4	0.0	9.0	6.8	8.3	0.4	0.0	1.1	0.4	2.3	0.0	0.4	0.4	266
72	Schwalbeninsel, Danube, at Stopfenreuth village	present Danube	1.0	3.0	0.7	5.7	33.3	0.3	6.3	6.3	40.0	1.0	0.0	0.0	0.0	0.7	0.0	1.7	0.0	300
outcrops Mitterndorf Basin																				

20_3	Neuribhof pit	Alps, Piesting Fan drainage area	13.1	12.7	3.8	8.9	34.4	0.7	2.4	7.9	10.0	1.7	2.7	0.3	0.3	0.7	0.3	0.0	0.0	291
20_4	Neuribhof pit	Alps, Piesting Fan drainage area	5.4	4.8	4.2	8.4	46.7	0.0	1.2	16.8	8.4	1.2	2.4	0.6	0.0	0.0	0.0	0.0	0.0	167
35	neben Loidl pit	Alps, Piesting Fan drainage area	5.9	5.9	6.3	4.2	56.5	0.0	0.7	10.1	2.8	1.7	3.8	0.4	0.0	0.4	0.0	1.1	0.0	287
22_2	Hitzehammer 2 pit	Alps, Piesting Fan drainage area	20.1	15.3	8.2	4.8	37.4	0.3	2.4	8.8	0.3	0.7	0.7	0.0	0.0	0.7	0.0	0.3	0.0	294
23_1	Tattendorf pit	Alps, Piesting Fan drainage area	10.1	13.0	2.2	9.4	39.9	1.4	4.3	6.2	5.8	1.1	5.8	0.4	0.0	0.0	0.0	0.4	0.0	276
23_2	Tattendorf pit	Alps, Piesting Fan drainage area	25.9	15.5	12.0	3.9	32.4	0.3	2.6	3.9	1.0	0.6	1.9	0.0	0.0	0.0	0.0	0.0	0.0	309
25_2	neben Fischadep pit	Alps, Piesting Fan drainage area	5.5	7.9	1.8	9.7	52.1	1.2	0.6	7.9	7.3	0.0	5.5	0.0	0.0	0.0	0.0	0.6	0.0	165
27	Hitzehammer 1 pit	Alps, Piesting Fan drainage area	4.0	7.3	4.5	2.8	44.5	0.4	5.7	11.3	12.1	0.0	6.5	0.0	0.0	0.4	0.0	0.4	0.0	247
47	Neuribhof pit	Alps, Piesting Fan drainage area	6.8	7.5	1.7	4.4	51.0	1.7	11.9	6.5	7.1	0.0	1.0	0.3	0.0	0.0	0.0	0.0	0.0	294
53	Tattendorf pit	Alps, Piesting Fan drainage area	2.4	6.0	3.0	3.6	38.7	0.0	6.0	6.5	14.9	1.2	15.5	0.0	0.0	0.6	0.6	1.2	0.0	168

60	Wopfinger pit	Alps, Piesting Fan drainage area	7.0	1.2	2.7	1.6	46.9	2.0	4.7	10.5	3.9	0.0	19.1	0.4	0.0	0.0	0.0	0.0	0.0	256
58	gegenüber Wopfinger pit	Alps, Piesting Fan drainage area	4.2	10.8	2.0	12.4	22.5	0.3	2.9	14.1	20.6	1.6	5.9	0.0	0.7	0.7	0.7	0.7	0.0	306
108	neben Loidl pit	Alps, Piesting Fan drainage area	3.2	4.2	5.3	1.1	70.4	0.4	2.8	10.2	0.0	0.7	1.4	0.0	0.0	0.0	0.4	0.0	0.0	284
33	Breitenau 4 pit	Alps, Schwarza Fan drainage area	4.0	6.9	5.0	5.0	22.8	1.0	0.0	41.6	12.9	0.0	0.0	0.0	0.0	0.0	0.0	1.1	0.0	101
34	Breitenau 4 pit	Alps, Schwarza Fan drainage area	8.6	5.3	0.5	16.0	17.6	1.1	0.0	39.0	10.7	0.0	0.5	0.5	0.0	0.0	0.0	0.0	0.0	187
46	pit NK (east)	Alps, Schwarza Fan drainage area	11.7	7.4	0.9	9.1	12.1	0.0	0.0	51.9	6.5	0.4	0.0	0.0	0.0	0.0	0.0	0.0	0.0	231
50	HS2 Pannon pit	Alps, Schwarza Fan drainage area	1.2	1.2	2.3	3.5	50.4	0.0	6.6	20.5	11.6	0.4	0.0	0.4	0.0	1.9	0.0	0.0	0.0	258
51	HS2 Pannon pit	Alps, Schwarza Fan drainage area	5.8	4.4	1.5	3.3	58.2	2.2	2.9	15.3	4.0	0.7	0.0	0.4	0.0	1.1	0.0	0.4	0.0	275
63	pit 2 street Weik_Neunk	Alps, Schwarza Fan drainage area	8.6	6.1	2.5	8.6	15.2	0.4	0.8	45.1	12.3	0.0	0.0	0.0	0.0	0.4	0.0	0.0	0.0	244
64	pit 2 street Weik_Neunk	Alps, Schwarza Fan drainage area	6.6	2.5	0.8	9.0	25.4	0.0	0.8	47.5	4.9	0.8	0.8	0.0	0.0	0.8	0.0	0.0	0.0	122

27.1	Bad Fischau pit	Alps, Schwarza Fan drainage area	6.9	6.3	1.6	11.1	37.0	0.5	0.5	23.3	9.5	0.5	1.6	0.5	0.0	0.5	0.0	0.0	0.0	189
27.2	Bad Fischau pit	Alps, Schwarza Fan drainage area	3.7	17.4	0.0	14.3	18.6	0.0	0.6	37.3	7.5	0.6	0.0	0.0	0.0	0.0	0.0	0.0	0.0	161
P31	pit 3 street Weik_Neunk	Alps, Schwarza Fan drainage area	4.4	13.2	3.2	19.2	12.0	0.8	4.4	34.4	4.8	1.6	1.6	0.0	0.0	0.0	0.4	0.0	0.0	250
P32	Cemex pit (at highway A2), section Kaiser	Alps, Schwarza Fan drainage area	7.9	6.4	1.1	10.2	9.0	0.4	1.9	48.9	9.4	1.1	2.6	0.0	0.0	0.4	0.4	0.4	0.0	266
P42	Cemex pit (at highway A2)	Alps, Schwarza Fan drainage area	6.6	8.7	4.2	6.9	20.1	0.0	2.8	41.7	5.9	1.0	0.3	0.0	0.0	0.0	1.7	0.0	0.0	288
P43	Cemex pit (at highway A2)	Alps, Schwarza Fan drainage area	6.6	10.0	2.1	9.3	11.4	0.0	7.6	41.5	9.0	0.3	1.0	0.0	0.0	0.0	1.0	0.0	0.0	289
P45a	Cemex pit (at highway A2)	Alps, Schwarza Fan drainage area	2.8	7.0	0.9	4.7	14.5	0.0	10.3	48.6	9.8	0.9	0.0	0.0	0.5	0.0	0.0	0.0	0.0	214
0.0																				
rivers, southern Vienna Basin																				
P117	Triesting at Guenselsdorf	Alps, Triesting drainage area	15.7	16.5	3.5	8.2	43.1	0.0	5.1	5.1	1.2	0.4	0.8	0.0	0.0	0.4	0.0	0.0	0.0	255
P118	Piesting at Neurifhof	Alps, Piesting drainage area	3.1	9.3	2.4	4.5	44.7	0.7	9.3	13.1	8.9	0.3	2.1	0.7	0.0	0.0	0.7	0.3	0.0	291

P119	Leitha at Zillingdorf	Alps, Leitha drainage area	0.0	5.5	0.7	5.5	69.6	0.0	0.7	8.8	8.1	0.4	0.0	0.4	0.0	0.0	0.0	0.4	0.0	273
P120	Leitha spring at nature trail	Alps, Leitha drainage area	3.0	5.7	1.3	4.7	29.9	0.0	3.4	35.9	13.1	0.7	1.3	0.0	0.0	0.0	0.7	0.3	0.0	298
P121	Warme Fische at Bad Fischau	Alps, Warme Fische drainage area	2.8	3.8	2.1	1.4	69.2	0.0	1.7	9.3	4.2	1.0	0.0	0.0	0.3	0.0	0.0	0.0	4.2	289
core THER-SCI-1																				
K1	core THER-SCI-1	Alps, Piesting Fan drainage area	8.5	13.5	3.1	4.2	38.5	0.4	4.6	15.8	4.2	1.2	5.8	0.0	0.0	0.0	0.4	0.0	0.0	260
K4	core THER-SCI-1	Alps, Piesting Fan drainage area	7.7	11.1	5.9	3.7	48.0	0.0	4.1	13.3	1.1	0.7	3.7	0.0	0.0	0.4	0.4	0.0	0.0	271
K13	core THER-SCI-1	Alps, Piesting Fan drainage area	7.0	10.7	5.6	1.9	31.5	1.1	5.9	18.5	5.6	0.0	10.7	0.0	0.7	0.0	0.0	0.7	0.0	270
K15	core THER-SCI-1	Alps, Piesting Fan drainage area	6.3	7.5	2.4	5.2	34.1	0.4	4.0	15.1	5.6	0.8	16.7	0.0	0.0	2.0	0.0	0.0	0.0	252
K18	core THER-SCI-1	Alps, Piesting Fan drainage area	6.3	16.7	8.9	4.1	40.7	0.4	3.7	11.1	2.6	0.4	4.8	0.0	0.0	0.4	0.0	0.0	0.0	270

K19	core THER-SCI-1	Alps, Piesting Fan drainage area	5.9	11.5	7.4	4.1	48.3	0.0	2.2	11.2	1.1	0.4	7.4	0.4	0.0	0.0	0.0	0.0	0.0	269
K20	core THER-SCI-1	Alps, Piesting Fan drainage area	7.4	6.4	3.0	2.7	43.6	0.7	8.1	18.8	4.0	3.4	0.7	0.3	0.0	1.0	0.0	0.0	0.0	298
K21	core THER-SCI-1	Alps, Piesting Fan drainage area	13.1	11.9	6.2	2.3	38.5	0.4	6.2	11.5	6.2	1.5	1.5	0.0	0.0	0.8	0.0	0.0	0.0	260
K25	core THER-SCI-1	Alps, Piesting Fan drainage area	2.9	13.6	3.9	14.6	35.0	0.0	5.8	11.7	5.8	1.0	5.8	0.0	0.0	0.0	0.0	0.0	0.0	103
K26	core THER-SCI-1	Alps, Piesting Fan drainage area	8.5	4.3	4.3	14.5	41.0	0.9	4.3	9.4	5.1	0.9	6.0	0.0	0.9	0.0	0.0	0.0	0.0	117
K28	core THER-SCI-1	Alps, Piesting Fan drainage area	6.5	4.9	1.9	11.3	32.4	1.0	1.9	18.1	4.2	0.3	17.5	0.0	0.0	0.0	0.0	0.0	0.0	309

Curriculum Vitae

MAG. BERNHARD SALCHER
<ul style="list-style-type: none">▪ Date of Birth: 04.05.1978▪ Place of Birth: Vienna▪ Adress: Nussdorfer Strasse 62/11, 1090 Wien▪ University of Vienna, Department for Geodynamic & Sedimentology, Althanstrasse 14, 1090 Wien; Tel: +436503247324, +43/1/4277/53442▪ e-mail: bernhard.salcher@univie.ac.at
EDUCATION:
<ul style="list-style-type: none">▪ 1996 Matura, Realgymnasium▪ 1998 – 2005 study of geology (1. class)▪ 2004 military service, bureau of the General Staff (Ministry of Defence).▪ Dec. 2005 Phd. expected graduation end of 2008.
ACTIVITIES AT THE UNIVERSITY:
<ul style="list-style-type: none">▪ 2001 – 2004 student's representation, mandatar of the faculty of natural sciences

JOBS & PROJECTS

- since June 2008, modeler in the Project: "deep Geothermal Exploration of eastern Vienna" (Geothermie Wien Ost).
- since March 2008, consultant of the OMV project: „geological evaluation of eastern Vienna for deep geothermal utilization“
- since October 2007, consultant of the project "Thermalp – Geothermal modelling of the southern Vienna Basin".
- since December 2005, PhD student "Sedimentology and modeling in the Mitterndorf pull-apart basin (Plio-/Pleistocene, Austria)", Dep. of Geodynamic and Sedimentology, University of Vienna (Austrian Science Fund, FWF, 18203).
- 2005 employee of the Dep. of Natural Resources and Applied Life Sciences
- 1999-2004 assistant of the hydrogeological project „Recovery of Groundwater, southwestern Innviertel“, Government of Upper Austria (diploma Thesis).
- 1998-2003 numerous works at civil engineers

PUBLICATIONS**Scientific articles:**

- Salcher, B. and Wagreich M. (2008, in review): Climate and tectonic controls on sequence development and river evolution in Austria's largest Pleistocene basin.
- Salcher, B., Meurers B., Decker, K. Wagreich, M. (2008, submitted): Detection of Pleistocene structures in the southern and central Vienna Basin using first order gravity derivatives, reflection seismic and well data
- Salcher, B., Hinsch R.. (2008, in review): Application of Airborne LiDAR data for glacial landform evaluation – a comparison with traditional methods, terminal area of the Salzach glacier, Austria
- Salcher, B., Faber R., Wagreich, M. (2008, in review): Numerical modeling of factors controlling sequence development of Pleistocene alluvial fans, Vienna Basin, eastern Austria
- Salcher, B. Götzl, G. (2007) Deep heat mining in the Austrian Alps – a preliminary look on possibilities and limitations. Proceedings of the Thirty Second Workshop on Geothermal Reservoir Engineering, Stanford University, California.

Posters (selection):

- Salcher, B., Faber R., Wagneich, M. (2008) Response of rivers to late Pleistocene and Holocene climate change and subsidence, Southern Vienna Basin, eastern Austria. EGU (accepted).
- Salcher, B., Faber R., Wagneich, M. (2007) 4 D modelling of alluvial fans. EGU.
- Salcher, B., Faber R., Wagneich, M. (2006) Sedimentation and simulation in the Pleistocene Mitterndorf basin (Vienna Basin, Austria), Geoberlin.
- Salcher, B., van Husen, Dirk., (2005) Evidence for a subglacial drainage system at the Salzach Foreland Glacier (Austria). EGU, General Assembly, 24– 29 April 2005, Vienna. EGU.

Talks (selection):

- Salcher, B., Decker, K., Meurers, B., Hölzel M., Wagneich, M. (2008) Hochauflösende Kartierung quartärer Störungen im südlichen Wiener Becken. Pangeo Austria.
- Salcher, B., Faber R., Wagneich, M. (2007) 4 D modelling of 2 Pleistocene alluvial fans in an active pull-apart basin in Eastern Austria. Alluvial Fans Scientific Meeting, Banff, Alberta.
- Salcher, B. Götzl, G. (2007) Deep heat mining in the Austrian Alps – a preliminary look on possibilities and limitations. Workshop on Geothermal Reservoir Engineering, Stanford University, California.

LANGUAGES

- German (first language)
- English (fluently), French (school)

APPLICATION SOFTWARE SKILLS

- ArcGIS, ArcView (ERSI)
- WinGeol, SedTec (Terramath)
- GoCAD (Earth Decison)
- div. Software (ERdas Imagine, Corel Draw, Surfer, Grapher)
- Petrel, Mathlab (beginner)